

## Supplementary Information

### A microbial platform for recyclable plastics with customizable properties

Zilong Wang<sup>1,2,3</sup>, Seokjung Cheong<sup>1,2,3</sup>, Hai Wang<sup>4\*</sup>, Jeremy Demarteau<sup>4</sup>, Alexander R. Epstein<sup>5</sup>, Baishakhi Bose<sup>6</sup>, Mei Zhao<sup>2,3†</sup>, Beibei Ge<sup>2,3‡</sup>, Alberto A. Nava<sup>2,3</sup>, Ramu Kakumanu<sup>3,6</sup>, Edward E. K. Baidoo<sup>3,6</sup>, Yan Chen<sup>3,6</sup>, Christopher J. Petzold<sup>3,6</sup>, Yifan Guo<sup>3,6,7,8</sup>, Nawa Raj Baral<sup>3,6</sup>, Nemi Vora<sup>3,6¶</sup>, Yuzhong Liu<sup>1,2,3</sup>, Rithwik Ghanta<sup>5§</sup>, Pablo Cruz-Morales<sup>3,6,15</sup>, Kevin Yin<sup>3,9</sup>, Robert W. Haushalter<sup>3,6</sup>, Kristin A. Persson<sup>4,5</sup>, Corinne D. Scown<sup>3,6,10,11</sup>, Brett A. Helms<sup>3,4,12</sup>, Jay D. Keasling<sup>1-3,6,13-15</sup>✉

<sup>1</sup>QB3 Institute, University of California, Berkeley, CA 94720, USA.

<sup>2</sup>Department of Chemical and Biomolecular Engineering, University of California, Berkeley, CA 94720, USA.

<sup>3</sup>Joint BioEnergy Institute, Emeryville, CA 94608, USA.

<sup>4</sup>The Molecular Foundry, Lawrence Berkeley National Laboratory, Berkeley, CA 94720, USA.

<sup>5</sup>Materials Sciences and Engineering, University of California, Berkeley, Berkeley, CA 94720, USA.

<sup>6</sup>Biological Systems and Engineering Division, Lawrence Berkeley National Laboratory, Berkeley, CA 94720, USA.

<sup>7</sup>Department of Chemistry, University of California, Berkeley, Berkeley, CA 94720, USA

<sup>8</sup>Department of Molecular and Cell Biology, University of California, Berkeley, Berkeley, CA 94720, USA

<sup>9</sup>Department of Plant and Microbial Biology, University of California, Berkeley, Berkeley, CA 94720, USA

<sup>10</sup>Energy Analysis and Environmental Impacts Division, Lawrence Berkeley National Laboratory, Berkeley, CA 94720, USA.

<sup>11</sup>Energy & Biosciences Institute, University of California, Berkeley, Berkeley, CA 94720, USA.

<sup>12</sup>Materials Sciences Division, Lawrence Berkeley National Laboratory, Berkeley, CA 94720, USA.

<sup>13</sup>Department of Bioengineering, University of California, Berkeley, CA 94720, USA.

<sup>14</sup>Center for Synthetic Biochemistry, Institute for Synthetic Biology, Shenzhen Institutes of Advanced Technologies, Shenzhen 518055, China.

<sup>15</sup>Novo Nordisk Foundation Center for Biosustainability, Technical University of Denmark, Lyngby, Denmark.

✉ e-mail: [keasling@berkeley.edu](mailto:keasling@berkeley.edu)

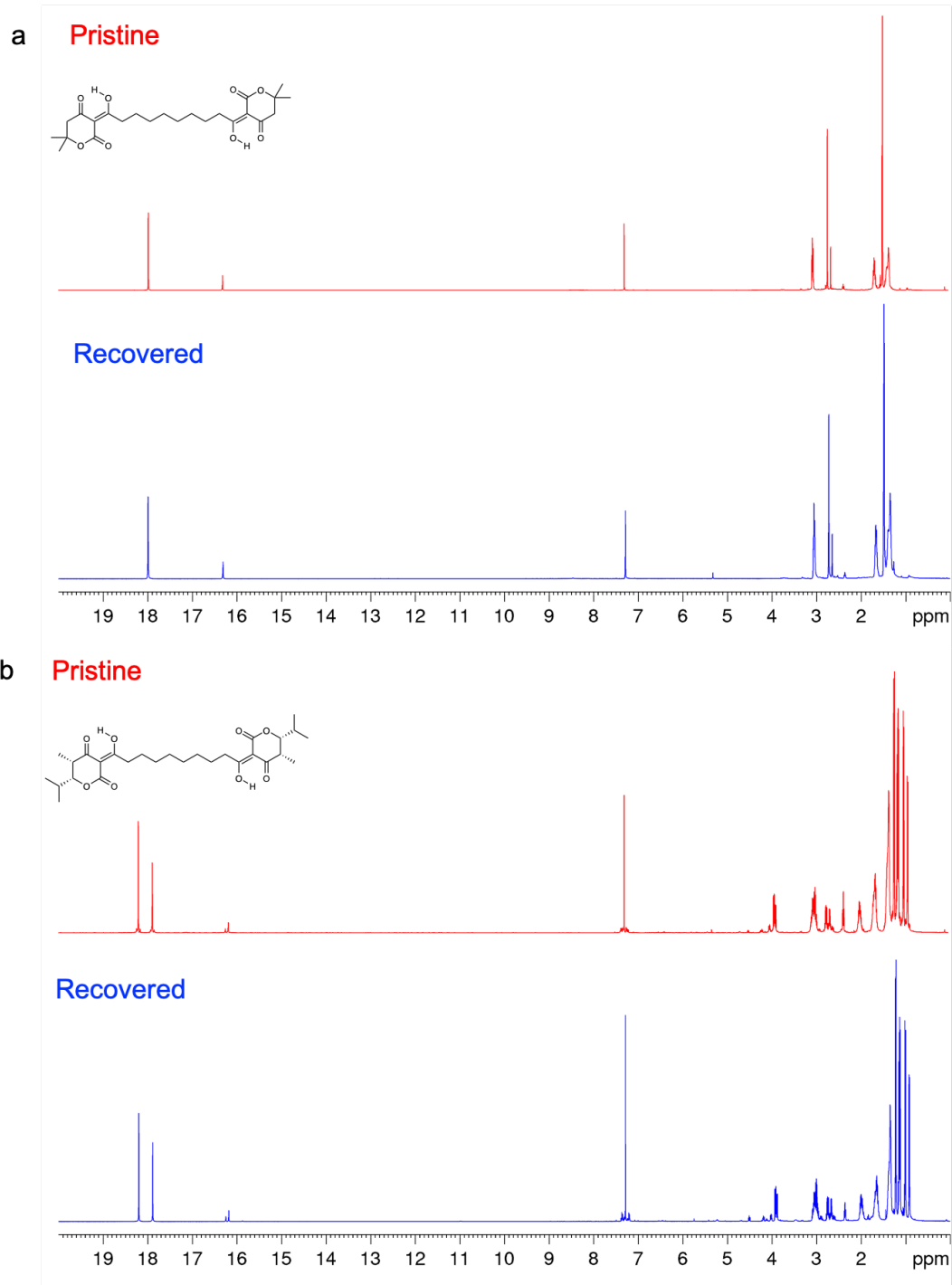
\*Present address: The Dow Chemical Company, Collegeville, PA 19426, USA.

†Present address: School of Food and Biological Engineering, Jiangsu University, 301 Xuefu Road, Zhenjiang, Jiangsu 212013, China.

‡Present address: State Key Laboratory of Biology of Plant Diseases and Insect Pests, Institute of Plant Protection, Chinese Academy of Agricultural Sciences, 2 Yuanmingyuan West Road, Beijing 100193, China.

¶Present address: Amazon.com, Inc, 410 Terry Ave N, Seattle, WA 98109, USA.

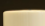
§Present address: Department of Chemical and Biomolecular Engineering, University of Illinois Urbana-Champaign




**Supplementary Fig. 1.**  $^1\text{H}$  NMR of original (pristine) triketone monomers and recovered from depolymerized PDKs: (a) *b*-TK 1 monomer and (b) *b*-TK 2 monomer (*top*).




The image shows three glass vials with white caps, each containing a yellow liquid. The vials are arranged side-by-side. The first vial on the left shows a clear yellow liquid. The middle vial shows a slightly darker yellow liquid. The vial on the right shows a very dark, almost black, liquid, indicating a significant color change upon the addition of Hg<sup>2+</sup>.



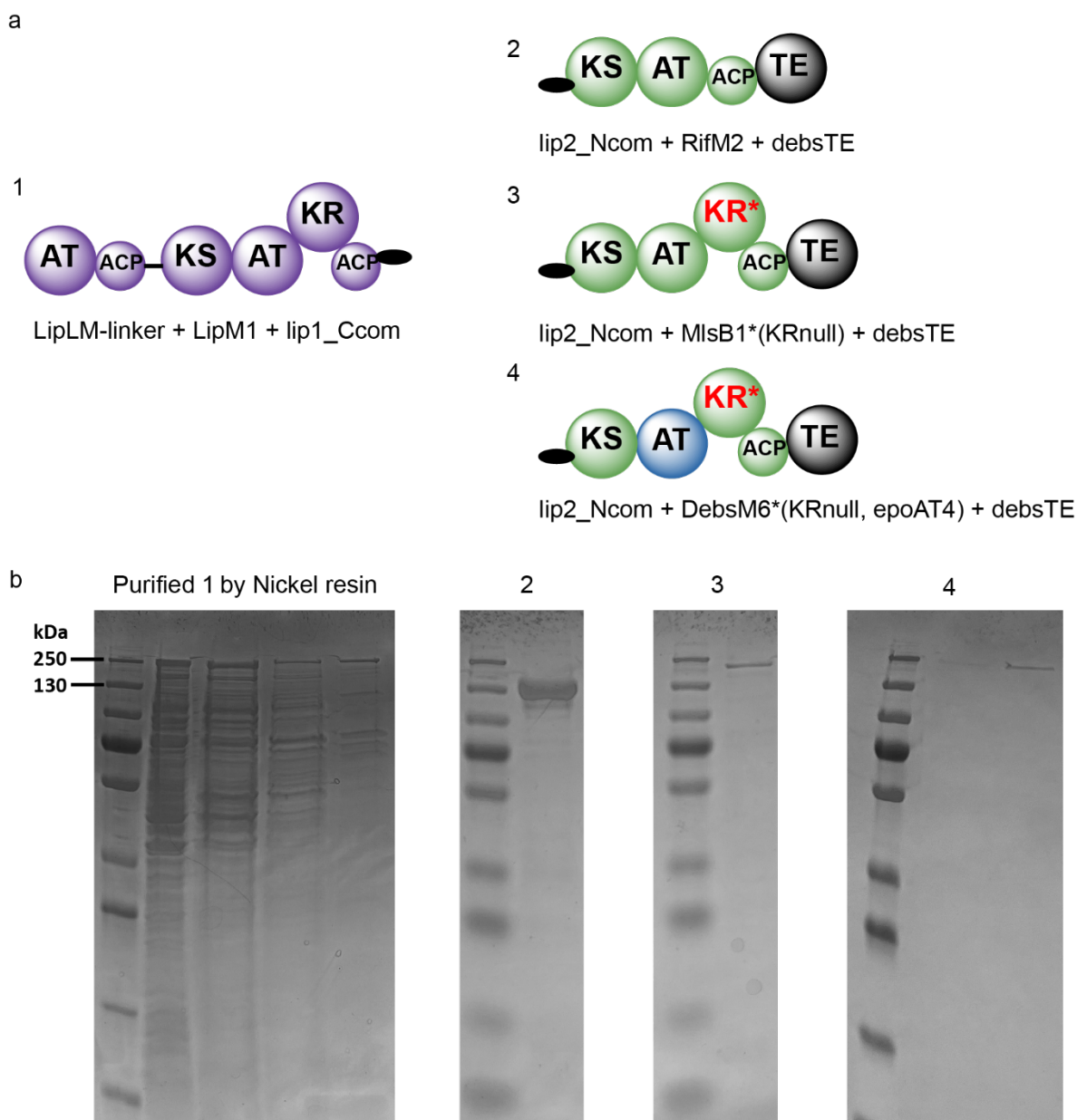
Three glass vials with white caps are shown side-by-side, each containing a clear liquid and a yellow, irregularly shaped polymer film. The film in the leftmost vial is the largest and most intact. The film in the middle vial is smaller and more fragmented. The film in the rightmost vial is the smallest and most fragmented, indicating significant degradation over time.



Three glass vials containing a yellow liquid. The middle vial shows a distinct yellow band at the interface between the two liquid layers, indicating a color change due to the addition of the polymer.

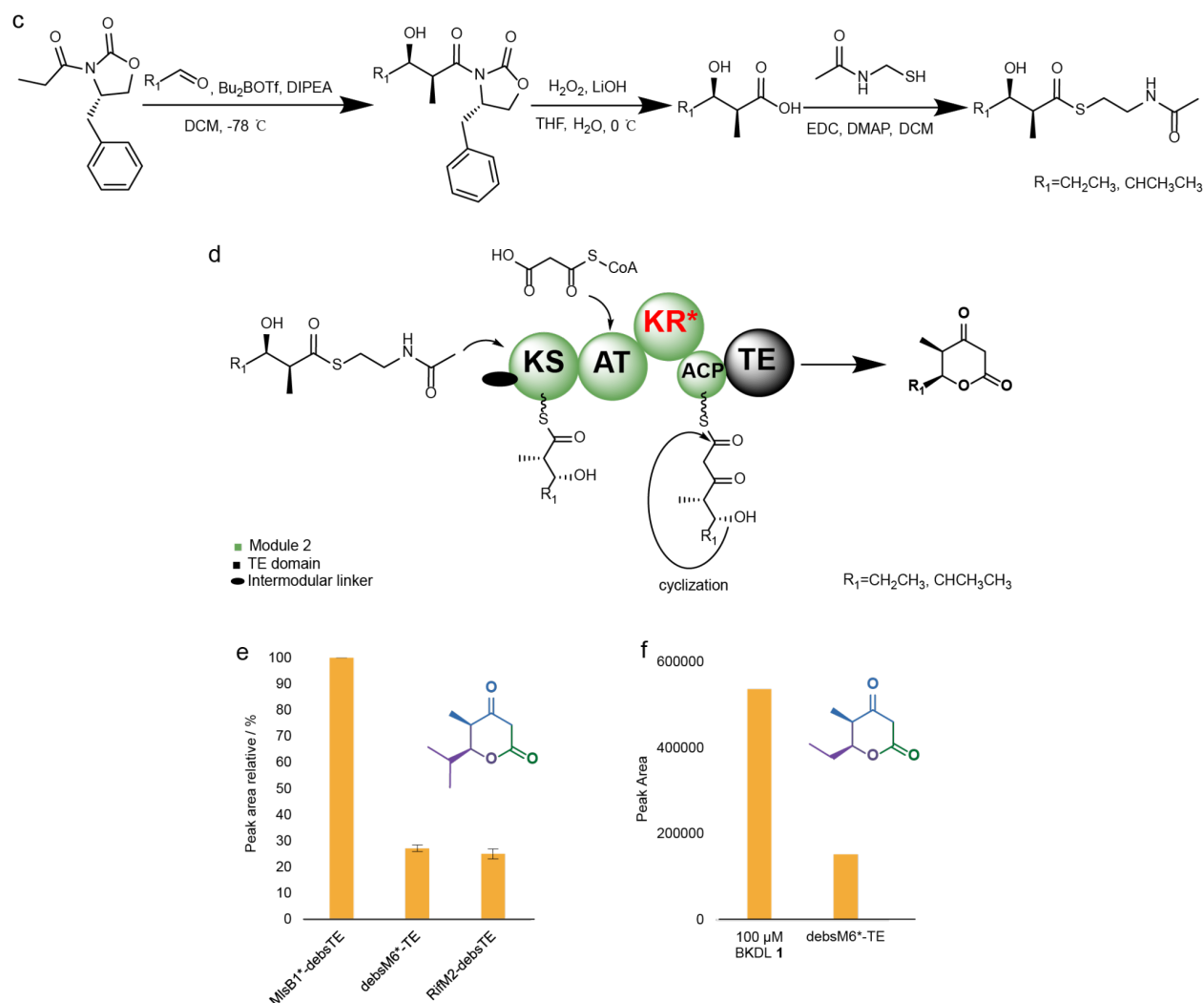


3

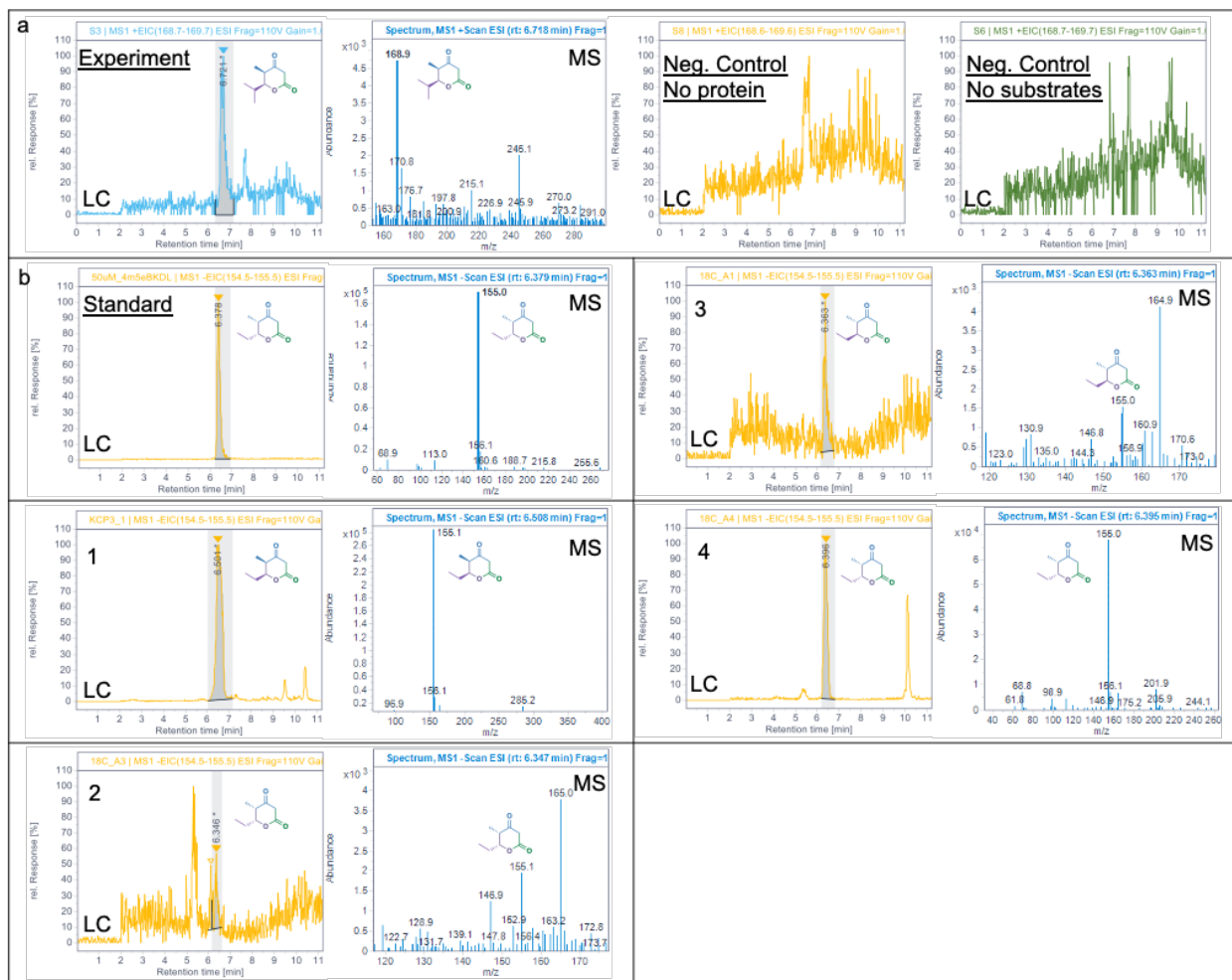


**Supplementary Fig. 3. Purification and *in vitro* assays of PKSs.** a) Architectures of Module 1 and Module 2s. b) Purified Module 1 and Module 2s. Purification of Module 1 by nickel resin is specifically shown. In purified 1, lanes from left to right are the samples in buffers with 5 mM, 10 mM, 20 mM and 200 mM imidazole. The top bands are the target proteins. In purified 2–4, only samples in the buffer with 200 mM imidazole are shown.

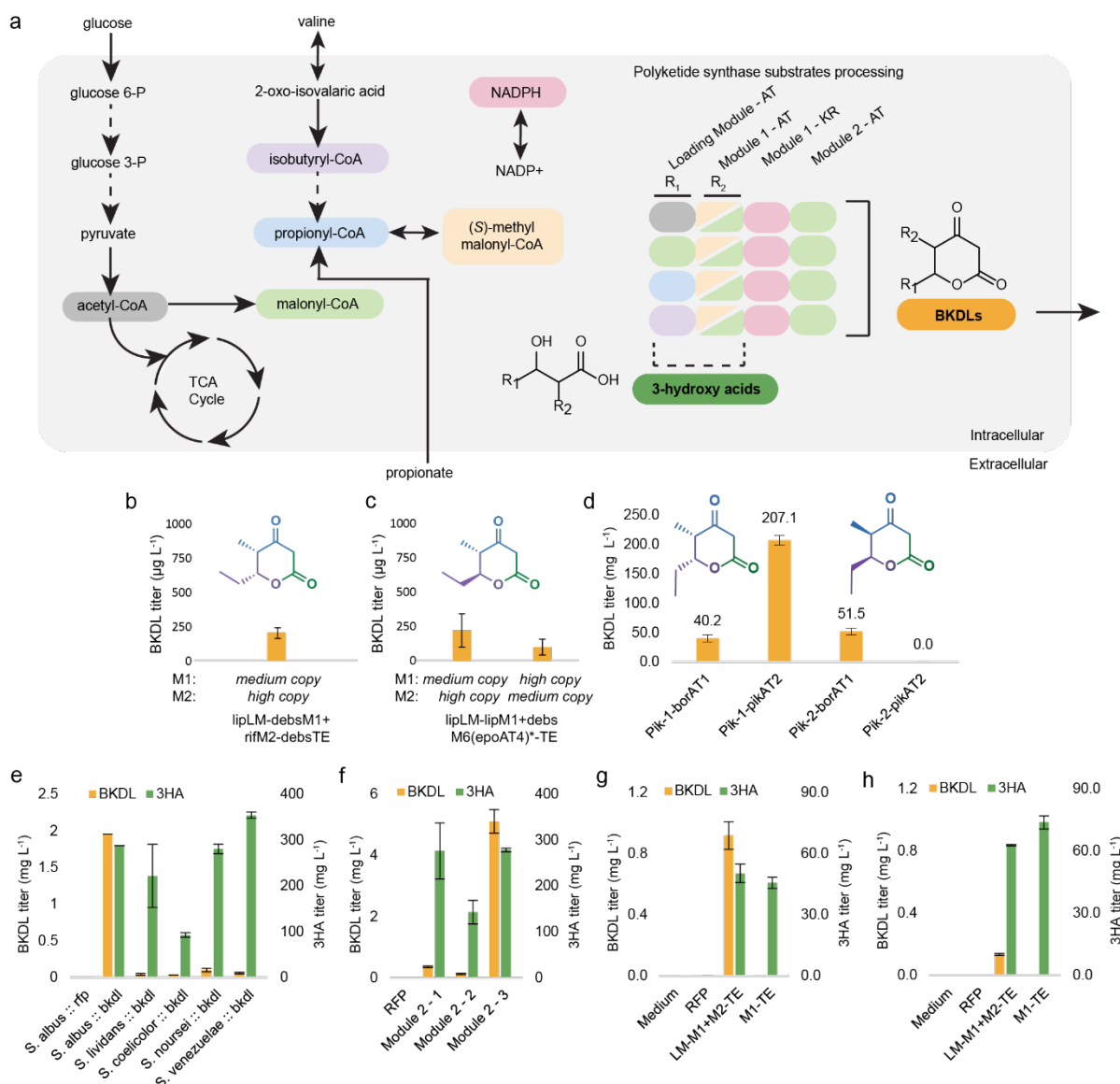




**Supplementary Fig. 3. Purification and *in vitro* assays of PKSs.** c) General synthetic pathway of 3-hydroxy alkyl thiolates (SNACs). d) *In vitro* enzymatic reaction of BKDL formation with SNACs substrate loaded in KS domain of PKS. The elongation of the polyketide is the same as the natural pathway. e) *In vitro* production of BKDL 4 using 3-hydroxy alkyl thiolates ( $R_1 = \text{CHCH}_3\text{CH}_3$ ) and various second extension modules (2–4 in (a)). f) *In vitro* production of BKDL 1 using 3-hydroxy alkyl thiolates ( $R_1 = \text{CH}_2\text{CH}_3$ ) and the second extension module (3 in (a)).

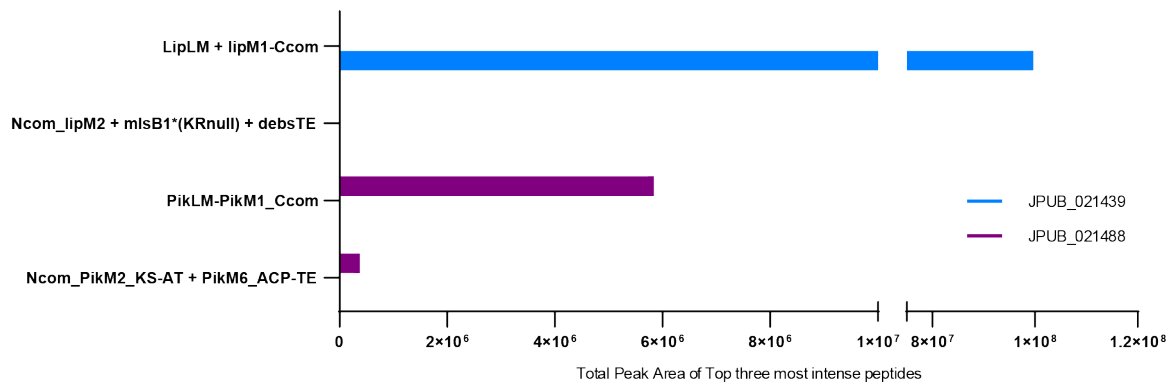


**Supplementary Fig. 4. BKDL identification by LC-MS of the *in vitro* reaction and *in vivo* production in *E. coli* K207-3.** a) LC-MS result of *in vitro* experiments for the production of BKDL 4. No product was detected in the negative controls. b) *In vivo* BKDL production in *E. coli* K207-3. 3  $\mu$ L 50  $\mu$ M standard solution or sample was injected in LC-MS. 1–4 were produced by Module 1 with Module 2 as (1) LipLM + DebsM1 + mlsA8\_Ccom with mlsA9\_Ncom + RifM2 + debsTE (JPUB\_021437), (2) LipLM + LipM1 + lip1\_Ccom with lip2\_Ncom + debsM6(epoAT4)\_KRnull + debsTE (JPUB\_021447), (3) PikLM + PikM1 + pikM5\_Ccom with pikM6\_Ncom + pikKS2-borAT-pikACP6 + pikTE (JPUB\_021467), (4) PikLM + pikM5(pikKS1) + pikM5\_Ccom with pikM6\_Ncom + pikKS2-borAT1-pikACP6 + pikTE (JPUB\_021479), respectively. See Supplementary Table 9 for the details of mass-to-charge.

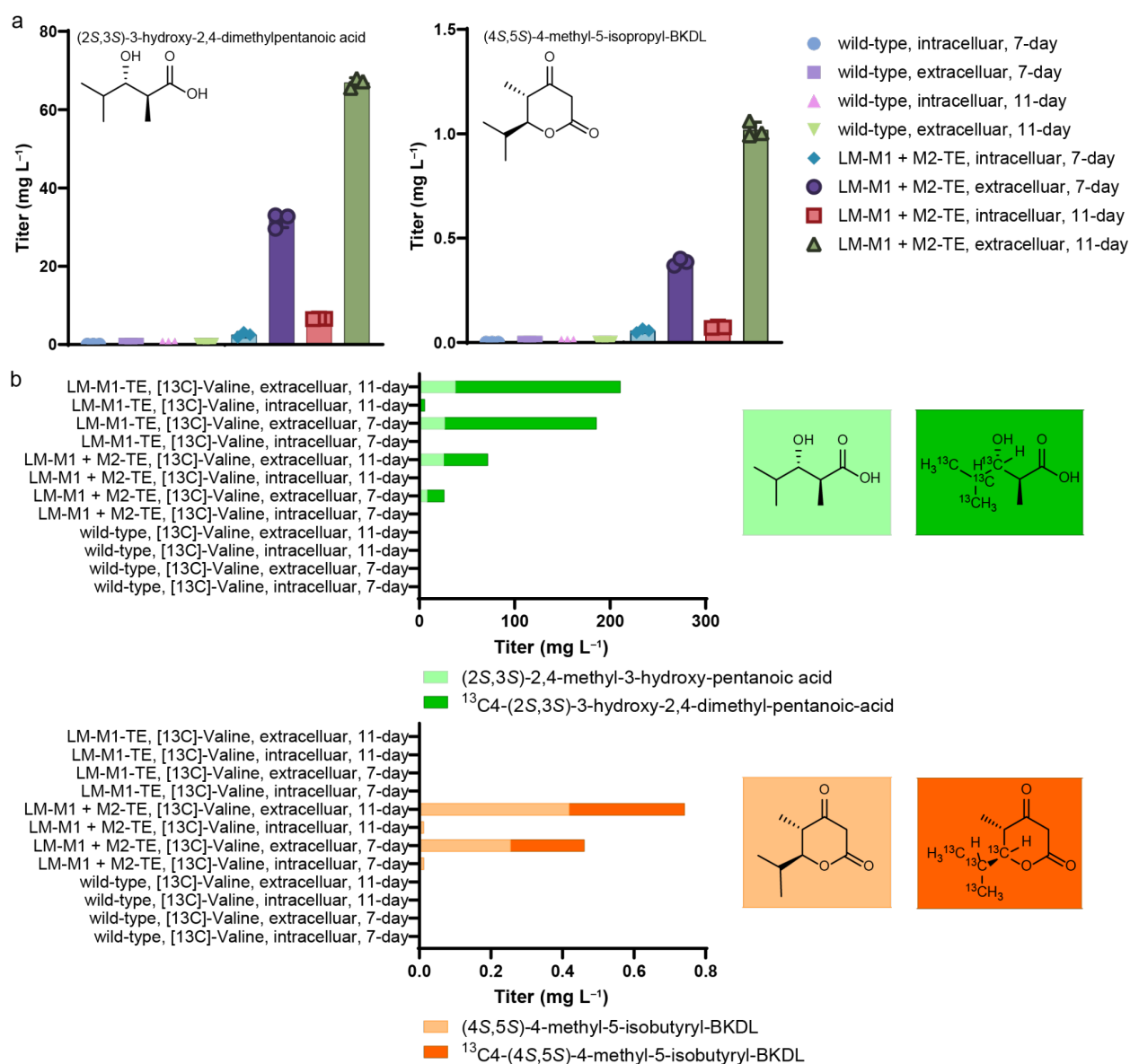


**Supplementary Fig. 5. Production and diversification of BKDLs.** a) The metabolic pathway of BKDL biosynthesis in *Streptomyces*. The key CoA substrates used by the PKS modules are highlighted with colored backgrounds in the left of the figure. The colors of the acyl-CoA intermediates correspond to the color of the PKS modules. Substitutions at R<sub>1</sub> and R<sub>2</sub> positions are determined by the incorporated substrates in the polyketide chain elongation. Specifically, R<sub>1</sub> is the chemical group linked to the acyl-CoA processed by the Loading Module, and R<sub>2</sub> is the chemical group linked to the β position of the malonyl-CoA processed by the AT domain in the Module 1. b–c) *In vivo* production by *E. coli* K207-3 of BKDLs with different stereochemistry at the δ carbon in the lactone ring. d) *E. coli* K207-3 production of BKDL with malonyl-AT-swapped Pik PKSs. Pik-1 is referred to as Pik127. Pik-2 refers to Pik167. Pik-1-borAT1 or pikAT2 produced BKDL 2 and Pik-2-borAT1 or pikAT2 produced BKDL 1. e) Selection of *Streptomyces* species with *bkdL* genes integrated into their genomes. 3-Hydroxy acid (3HA) and BKDL production are measured to demonstrate the capability of BKDL biosynthesis. f) BKDL production by three selected module 2s with LipLM-lipM1 as module 1. g–h) High throughput screen of BKDL production in 24- or 96-well plates. g) Production of BKDLs and 3HAs at 30 °C in 96 well plates with 0.5 mL cell cultures, one 4.5 mm sterile glass bead, 50 % humidity, and water compensation every two days.

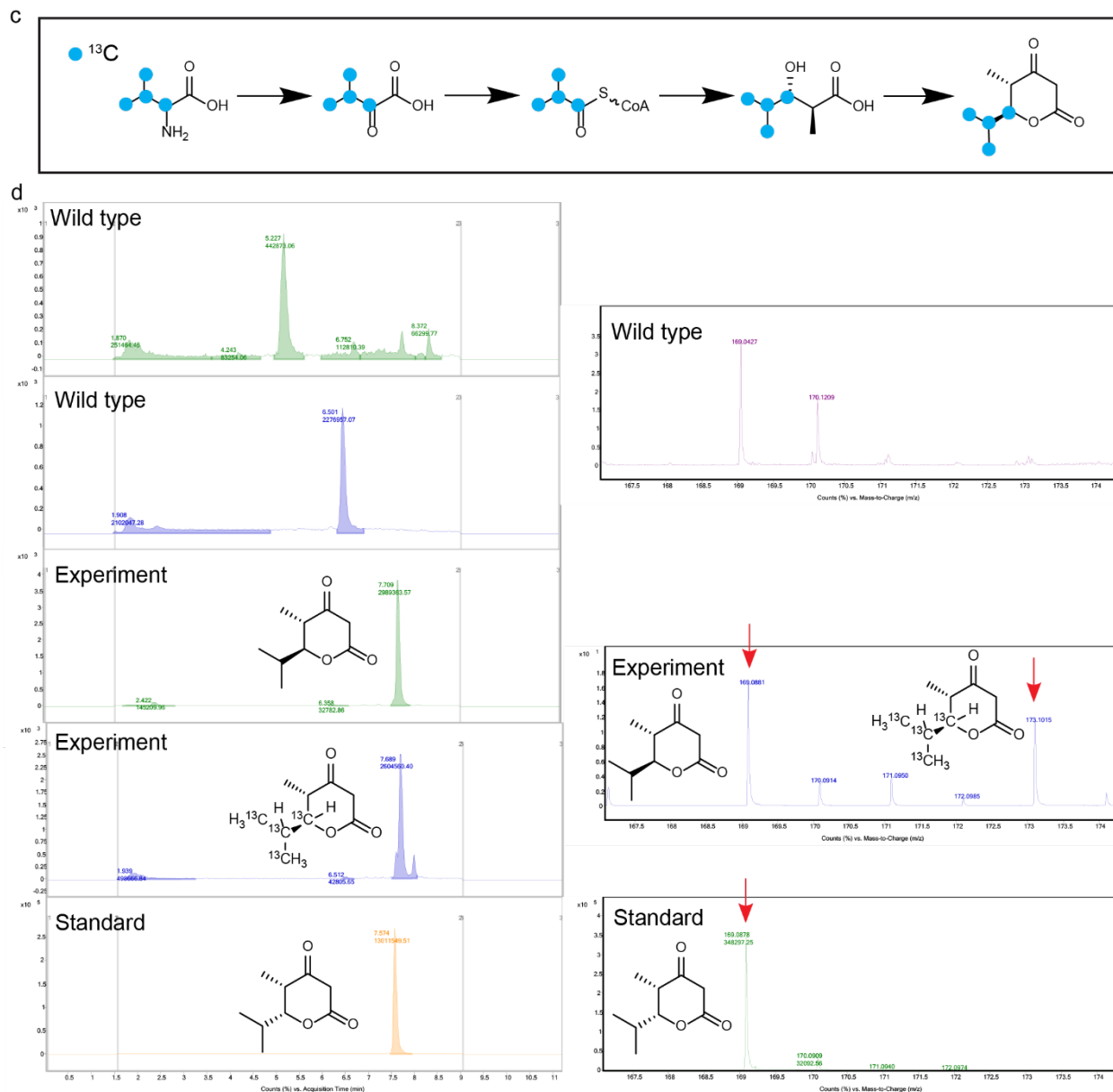
h) Production of BKDLs and 3HAs at 30 °C in 24 well plates with 2 mL cell cultures, two sterile glass beads, 70% humidity. All productions were quantified by LC-MS with chemically synthesized standards.

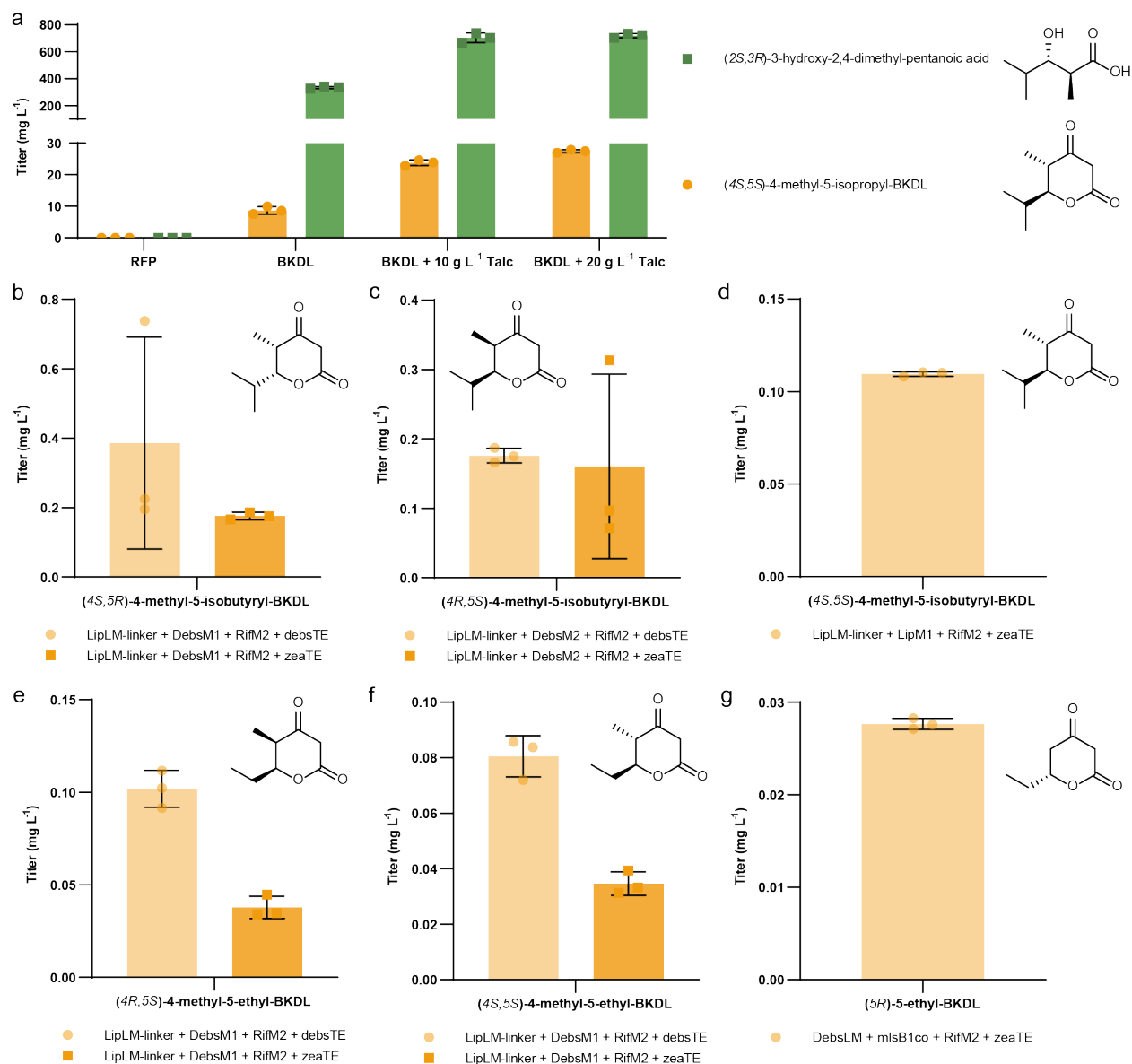


**Supplementary Fig. 6. Proteomics analysis of module 1 and module 2 expression in *S. albus* J1074 strains grown in shake flasks.**



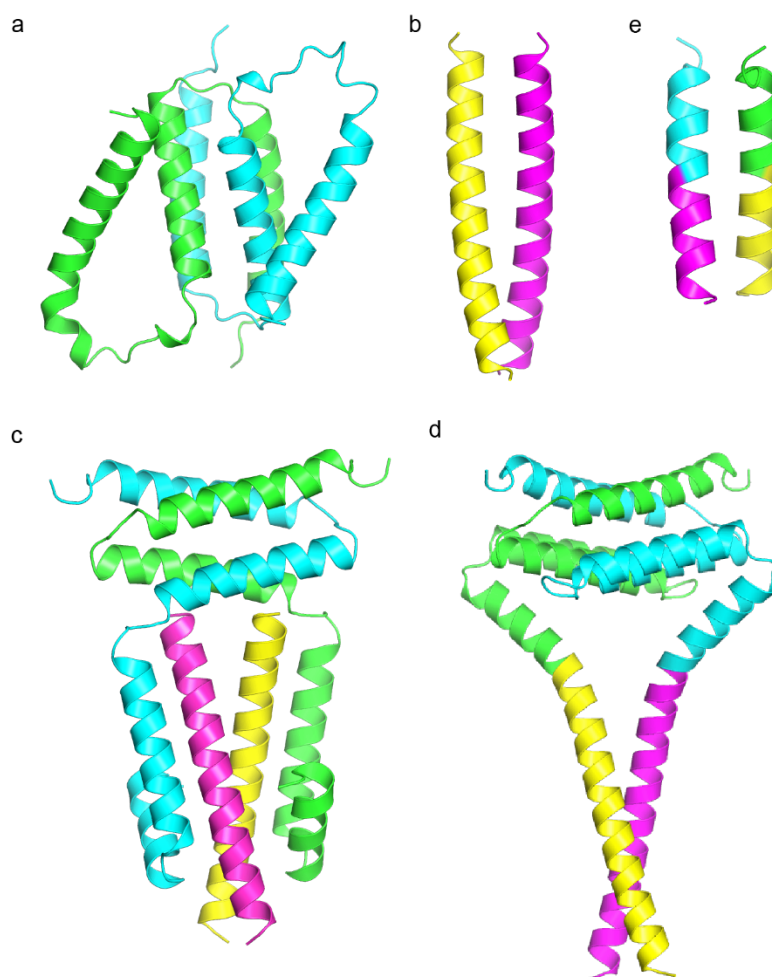
**Supplementary Fig. 7. Confirmation of BKDL production by *S. albus* J1074 using <sup>13</sup>C labeling.** a) Quantification of intracellular and extracellular production of 3-hydroxy acid and BKDL. Cultures were grown in the 250 mL baffled flask with 30 mL R5 medium supplemented with L-valine, incubated at 30 °C. b) Demonstration of 3-hydroxy acid and BKDL production with <sup>13</sup>C-L-valine supplemented into the medium. Cultures were grown in 250-mL baffled flasks with 30 mL R5 medium supplemented with <sup>13</sup>C-L-valine, incubated at 30 °C. 3 µL supernatant or cell pellets after lysis by acetonitrile were analyzed by LC-MS. Chemically synthesized 3-hydroxy acid and BKDL were used to construct the standard curves. Wild type is *S. albus* J1074. LM-M1 is LipLM-lipM1-lip1\_Ccom. M2-TE is lip2\_Ncom-MIsB1\*(KRnull)-debsTE. The strain is JPUB\_021439. LM-M1-TE is LipLM-lipM1-debsTE (JPUB\_010343). LM-M1 and LM-M1-TE were integrated at  $\Phi C31$  integration site in the genome. M2-TE was integrated at the VWB integration site in the genome.



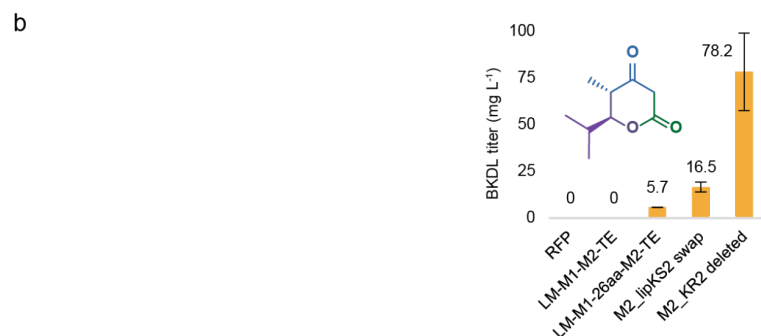
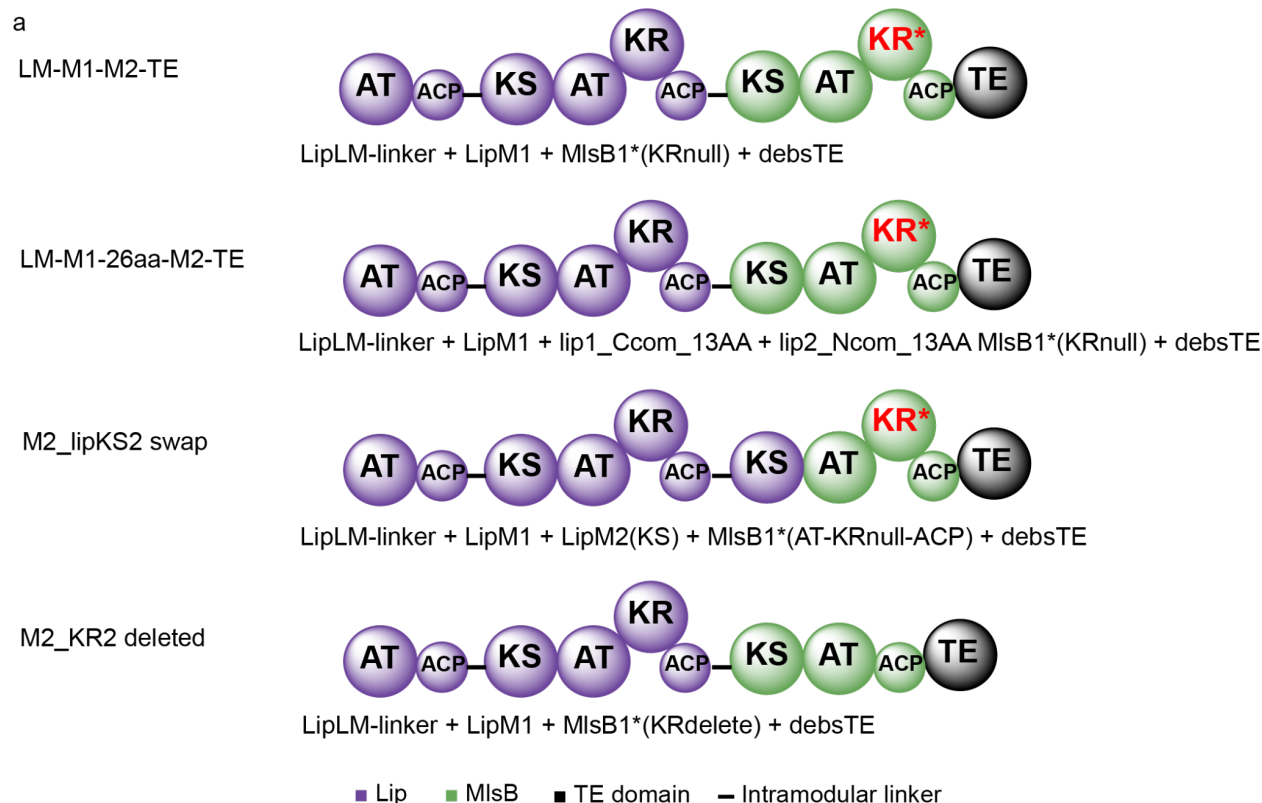


**Supplementary Fig. 8. Diversified BKDLs produced from *S. albus* J1074.** a) Optimization of BKDL 6 titers using *S. albus* J1074 (JPUB\_021439) grown with microparticles in shake flasks. 10 g L<sup>-1</sup> or 20 g L<sup>-1</sup> Talc, hydrated magnesium silicate, was added at the beginning of the production run to break the cell clump. Production was performed in 250 mL shake flasks with 30 mL R5 medium for 7 days. b–g) 96-well plate cell growth was incubated at 30 °C for 4 days, 200 rpm, with one 4.5 mm sterile glass bead in 0.5 mL R5 medium. Negative control was *S. albus* J1074 with RFP integrated at the same integration site (JPUB\_021445), without detection of any BKDL products. Supernatants were analyzed using LC-MS and compared with the standards. The chemical standards were made at 12.5, 25 and 50 µM to generate the standard curves. All experiments have three biological replicates.

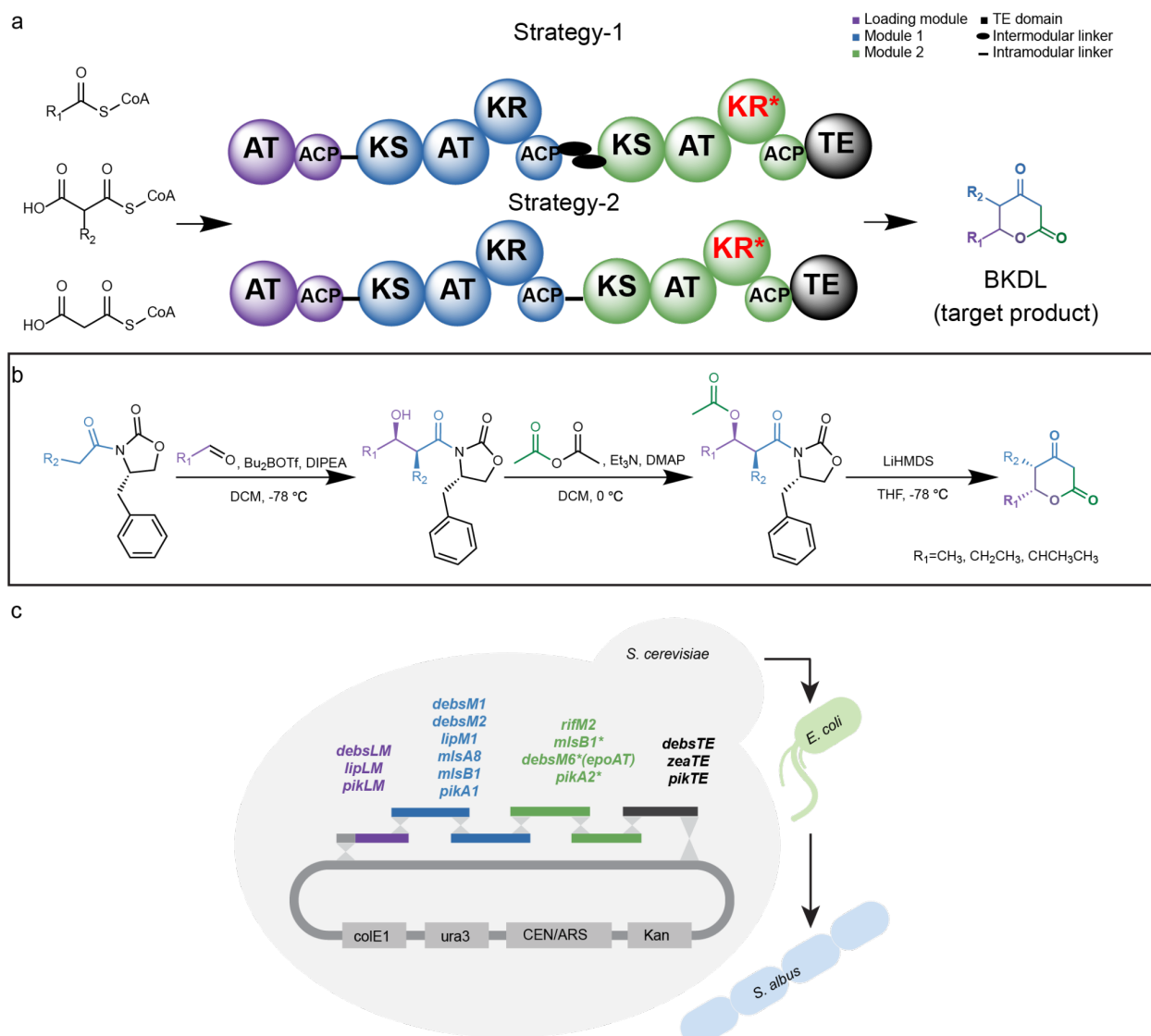




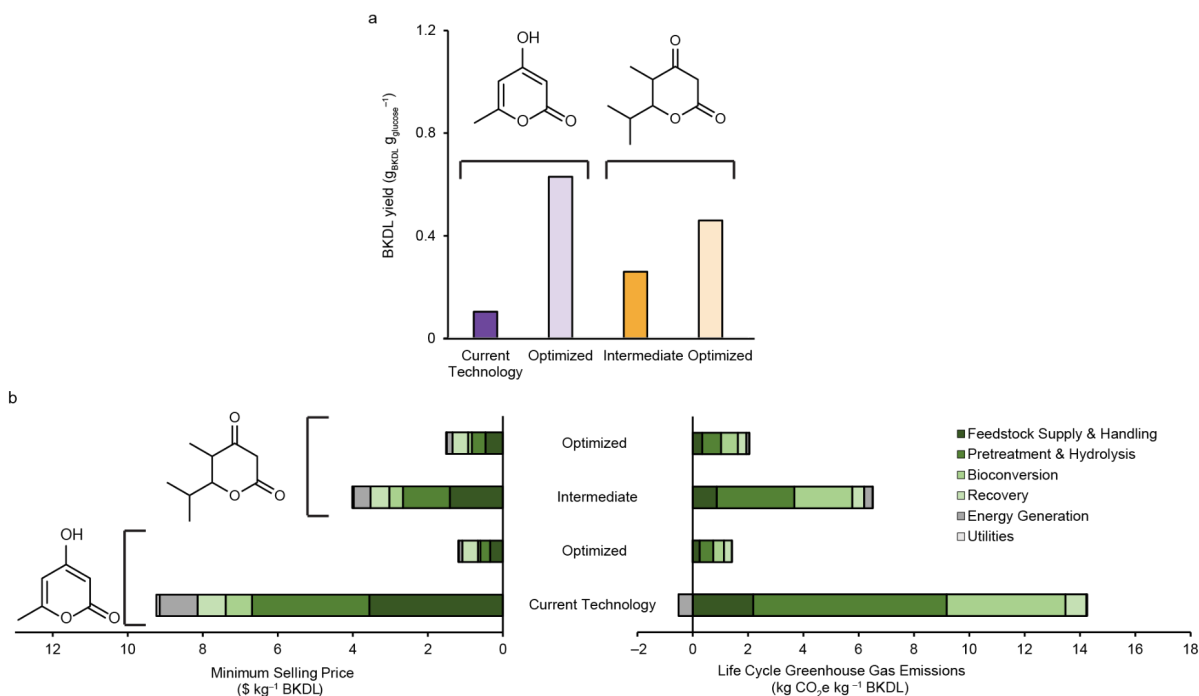
**Supplementary Fig. 9. Alpha-fold predicted structures of intermodular docking domains between Lip PKS module 1 and module 2.** a) The C-terminal docking domain of Module 1, lip1\_Ccom. b) The N-terminal docking domain of Module 2, lip2\_Ncom. c) The natural structure of unfused docking domains. d) The structure of fused docking domains, lip1\_Ccom-lip2\_Ncom. e) The structure of fused truncated docking domain, lip1\_Ccom\_13AA-lip2\_Ncom\_13AA. Green and cyan represent the lip1\_Ccom. Yellow and magenta represent the lip2\_Ncom. AA is the abbreviation of amino acids.



**Supplementary Fig. 10. Fused PKSs for BKDL production.** a) Module 1 and module 2 were fused in two different ways, Fusion 1 and Fusion 2. In Fusion 1, the intermodular docking domains were fused keeping all amino acids, while Fusion 2 only keeps 13 amino acid residues from each pair of docking domains. b) Production of BKDL 6 by the fused Module 1 and Module 2. LM, LipLM. M1, lipM1. M2, mlsB1\*. TE, debstsTE. lipKS2 swap and KR2 deletion were abbreviated with M2\_lipKS swap and M2\_KR2 deleted. The strains from left to right are JPUB\_021445, JPUB\_021510, JPUB\_021513, JPUB\_021515 and JPUB\_021511.

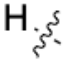
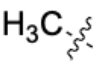
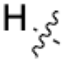
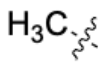
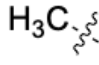
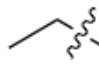
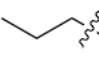
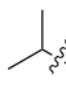
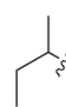
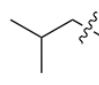
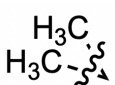


**Supplementary Fig. 11. Recombination of PKSs for making BKDLs.** a) Two strategies of PKS recombination. Strategy-1 uses two separate PKSs collaborated through the docking domain. Strategy-2 uses one fused PKS with an artificial linker. b) The chemical synthesis pathway for BKDLs. c) The hybrid PKS was assembled in *S. cerevisiae* using its native homologous recombination system. The sequence-verified *bkdL* genes were then tested in *E. coli* and *S. albus*. Abbreviations: KS, ketosynthase; AT, acyltransferase; KR, ketoreductase; KR\*, inactive ketoreductase; ACP, acyl carrier protein; TE, thioesterase.

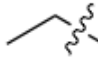
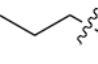
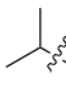
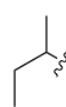
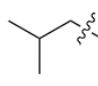


**Supplementary Fig. 12. Systems analysis of the bio production of BKDL including prior work on bioTAL.** a) Annual bio production and yield of the TAL and BKDL under the different scenarios, adjusting for factors such as the product yield and projected efficiencies gained at industrial scale. b) Minimum selling price (MSP) and Life cycle GHG emissions contributions for bio production of TAL and BKDL across all four scenarios considered in this study. The optimized and current technology results from the production of bioTAL are from Demartea et al., 2022<sup>1</sup>.

**Supplementary Table 1. Calculated free energy barrier of hydrolysis for BKDL-based diketoenamines.**

	$\Delta G^\ddagger$ ( $\text{kJ mol}^{-1}$ )			
	trans		cis	
				
	121.4458082	118.1867692	121.4459644	115.6604326
	124.5108437	122.1569145	125.4859302	121.9092489
	122.7122354	126.3847792	121.1720474	123.2852058
	121.527017	120.4446273	121.5268373	121.5200837
	120.2447452	123.5308746	120.2449983	122.8511114
	122.3506736	121.0832229	122.3102172	119.9634309
	achiral			
	124.0326794			

**Supplementary Table 2. Calculated solvation free energy for BKDL-based diketoenamines.**

	$\Delta G \text{ (kJ mol}^{-1}\text{)}$			
	trans		cis	
	$\text{H} \begin{array}{c} \diagup \\ \diagdown \end{array}$	$\text{H}_3\text{C} \begin{array}{c} \diagup \\ \diagdown \end{array}$	$\text{H} \begin{array}{c} \diagup \\ \diagdown \end{array}$	$\text{H}_3\text{C} \begin{array}{c} \diagup \\ \diagdown \end{array}$
$\text{H}_3\text{C} \begin{array}{c} \diagup \\ \diagdown \end{array}$	-712.46794	-699.58624	-712.47189	-697.90077
	-709.04905	-697.13436	-710.03033	-698.49535
	-703.06358	-697.47339	-700.92954	-693.72176
	-700.86134	-690.59286	-700.86117	-692.72131
	-696.30496	-690.99711	-696.3045	-692.37259
	-696.53537	-686.52061	-696.48068	-685.68097
	achiral			
$\begin{array}{c} \text{H}_3\text{C} \\ \text{H}_3\text{C} \end{array} \begin{array}{c} \diagup \\ \diagdown \end{array}$	-702.13711			

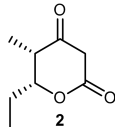
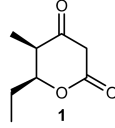
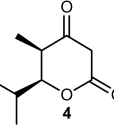
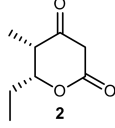
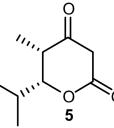
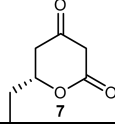
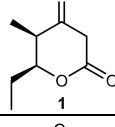
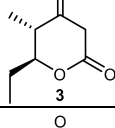
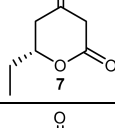
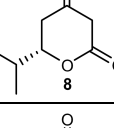
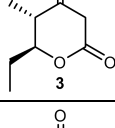
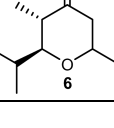
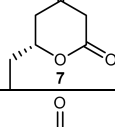
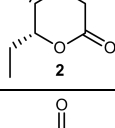
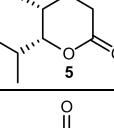
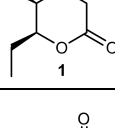
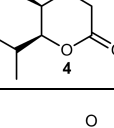
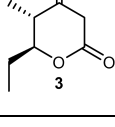
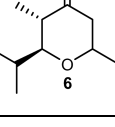
**Supplementary Table 3. Base plasmids and strains used in this study.**

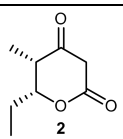
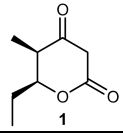
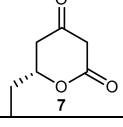
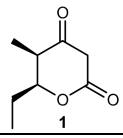
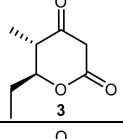
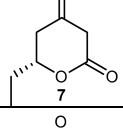
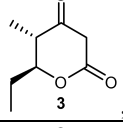
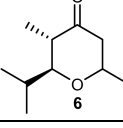
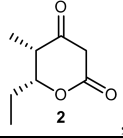
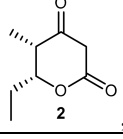
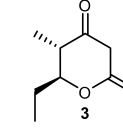
Name	Description	Source/reference
<b>Plasmids</b>		
FICUS (JBx_098142)	Yeast assembly backbone	This study
pET-28a (+)	Protein expression vector	This study
pBbA5a	Cloning vector, high copy	This study
pBbE5k	Cloning vector, high copy	This study
pBbS5k	Cloning vector, high copy	This study
pJH020	Cloning vector, high copy	This study
p21 (JPUB_009893)	mCherry gene under gapdh promoter from <i>E. lenta</i> , ΦC31 attP and integrase, apramycin resistance	This study
pVWB	mCherry gene under gapdh promoter from <i>E. lenta</i> , VWB attP and integrase, spectinomycin resistance	This study
<b>Strains</b>		
<i>E. coli</i>		
DH5α	Cloning host	NEB
BL21(DE3)	Protein expression host	NEB
ET12567/pUZ8002	Donor strain for biparental conjugation between <i>E. coli</i> and <i>Streptomyces</i>	This study
ET12567/pUB307	Donor strain for triparental conjugation between <i>E. coli</i> and <i>Streptomyces</i>	This study
<i>S. albus</i>		
J1074	Wild type host strain	ATCC
<i>S. lividans</i>		
TK24	Wild type host strain	ATCC
<i>S. coelicolor</i>		
M1152	Wild type host strain	ATCC
<i>S. venezuelae</i>		
10712	Wild type host strain	ATCC
<i>S. noursei</i>		
11455	Wild type host strain	ATCC

**Supplementary Table 4. Recombined PKSs used in this study.** Strategy-1 uses two separate PKSs that pair with each other through docking (communication) domains: module 1 has a C-terminal communication domain (Ccom) and module 2 has an N-terminal communication domain (Ncom), which are paired intermodular docking domains found in natural PKSs. LM-linker is the loading module with its downstream intramodular linker, usually 8-20 amino acid residues. Strategy-2 uses a single PKS with module 1 and module 2 fused with a complete intermodular docking domain or a truncated docking domain. For easier cloning, some of the genes were codon optimized, as indicated by the co suffix, to reduce the repeats or high GC contents. PKS abbreviations: lip, lipomycin; mls, mycolactone; rif, rifamycin; debs, 6-deoxyerythronolide B synthase; nat, naphthomycin; blv75, genome-mined gene (GenBank: SEE85242.1); epo, epothilone; pik, pikromycin; bor, borrelidin; zea, zearalenone.

No.	Strategy-1		Target BKDL
	Module 1	Module 2	
01	LipLM-linker + LipM1 + mlsA8co_Ccom	mlsA9_Ncom + RifM2 + debsTE	
02	LipLM-linker + mlsB1co + mlsA8co_Ccom		
03	DebsLM-linker + DebsM1 + mlsA8co_Ccom		
04	LipLM-linker + DebsM2 + mlsA8co_Ccom		
05	LipLM-linker + DebsM1 + mlsA8co_Ccom		
06	DebsLM-linker + mlsB1co + mlsA8co_Ccom		
07	DebsLM-linker + DebsM2 + mlsA8co_Ccom		
08	LipLM-linker + LipM1 + mlsA8co_Ccom	mlsA9_Ncom + RifM2 + zeaTE	
09	LipLM-linker + mlsB1co + mlsA8co_Ccom		



10	DebsLM-linker + DebsM1 + mlsA8co_Ccom		
11	LipLM-linker + DebsM2 + mlsA8co_Ccom		 , 
12	LipLM-linker + DebsM1 + mlsA8co_Ccom		 , 
13	DebsLM-linker + mlsB1co + mlsA8co_Ccom		
14	DebsLM-linker + DebsM2 + mlsA8co_Ccom		
15	DebsLM-linker + LipM1 + ppsB_Ccom	ppsC_Ncom + RifM2 + debsTE	
16	LipLM-linker + mlsB1co + ppsB_Ccom		 , 
17	LipLM-linker + LipM1 + ppsB_Ccom		 , 
18	DebsLM-linker + mlsB1co + ppsB_Ccom		
19	LipLM-linker + DebsM1 + ppsB_Ccom		 , 
20	LipLM-linker + DebsM2 + ppsB_Ccom		 , 
21	LipLM-linker + LipM1 + lip1_Ccom	lip2_Ncom + RifM2 + debsTE	 , 
22		lip2_Ncom + DebsM6*(KRnull, epoAT4) + debsTE	

23		lip2_Ncom + MlsB1*(KRnull) + debsTE	
24		lip2_Ncom + NatM2 + blv75TE	
25	PikLM-linker + PikM1 + pikM5_Ccom	pikM6_Ncom + Pik_KS2-borAT1-pikACP6 + pikTE	
26		pikM6_Ncom + Pik_KS2-AT2-pikACP6 + pikTE	
27	PikLM-linker + Pik_KS1-AT5-KR5-ACP5+ pikM5_Ccom	pikM6_Ncom + PikM6*(borAT1) + pikTE	
28		pikM6_Ncom + PikM6*(pikAT2) + pikTE	
29	PikLM-linker + PikM1*(pikAT2) + pikM5_Ccom	pikM6_Ncom + Pik_KS2-AT2-pikACP6 + pikTE	
<b>Strategy-2</b>			
30	DebsLM-linker + DebsM2 + RifM2 + debsTE		
31	DebsLM-linker + DebsM2 + RifM2 + zeaTE		
32	DebsLM-linker + LipM1 + RifM2 + debsTE		
33	DebsLM-linker + LipM1 + RifM2 + zeaTE		
34	DebsLM-linker + mlsB1co + RifM2 + zeaTE		
35	LipLM-linker + LipM1 + RifM2 + zeaTE		 , 
36	LipLM-linker + DebsM1 + RifM2 + debsTE		
37	LipLM-linker + DebsM1 + RifM2 + zeaTE		
38	LipLM-linker + DebsM2 + RifM2 + debsTE		
39	LipLM-linker + DebsM2 + RifM2 + zeaTE		
40	LipLM-linker + LipM1 + RifM2 + debsTE		
41	LipLM-linker + LipM1 + DebsM6*(KRnull, epoAT4) + debsTE		
42	LipLM-linker + LipM1 + MlsB1*(KRnull) + debsTE		
43	LipLM-linker + LipM1 + MlsB1*(KRdelete) + debsTE		
44	LipLM-linker + LipM1 + lip1_Ccom_13AA + lip2_Ncom_13AA MlsB1*(KRnull) + debsTE		
45	LipLM-linker + LipM1 + LipM2(KS) + MlsB1*(AT-KRnull-ACP) + debsTE		



**Supplementary Table 5. Combinatorial PKSs tested in *E. coli* K207-3.** Strains contain the information of plasmids in <https://public-registry.jbei.org>. PKS abbreviations: lip, lipomycin; mls, mycolactone; rif, rifamycin; debs, 6-deoxyerythronolide B synthase; nat, naphthomycin; blv75, genome-mined gene (GenBank: SEE85242.1); epo, epothilone; pik, pikromycin; bor, borrelidin.

Strain	Vector 1 <sup>a</sup>	Loading Module	Module 1	Ccom	Vector 2 <sup>a</sup>	Ncom	Module 2 <sup>b</sup>	TE	Accession Code
KC1	pBbA5a	lipLM	lipM1	mlsA8	pBbS5k	mlsA9	rifM2	debsTE	JPUB_021430
KC2	pBbA5a	lipLM	mlsB1	mlsA8	pBbS5k	mlsA9	rifM2	debsTE	JPUB_021433
KC3	pBbA5a	lipLM	debsM2	mlsA8	pBbS5k	mlsA9	rifM2	debsTE	JPUB_021435
KC4	pBbA5a	lipLM	debsM1	mlsA8	pBbS5k	mlsA9	rifM2	debsTE	JPUB_021437
KC10	pBbA5a	lipLM	lipM1	lip1	pBbE5k	lip2	debsM6(epoAT4) KRnull	debsTE	JPUB_021447
KC13	pBbA5a	lipLM	lipM1	lip1	pBbE5k	lip2	mlsB1 <sup>c</sup> KRnull	debsTE	JPUB_021450
KC15	pBbA5a	lipLM	lipM1	lip1	pJH0204	lip2	natM2	blv75_TE	JPUB_021452
KC16	pBbE5k	lipLM	lipM1	lip1	pBbA5a	lip2	debsM6(epoAT4) KRnull	debsTE	JPUB_021454
KC18	pBbE5k	lipLM	lipM1	lip1	pBbA5a	lip2	mlsB1 <sup>c</sup> KRnull	debsTE	JPUB_021457
KC19	pBbE5k	lipLM	lipM1	lip1	pBbA5a	lip2	rifM2	debsTE	JPUB_021459
KC20	pBbE5k	lipLM	lipM1	lip1	pBbA5a	lip2	natM2	blv75_TE	JPUB_021461
K207-3 pik167(borAT1)	pCDF	pikLM	pikM5 (pikKS1)	pik5	pET	pik6	pikM6(borAT1)	pikTE	JPUB_021463
KCP2	pBbS5k	pikLM	pikM1	pik5	pBbA5a	pik6	pikKS2-borAT1-pikACP6	pikTE	JPUB_021467
KCP3	pBbS5k	pikLM	pikM1	pik5	pBbA5a	pik6	pikKS2-pikAT2-pikACP6	pikTE	JPUB_021470
KCP5	pBbS5k	pikLM <sup>d</sup>	pikM5 (pikKS1)	pik5	pBbA5a	pik6	pikM6 <sup>e</sup> (borAT1)	pikTE	JPUB_021472
KCP6	pBbS5k	pikLM <sup>d</sup>	pikM5 (pikKS1)	pik5	pBbA5a	pik6	pikM6(borAT1)	pikTE	JPUB_021475
KCP7	pBbS5k	pikLM <sup>d</sup>	pikM5 (pikKS1)	pik5	pBbA5a	pik6	pikM6(borAT1)	pikTE	JPUB_021477
KCP8	pBbS5k	pikLM <sup>d</sup>	pikM5 (pikKS1)	pik5	pBbA5a	pik6	pikM6 <sup>e</sup> (borAT1)	pikTE	JPUB_021479
KCP10	pBbS5k	pikLM	pikM1 (pikAT2)	pik5	pBbA5a	pik6	pikKS2-borAT1-pikACP6	pikTE	JPUB_021481

KCP11	pBbS5k	pikLM	pikM1 (pikA T2)	pik5	pBbA5a	pik6	pikKS2- pikAT2- pikACP6	pikTE	JPUB_0 21483
-------	--------	-------	-----------------------	------	--------	------	-------------------------------	-------	-----------------

Note:

- a. For Biobrick vectors with 'pBb', 'E' means high copy ColE1; 'A' means medium copy p15A; 'S' means low copy SC101; '5' means lacUV5 promoter; 'a' means ampR; 'k' means kanR. pJH0204 is a high copy plasmid with ColE1, kanR and lacUV5 promoter. pCDF is a medium copy plasmid with CloDF13, specR and T7 promoter, while pET is a high copy plasmid with ColE1, kanR and T7 promoter.
- b. Parentheses means swapped domain; 'KRnull' means KR inactivated.
- c. Wild-type gene. Otherwise, genes are codon optimized, except genes encoding pikromycin modules which are wild-type.
- d. With G518V mutation.
- e. With H320R mutation.

**Supplementary Table 6. Combinatorial PKSs tested in *Streptomyces*.** Strains contain the information of integrated genes and conjugation plasmids in <https://public-registry.jbei.org>. PKS abbreviations: lip, lipomycin; mls, mycolactone; rif, rifamycin; debs, 6-deoxyerythronolide B synthase; epo, epothilone; pik, pikromycin; bor, borrelidin; zea, zearalenone.

Strain	Integr ation site	Gene 1	Integr ation site	Gene 2	Accessio n Code
<i>S. albus</i>	ΦC31	RFP			JPUB_02 1445
<i>S. albus</i>	ΦC31	LipLM-lipM1 + debsTE			JPUB_01 0343
<i>S. albus</i>	ΦC31	LipLM + LipM1 + lip1_Ccom	VWB	lip2_Ncom + RifM2 + debsTE	JPUB_02 1484
<i>S. albus</i>	ΦC31		VWB	lip2_Ncom + DebsM6*(KRnull, epoAT4) + debsTE	JPUB_02 1486
<i>S. albus</i>	ΦC31		VWB	lip2_Ncom + MlsB1*(KRnull) + debsTE	JPUB_02 1439
<i>S. lividans</i>	ΦC31		VWB		JPUB_02 1441
<i>S. coelicolor</i>	ΦC31		VWB		JPUB_02 1442
<i>S. venezuelae</i>	ΦC31		VWB		JPUB_02 1444
<i>S. noursei</i>	ΦC31		VWB		JPUB_02 1443
<i>S. albus</i>	ΦC31	PikLM-PikM1_Ccom	TG1	Ncom_PikM2_KS-AT + PikM6_ACP-TE	JPUB_02 1488
<i>S. albus</i>	ΦC31				
<i>S. albus</i>	ΦC31	DebsLM + DebsM2 + RifM2 + debsTE			JPUB_02 1491
<i>S. albus</i>	ΦC31	DebsLM + DebsM2 + RifM2 + zeaTE			JPUB_02 1509
<i>S. albus</i>	ΦC31	DebsLM + LipM1 + RifM2 + debsTE			JPUB_02 1499
<i>S. albus</i>	ΦC31	DebsLM + LipM1 + RifM2 + zeaTE			JPUB_02 1501
<i>S. albus</i>	ΦC31	DebsLM + mlsB1co + RifM2 + zeaTE			JPUB_02 1507
<i>S. albus</i>	ΦC31	LipLM + LipM1 + RifM2 + zeaTE			JPUB_02 1493
<i>S. albus</i>	ΦC31	LipLM + DebsM1 + RifM2 + debsTE			JPUB_02 1495
<i>S. albus</i>	ΦC31	LipLM + DebsM1 + RifM2 + zeaTE			JPUB_02 1497
<i>S. albus</i>	ΦC31	LipLM + DebsM2 + RifM2 + debsTE			JPUB_02 1503

<i>S. albus</i>	ΦC31	LipLM + DebsM2 + RifM2 + zeaTE	JPUB_02 1505
<i>S. albus</i>	ΦC31	LipLM + LipM1 + MlsB1*(KRnull) + debsTE	JPUB_02 1510
<i>S. albus</i>	ΦC31	LipLM + LipM1 + MlsB1*(KRdelete) + debsTE	JPUB_02 1511
<i>S. albus</i>	ΦC31	LipLM + LipM1 + lip1_Ccom_13AA + lip2_Ncom_13AA MlsB1*(KRnull) + debsTE	JPUB_02 1513
<i>S. albus</i>	ΦC31	LipLM + LipM1 + LipM2(KS) + MlsB1*(AT-KRnull-ACP) + debsTE	JPUB_02 1515

**Supplementary Table 7. Media used in this study.**

Medium	Composition	Source
LB		Sigma-Aldrich, L2542
TSB		EMD Millipore, 1.00525.5007
LB -EZ-Rich	EZ-rich supplemented with 10 g L <sup>-1</sup> tryptone, 5 g L <sup>-1</sup> yeast extract, 5 mM calcium pantothenate and 20 g L <sup>-1</sup> glycerol and replacement of 1.32 mM K <sub>2</sub> HPO <sub>4</sub> to 2.8 mM Na <sub>2</sub> HPO <sub>4</sub> .	This study
R5	103 g L <sup>-1</sup> sucrose, 0.25 g L <sup>-1</sup> K <sub>2</sub> SO <sub>4</sub> , 10.12 g L <sup>-1</sup> MgCl <sub>2</sub> ·6H <sub>2</sub> O, 10 g L <sup>-1</sup> glucose, 0.1 g L <sup>-1</sup> casamino acids, 5 g L <sup>-1</sup> yeast extract, 5.73 g L <sup>-1</sup> TES (pH 7.2), 0.08 mg L <sup>-1</sup> ZnCl <sub>2</sub> , 0.4 mg L <sup>-1</sup> FeCl <sub>3</sub> ·6H <sub>2</sub> O, 0.02 mg L <sup>-1</sup> CuCl <sub>2</sub> ·2H <sub>2</sub> O, 0.02 mg L <sup>-1</sup> MnCl <sub>2</sub> ·4H <sub>2</sub> O, 0.02 mg L <sup>-1</sup> Na <sub>2</sub> B <sub>4</sub> O <sub>7</sub> ·10H <sub>2</sub> O, 0.02 mg L <sup>-1</sup> (NH <sub>4</sub> ) <sub>6</sub> Mo <sub>7</sub> O <sub>24</sub> ·4H <sub>2</sub> O, and 0.28 g L <sup>-1</sup> NaOH.	This study



**Supplementary Table 8. Primers used in this study.**

Primer	Primer sequence
j5_00001_(RifM2_3)_forward	GCGAGTATCTGAAAGGGGATACGCCATATGGCGGATCTTTCGAAGTTGTCT
j5_00002_(RifM2_3)_reverse	CCAAGGGGTTATGCTAGTTACTCGAGTTATGCGGCCGCAAGCT
j5_00003_(pk21)_forward	TAACTCGAGTAACTAGCATAACCCCTTGG
j5_00004_(pk21)_reverse	CATATGGCGTATCCCCTTTCAGATACTCGC
j5_00005_(RifM2_5)_forward	GCGAGTATCTGAAAGGGGATACGCCATATGACCGCGACACCGGACCG
j5_00006_(RifM2_5)_reverse	CCAAGGGGTTATGCTAGTTACTCGAGTTAACCAGCTTCATTGAAGAAGCTCAAACGCGC
j5_00007_(RifM2_6)_forward	GCGAGTATCTGAAAGGGGATACGCCATATGTCTGAACATCGCGGTAGC
j5_00008_(RifM2_9)_forward	GCGAGTATCTGAAAGGGGATACGCCATATGAGCACTATCGAAGAACGCG
j5_00009_(RifM2_12)_forward	GCGAGTATCTGAAAGGGGATACGCCATATGACACCGAGCATCGGTGGAG
j5_00010_(RifM2_15)_forward	GCGAGTATCTGAAAGGGGATACGCCATATGGTTAGCACCGAGGAAAACCTGCG
gapdh_R_LipLM	CCTGCGCTACCGCGATGTTTCAGACATATGGCGTATCCCCTTTCAGATACTCGCACT
gapdh_R_debsLM	GCTGTTCAGACAACTTCGAAAGATCCGCCATATGGCGTATCCCCTTTCAGATACTCGCACT
gapdh_R_acpP-mlslinker	TTTCTTAACGCGTTCTTCGATAGTGCTCATATGGCGTATCCCCTTTCAGATACTCGCACT
gapdh_R_ppsAmmZ	GCTTCTCCACCGATGCTCGGTGTCATATGGCGTATCCCCTTTCAGATACTCGCACT
gapdh_F_debsTE	CGTTGACAAGCTTGCGGCCGCATAActcgagTAGCCGTTTCGCGCCGCC
gapdh_F_zeaTE	GCGCGTTTGAGTTCTTCAATGAAGCTGGTTAAActcgagTAGCCGTTCGCGCCGCC
2nd-gapdh_F_mlsA8_end	AGGGTGGCCGTGGCGTGAACATAActcgagCGAGACACCCGGGAAGCCTGATCTAC
2nd-gapdh_F_ppsA_Ccom	CTCCCGAGGGCCCTGGGTAAActcgagCGAGACACCCGGGAAGCCTGATCTAC
2nd-gapdh_F_ppsB_Ccom	GCAGAGGCTGCGAGGAACCTGActcgagCGAGACACCCGGGAAGCCTGATCTAC
2nd-gapdh_F_pks12_Ccom	CGGCGTTTCGGAACGACGACGAGTAGctcgagCGAGACACCCGGGAAGCCTGATCTAC
2nd-gapdh_R_mlsA9_Ncom	ACGCAGGTTTCTCTCGGTGCTAACCATATGGCGTATCCCCTTTCAGATACTCGCACT
2nd-gapdh_R_ppsB_Ncom	CGAGATGCGGCTGTACACAGATCGCATATGGCGTATCCCCTTTCAGATACTCGCACT
2nd-gapdh_R_ppsC_Ncom	CGGTCCGGTGTCGCGGTCATATGGCGTATCCCCTTTCAGATACCTCGCACT
2nd-gapdh_R_pks12_Ncom	GGTCGCATGCTGGAGTTGATCAACCATATGGCGTATCCCCTTTCAGATACTCGCACT
2nd-gapdh_F_lip1Ccom	ATACCGAACTGGGCATCTAAAggatccCGAGACACCCGGGAAGCCTGATCTAC
2nd-gapdh_R_lip2Ncom	AGTTTATCGTGGTCAGCCATATGGCGTATCCCCTTTCAGATACTCGCACT
pks12_Ncom_F	ATGGTTGATCAACTCCAGCATGCGACC
debsTE_R	TTATGCGGCCGCAAGCTTGTCACG
zeaTE_R	TTAACCAGCTTCATTGAAGAACTCAAACGCGC

ppsB Ncom F	ATGCGATCTGTGTACAGCCGCATCTCG
debsTE R	TTATGCGGCCGCAAGCTTGTCAACG
zeaTE R	TTAACCAGCTTCATTGAAGAACTCAAACGCGC
Bbpro.(Lip2Ncomm)_R	CCATATGTATATCTCCTTCTTAAAAGATCTTTTGAATTC
Bbterm.(debsTE)_F	AGGATCCAAACTCGAGTAAGGATCTCC
DebsTE.(bbterm)_R	GGAGATCCTTACTCGAGTTTGGATCCTCAACCGCTGTTGCCG CA
Lip1.(bbpro)_F	CAAAAGATCTTTTAAGAAGGAGATATACATATGGTTTCTGAAC ATCGCGGTAGC
Lip1.(bbterm)_R	GGAGATCCTTACTCGAGTTTGGATCCTTAGATGCCCAGTTCGG TATCAATAAACGCC
Lip2Ncomm.(bbpro)_F	CAAAAGATCTTTTAAGAAGGAGATATACATATGGCGGACCAT GATAAACTGGTGGA
MlsB1wt_KRnull_F	CGTTTGTTCATGTTCTCGGCAGTAGCCGGAATCTGG
MlsB1wt_KRnull_R	CCAGATTCCGGCTACTGCCGAGAACATGACAAACG
Ncomm-lipLM_F	GTGCCGCATGACGAACCAATTGCG
Ncomm-lipLM_R	CGCAATTGGTTCGTCATGCGGCAC
Ncomm-lipLM-lip1KSAT1_F	CATAGCCGTCGTCCGGTTTTTCGTCTTT
Ncomm-lipLM-lip1KSAT1_R	AAAGACGAAAACCGGACGACGGCTATG
BbTerm.(Mtb)_F	GGATCCAAACTCGAGTAAGGATCTCC
BbPro.(Mtb)_R	CATATGTATATCTCCTTCTTAAAAGATCTTTTGAATTC
BLV75_TE.(Bbterm)_R	GGAGATCCTTACTCGAGTTTGGATCCTAACGTTCCAGCAGCC ATGCGT
lip2Ncomm_co.(Bbpro)_F	CAAAAGATCTTTTAAGAAGGAGATATACATATGGCTGACCACG ATAAACTAGTAGATTATTTGAAG
borAT.(pik67)_F	GGACGAACGCGCACGTCGTCCTGGAGGAGGCGCCTGAAGAGG GC
borAT.(pik27)_R	CAGCCAATAGTGTTGATGTTGGAACGGG
pikAT2.(pik27)_F	GGACGAACGCGCACGTCGTGCTGGAGCAGGCGCCGGATGCTG CTGG
pikAT2.(pik27)_R	CAGCCAGTAGCGGTCGCGC
pikAT2.(pik67)_F	GGACGAACGCGCACGTCGTCCTGGAGCAGGCGCCGGATGCTG CTGG
pik27.(borAT)_F	CCCGTTCCAACATCAACACTATTGGCTGAGCCCCGCGGGTCCC GGC

pik27.(borAT)_R	CTCCAGCACGACGTGCGCG
pik27.(pikAT2)_F	CCTTCCGGCGCGACCGCTACTGGCTGAGCCCCGCGGGTCCCCGGC
pik67.(borAT)_F	CCCGTTCCAACATCAACACTATTGGCTGCCCCGCGGGTCCCCGGC GAG
pik67.(borAT)_R	CTCCAGGACGACGTGCGCGTTC
pik67.(pikAT2)_F	CCTTCCGGCGCGACCGCTACTGGCTGCCCCGCGGGTCCCCGGCGA G
pBbA5a.(pik6_NDD)_R	CGTTGGAACCTCGTCATATGTATATCTCCTTCTTAAAAGATCTTT TGAATTC
pBbA5a.(pikTE)_F	GGGGGCGGGCAAGTAAGGATCCAAACTCGAGTAAGGATCTCC
pBbS5k.(pik5_CDD)_F	CCCCGTAACACCTGAGGATCCAAACTCGAGTAAGGATCTCC
pBbS5k.(pik1)_R	GTCCTGGTAATTCCGGCTGAAGACATATGTATATCTCCTTCTTA AAAGATCTTTGA
pik_ACP7.(pik6)_F	CCCGCGGGTCCCCGGCGAGG
pik5_CDD.(pBbS5k)_R	CGAGTTTGGATCCTCAGGTGTTACGGGGGCC
pikKS6_H320R_F	TGGCGGATCAGGCGCTGCTGGGAGG
pikKS6_H320R_R	CCTCCCAGCAGCGCCTGATCCGCCA
pik6_NDD.(pBbA5a)_F	GAAGGAGATATACATATGACGAGTTCCAACGAACAGTTGGTG GA
pikTE.(pBbA5a)_R	GTTTGGATCCTTACTTGCCCCGCCCCCTCGATGC
pik1.(pBbS5k)_F	GGAGATATACATATGTCTTCAGCCGGAATTACCAGGACCG
pik1.(pik2)_R	TCGACAACCACCGGGGCCTCTTCG
pik2.(pik1)_F	CTCGAAGAGGCCCCGGTGGTTGTCGAGGGTGCTTCGGTCGTCG
pik6.(pikACP6)_R	GCGGGCGCCTCGCCGGGACCCGCGGGGCTGATCCAGTACGAG CGGTGCTG
pik6.(pik1)_F	CTCGAAGAGGCCCCGGTGGTTGTCGACTCCCCGGCCGTCGAG
pik12.(pikAT2)_F	CCTTCCGGCGCGACCGCTACTGGCTGGAGAACTCCCCGCCGC CC
pik12.(pikAT2)_R	GCATCCGGCGCCTGGACAACCACCGGGGCCTCTTCG
pikAT2.(pik12)_F	CCCGGTGGTTGTCCAGGCGCCGGATGCTGCTGG
pikAT2.(pik12)_R	CAGCCAGTAGCGGTGCGCG

**Supplementary Table 9. Details of mass and mass-to-charge of compounds identified in this study.**

Compound	Formula	Mass	[M-H] <sup>-</sup>
triacetic acid lactone (internal standard)	C6 H6 O3	126.032	125.024
4-methyl-5-ethyl-BKDL (BKDL 1, 2, 3)	C8 H12 O3	156.079	155.071
4-methyl-5-isobutyryl-BKDL (BKDL 4, 5, 6)	C9 H14 O3	170.094	169.087
5-ethyl-BKDL (BKDL 7)	C7 H10 O3	142.063	141.056
3-hydroxy-2-methyl-pentanoic acid (hydrolyzed side product of BKDL 1, 2, 3)	C6 H12 O3	132.077	131.071
3-hydroxy-2,4-dimethyl-pentanoic acid (hydrolyzed side product of BKDL 4, 5, 6)	C7 H14 O3	146.094	145.087
3-hydroxy-pentanoic acid (hydrolyzed side product of BKDL 7)	C5 H10 O3	118.063	117.056

**Supplementary Table 10. List of major equipment used in bioproduction of BKDL (costs derived from SuperPro).**

Name	Type	Quantity	Size (Capacity)	Unit	Quantity Price (\$ per Unit)	Total Price (\$)
SG-101	Steam Generator	1	301.21	MT/h	37,024,000	37,024,000
R-101	Stirred Reactor	1	944.27	m3	6,590,000	6,590,000
S-104	Shredder	4	26.04	MT/h	4,815,000	19,260,000
ET-101	Extraction Steam Turbine-Generator	2	22,795.09	kW	3,693,000	7,386,000
D-403	Distillation Column	1	2,104.82	m3	2,397,000	2,397,000
FR-102	Fermentor	3	2,587.74	m3	1,816,000	10,896,000
DC-102	Decanter Centrifuge	1	124,193.65	L/h	1,574,000	1,574,000
DC-101	Decanter Centrifuge	1	116,931.30	L/h	1,494,000	1,494,000
C-101	PBA Column	4	2,485.44	L	1,420,000	5,680,000
FR-106	Fermentor	2	1,900.16	m3	1,333,000	2,666,000
CSP-110	Component Splitter	1	174.12	MT/h	968,000	968,000
ST-207	Receiver Tank	1	2,189.29	m3	656,000	656,000
ST-407	Flat Bottom Tank	1	393.74	kgal	517,000	517,000
BT-205	Blending Tank	1	79,413.06	L	441,000	441,000
V-109	Blending Tank	2	46,417.75	L	367,000	734,000
V-101	Blending Tank	1	34,497.77	L	335,000	335,000
BC-101	Belt Conveyor	1	100.00	m	268,000	268,000
FR-105	Fermentor	1	380.08	m3	267,000	267,000
V-103	Flat Bottom Tank	4	753.06	m3	257,000	1,028,000
RVF-101	Rotary Vacuum Filter	11	76.77	m2	216,000	2,376,000
ST-311	Flat Bottom Tank	1	368.84	m3	181,000	181,000
UF-101	Ultrafilter	106	79.67	m2	135,000	14,310,000
HX-111	Heat Exchanger	4	92.52	m2	116,000	464,000
DDR-101	Drum Dryer	1	0.21	m2	84,000	84,000
HX-104	Heat Exchanger	2	53.29	m2	83,000	166,000
HX-101	Heat Exchanger	1	48.45	m2	79,000	79,000
PM-104	Centrifugal Pump	1	6.70	kW	42,000	42,000
P-224	Centrifugal Pump	1	6.26	kW	41,000	41,000
CT-101	Cooling Tower	3	26,433.84	L	41,000	123,000
ST-302	Hopper	1	2.85	kgal	40,000	40,000
PM-105	Centrifugal Pump	1	3.89	kW	33,000	33,000
PM-102	Centrifugal Pump	1	3.64	kW	32,000	32,000

411P	Centrifugal Pump	1	0.86	HP-E	31,000	31,000
HX-304	Heat Exchanger	2	74.26	m2	29,000	58,000
FR-104	Fermentor	1	38.05	m3	27,000	27,000
502P	Centrifugal Pump	1	0.50	HP-E	25,000	25,000
ST-301	Blending Tank	1	11.51	kgal	24,000	24,000
PM-124	Centrifugal Pump	1	86.01	kW	23,000	23,000
C-102	Distillation Column	1	0.02	m3	22,000	22,000
PM-101	Centrifugal Pump	1	1.14	kW	20,000	20,000
P-300	Centrifugal Pump	1	0.86	HP-E	15,000	15,000
PM-103	Centrifugal Pump	1	0.00	kW	9,000	9,000
P-760	Centrifugal Pump	1	0.00	kW	9,000	9,000
P-720	Centrifugal Pump	1	0.01	kW	9,000	9,000
PM-108	Centrifugal Pump	1	18.17	kW	8,000	8,000
HX-105	Heat Exchanger	1	0.59	m2	8,000	8,000
HX-102	Heat Exchanger	1	0.25	m2	8,000	8,000
PM-113	Centrifugal Pump	1	18.17	kW	7,000	7,000
M-103	Centrifugal Fan	43	8,873,223.89	L/h	7,000	280,000
512P	Centrifugal Pump	1	0.00	HP-E	6,000	6,000
BT-303	Blending Tank	1	617.24	L	6,000	6,000
P-302	Gear Pump	1	0.30	kW	2,000	2,000
P-301	Gear Pump	1	0.30	kW	2,000	2,000
FR-101	Fermentor	1	0.43	m3	1,000	1,000

**Supplementary Table 11. Material balance for BKDL production for the intermediate scenario.**

<b>Material</b>	<b>Input (kg per year)</b>	<b>Output (kg per year)</b>
Acetate (bound)	11,962,500	21,463
Ash	32,505,000	33,889,612
BKDL	0	63,237,622
Cellulose	231,330,000	31,083,796
Ionic liquid	3,473,684	3,181,788
Corn steep liquor	2,587,706	0
Diammonium phosphate	324,295	0
<i>Streptomyces</i>	6	92,019,796
Ethyl acetate	6,379,124	6,379,124
Glucose	0	35,450,788
Hemicellulose	128,865,000	21,737,943
Hydrolase	4,626,600	752,604
Lactic acid	0	9,039,542
Lignin	104,032,500	128,793
Methane	5,544,000	0
Methanol	2,894	2,894
Other solids	151,305,000	1,340,004
Return cooling water	8,395,200,000	0
Soluble lignin	0	285,617
Sulfuric acid	110,498,632	106,527,250
Water	1,582,686,415	10,138,996,405
Xylose	0	19,322,326
<b>TOTAL</b>	<b>10,771,323,356</b>	<b>10,563,397,367</b>

\*Only make-up amount is shown in the mass-balance stream. Solvent recycling is assumed to be 95% for the intermediate scenario.

**Supplementary Table 12. Major costs and revenue for BKDL production for different scenarios.**

<b>Scenario</b>	<b>Installed ISBL equipment cost</b>	<b>Total capital investment</b>	<b>Operating cost</b>	<b>MSP (\$ per kg)</b>
Intermediate (BKDL)	\$95,584,838	\$406,474,629	\$121,965,290	\$4.02
Optimized (BKDL)	\$112,598,438	\$415,958,009	\$124,629,712	\$1.51
State of Technology (bioTAL)	\$81,911,313	\$ 448,460,310	\$107,876,774	\$9.24
Optimized (bioTAL)	\$138,511,325	\$651,527,281	\$137,960,350	\$1.19

ISBL = Inside Battery Limit. This includes pretreatment, bioconversion, BKDL recovery and separation stages.



**Supplementary Table 13. Material and energy inputs for BKDL production (intermediate scenario).**

<b>Material input</b>	<b>Amount</b>	<b>Unit</b>
Ionic liquid	0.05	kg per kg BKDL
Ionic Liquid (recycle)	1.78	kg per kg BKDL
Corn liquor	0.04	kg per kg BKDL
Diammonium phosphate	0.01	kg per kg BKDL
<i>Streptomyces</i>	0.0705	mg per kg BKDL
Ethyl acetate	1.92	kg per kg BKDL
Ethyl acetate (makeup)	0.10	kg per kg BKDL
Hydrolase	0.07	kg per kg BKDL
Methane	0.09	kg per kg BKDL
Methanol	869.4	mg per kg BKDL
Methanol (makeup)	45.8	mg per kg BKDL
Stover	13.05	kg per kg BKDL
Sulfuric acid	1.56	kg per kg BKDL
Water	88.28	kg per kg BKDL
Electricity required	5.1	kWh per kg BKDL
Electricity generated	5.14, resulting in electricity credit of – 0.04 kWh per kg of BKDL	kWh per kg BKDL

**Supplementary Table 14. Process parameters and assumptions used for bioproduction of BKDL.**

Process Parameters	Units	Intermediate	Optimized	Source
Corn stover	bone-dry metric ton(bdt)/day	2000	2000	Xu, et al., 2016 <sup>2</sup>
Delivered cost of corn stover	\$/bdt	87.83	71.26	Davis et al., 2018 <sup>3</sup>
Cellulose	wt%	28.04	35.1	Xu, et al., 2016 <sup>2</sup>
Hemicellulose	wt%	15.62	19.5	Humbird et al., 2011 <sup>4</sup>
<b>Ionic liquid (IL) pre-treatment</b>				
Solids loading rate	wt%	30	30	Baral et al. 2019 <sup>5</sup>
Ionic liquid ([Ch][Lys]) loading rate	kg/kg-dry biomass	0.29	0.125	Baral et al. 2019 <sup>5</sup>
Ionic liquid ([Ch][Lys]) cost	\$/kg	2	0.5	Xu et al.,2016 <sup>2</sup>
Sulfuric acid loading	kg/kg- IL	0.2	0.07	Magurudeniya et al., 2021 <sup>6</sup>
Sulfuric acid price	\$/kg	0.14	0.14	Alibaba
Lignin to soluble lignin	wt%	31	17	Magurudeniya et al., 2021 <sup>6</sup>
Pretreatment time	h	3	1	Magurudeniya et al., 2021 <sup>6</sup>
IL recovery rate	wt%	97	99	Xu et al.,2016 <sup>2</sup>
<b>Enzymatic hydrolysis</b>				
Solids loading rate	wt%	25	25	Baral et al. 2019 <sup>5</sup>
Enzyme loading rate	mg/g-glucan	20	10	Baral et al. 2019 <sup>5</sup>
Cellulose to glucose	wt%	84	95	Baral et al. 2019 <sup>5</sup>
Xylan to xylose	wt%	80	90	Baral et al. 2019 <sup>5</sup>
Temperature	°C	48	48	Humbird et al.,2011 <sup>4</sup>
Hydrolysis time	h	72	48	Baral et al. 2019 <sup>5</sup>
Enzyme (hydrolase) price	\$/kg-protein	4.29	4.29	Xu et al.,2016 <sup>2</sup>
<b>Bioconversion</b>				
Cost of corn steep liquor	\$/kg	0.1	0.1	Baral et al. 2019 <sup>5</sup>
Cost of diammonium phosphate	\$/kg	1	1	Baral et al. 2019 <sup>5</sup>
Aeration rate	vvm	0.5	0.5	Experimental results
Power consumption	kW/m <sup>3</sup>	0.5	0.5	Baral et al. 2019 <sup>5</sup>

Power dissipation to heat	%	40	40	Baral et al. 2019 <sup>5</sup>
Temperature	°C	30	30	Experimental results
Bioconversion time	h	96 <sup>*</sup>	60 <sup>†</sup>	*Based on experimental results. †Modeling assumption
Glucose to BKDL	wt%	50.6	90	x% of theoretical yield, calculations
Xylose to BKDL	g BKDL/g xylose	0.234	0.414	Modeling assumption, 90% of glucose conversion
<b>Onsite energy generation</b>				
Boiler heat loss		5%	5%	Vakkilainen et al. 2017 <sup>7</sup>

## Materials

All the reagents were purchased from Sigma Aldrich, otherwise specifically mentioned. Dibutylboron trifluoromethanesulfonate solution (Bu<sub>2</sub>BOTf, 1.0 M in CH<sub>2</sub>Cl<sub>2</sub>), diisopropylethylamine (>99%), propionaldehyde (>97%), NaHCO<sub>3</sub> (>99%), magnesium sulfate (MgSO<sub>4</sub>, anhydrous), sodium sulfate (Na<sub>2</sub>SO<sub>4</sub>, >99%), 1-ethyl-3-(3-dimethylaminopropyl)carbodiimide hydrochloride (EDC, >99%), dimethylaminopyridine (DMAP, >99%), isobutyraldehyde (99%), lithium bis(trimethylsilyl)amide solution (LiHMDS 1.0 M in THF), ammonium chloride (NH<sub>4</sub>Cl), lithium hydroxide (LiOH), triethylamine (Et<sub>3</sub>N, >99%), *N,N'*-dicyclohexylcarbodiimide (DCC, >99%), tris(2-aminoethyl)amine (TREN, 96%) were purchased from Sigma Aldrich. *N*-acetylcysteamine (85%) was purchased from Sigma Aldrich. (*S*)-4-benzyl-3-propionyloxazolidin-2-one (>99%,) was purchased from Chemimpex. Bio-based sebacic acid (99%) was purchased from Arkema. Dihydro-6,6-dimethyl-2*H*-pyran-2,4(3*H*)-dione was synthesized according to previously reported procedures<sup>8</sup>. Tetrahydrofuran (THF, ≥99.9%), dichloromethane (DCM, ≥99.9%), methanol (MeOH, >99.8%), ethanol (90%), hydrochloric acid (HCl, 36.5–38%), ethyl acetate (EtOAc, ≥99.9%), hexane (≥99.9%), were purchased from VWR. 30 wt% H<sub>2</sub>O<sub>2</sub> solution, phosphate buffer solution (BioUltra, Na<sub>2</sub>HPO<sub>4</sub>, 0.5 M in H<sub>2</sub>O) and brine solution (NaCl, 5.0 M in H<sub>2</sub>O) were purchased by Sigma Aldrich. Chloroform-*d* (CDCl<sub>3</sub>, 99.8% D) was purchased from Cambridge Isotope Laboratories. BKDL 7 was ordered from Enamine (USA). All solvents and reagents were used without further purification.

## Instrumentation

**<sup>1</sup>H, <sup>13</sup>C and Heteronuclear Single Quantum Coherence (HSQC) Solution State Nuclear Magnetic Resonance (NMR) Spectroscopy.** <sup>1</sup>H, <sup>13</sup>C and HSQC solution state NMR spectroscopy was carried out using a Bruker Avance II at 500 and 125 MHz, respectively. Chemical shifts are reported relative to the residual solvent signal (<sup>1</sup>H: δ = 7.26 ppm (CDCl<sub>3</sub>); <sup>13</sup>C: δ = 77.16 ppm (CDCl<sub>3</sub>)). NMR data are reported as follows: chemical shift (multiplicity, coupling constants (where applicable), number of hydrogens). Splitting patterns are reported as s (singlet), d (doublet), t (triplet), and m (multiplet). All spectra were processed using Bruker TopSpin 4.1.1 software.

**Differential Scanning Calorimetry (DSC).** DSC data were acquired using a TA Instruments Q200 Differential Scanning Calorimeter. TAL-PDK samples were heated over a temperature range of 0–200 °C at a rate of 10 °C min<sup>-1</sup> under an N<sub>2</sub> atmosphere. For each sample, data acquisition runs consisted of a heating step, a cooling step, and a second heating step. Glass transition temperatures (*T<sub>g</sub>*) and melting temperatures (*T<sub>m</sub>*) were interpreted and reported from the second heating curve.

## Supplementary Methods

**Genome mining.** blv75, was obtained from mining of 36,334 genomes which were downloaded from the ref seq database by March 2021 using the script available here:

[https://github.com/WeMakeMolecules/fun-git/blob/main/download\\_bacterial\\_genomes.sh](https://github.com/WeMakeMolecules/fun-git/blob/main/download_bacterial_genomes.sh)

The genomes were then annotated using Antismash<sup>9</sup>. The domain annotations were then processed to obtain a polyketide-coding genes with the desired domain organization. This process was done using the script available here:

[https://github.com/WeMakeMolecules/Megasynthase\\_string\\_miner/tree/main](https://github.com/WeMakeMolecules/Megasynthase_string_miner/tree/main)

This process led to a set of 25 candidate PKS genes:

Strain	Genome assembly ID	Gene ID	PKS monomers	Domain organization
<i>Streptomyces</i> sp. CB03578	GCF00190502 5	6666666.306093.peg.49 34	mal	KS-AT-ACP-Thioesterase
<i>Streptomyces</i> sp. CNQ 525	GCF00070128 5	6666666.306109.peg.59 82	mal	KS-AT-ACP-Thioesterase
<i>Streptomyces</i> sp. FBKL.4005	GCF00225115 5	6666666.306147.peg.81 97	mal	KS-AT-ACP-Thioesterase
<i>Streptomyces</i> sp. FXJ1.172	GCF00163694 5	6666666.306153.peg.55 82	mal	KS-AT-ACP-Thioesterase
<i>Streptomyces</i> sp. GBA 94 10	GCF00049563 5	6666666.306157.peg.30 10	mal	KS-AT-ACP-Thioesterase
<i>Streptomyces</i> sp. GBA 94 10	GCF00049563 5	6666666.306157.peg.53 48	mal	KS-AT-ACP-Thioesterase
<i>Streptomyces</i> sp. IMTB 2501	GCF00195388 5	6666666.306168.peg.82 9	mal	KS-AT-ACP-Thioesterase
<i>Streptomyces</i> sp. MBT76	GCF00144565 5	6666666.306626.peg.82 3	mal	KS-AT-ACP-Thioesterase
<i>Streptomyces</i> sp. Mgl	GCF00015488 5	6666666.306627.peg.58 41	mal	KS-AT-ACP-Thioesterase
<i>Streptomyces</i> sp. Mgl	GCF00041226 5	6666666.306628.peg.61 42	mal	KS-AT-ACP-Thioesterase
<i>Streptomyces</i> sp. NBRC 109706	GCF00097448 5	6666666.306642.peg.56 16	mal	KS-AT-ACP-Thioesterase
<i>Streptomyces</i> sp. NRRL S 118	GCF00071633 5	6666666.307484.peg.70 48	mal	KS-AT-ACP-Thioesterase
<i>Streptomyces</i> sp. PAMC 26508	GCF00036480 5	6666666.309611.peg.55 80	mal	KS-AT-ACP-Thioesterase
<i>Streptomyces</i> sp. PVA 94 07	GCF00049575 5	6666666.306765.peg.76	mal	KS-AT-ACP-Thioesterase
<i>Streptomyces</i> sp. PVA 94 07	GCF00049575 5	6666666.306765.peg.18 87	mal	KS-AT-ACP-Thioesterase
<i>Streptomyces</i> sp. RTd22	GCF00164056 5	6666666.306776.peg.36 45	mal	KS-AT-ACP-Thioesterase
<i>Streptomyces</i> sp. SirexAA E	GCF00017719 5	6666666.306792.peg.56 60	mal	KS-AT-ACP-Thioesterase

<i>Streptomyces yokosukanensis</i> DSM 40224	GCF00151403 5	6666666.306876.peg.99 0	mal	KS-AT-ACP-Thioesterase
<i>Rhodococcus</i> sp. 14 2470 1a	GCF00225942 5	6666666.305111.peg.64 7	ccmal-mal	KS-AT-DH-KR-ACP-KS-AT-ACP-Thioesterase
<i>Streptomyces</i> sp. NBRC 110030	GCF00141767 5	6666666.306647.peg.46 33	ccmal-mal	KS-AT-DH-KR-ACP-KS-AT-ACP-Thioesterase
<i>Streptomyces</i> sp. PAN FS17	GCF90010546 5	6666666.306756.peg.82 26	ohmal-mal	KS-AT-DHt-KR-ACP-KS-AT-ACP-Thioesterase
<i>Sorangium cellulosum</i>	BGC0000080. 1	6666666.297074.peg.19	ohmal-pk	KS-AT-KR-ACP-KS-AT-ACP-Thioesterase
<i>Kitasatospora azatica</i> KCTC 9699	GCF00074478 5	6666666.300889.peg.35 70	ohmal-pk	KS-AT-KR-ACP-KS-AT-ACP-Thioesterase
<i>Streptomyces himastatinicus</i> ATCC 53653	GCF00015891 5	6666666.305862.peg.42 25	ohmal-mal	KS-AT-KR-ACP-KS-AT-ACP-Thioesterase
<i>Streptomyces</i> sp KS 5 (BLV75)	GCF90010527 5	6666666.306174.peg.91 31	ohmal-mal	KS-AT-KR-ACP-KS-AT-ACP-Thioesterase

**LC-QTOF-MS analysis.** The LC-MS analysis was conducted on a Kinetex XB-C18 column (100-mm length, 3.0-mm internal diameter, and 2.6- $\mu$ m particle size; Phenomenex, Torrance, CA USA) using a 1260 Infinity HPLC system (Agilent Technologies, Santa Clara, CA, USA). A sample injection volume of 3  $\mu$ L was used throughout. The sample tray and column compartment were set to 6 and 25  $^{\circ}$ C, respectively. The mobile phase was composed of 0.1 % formic acid (Sigma-Aldrich, St. Louis, MO, USA) in water (solvent A) and 0.1 % formic acid in methanol (solvent B), unless stated otherwise. BKDL was separated via gradient elution under the following conditions: linearly increased from 20 %B to 72.1 %B in 6.5 min, linearly increased to 95 %B in 1.3 min, then held at 95 %B for 2 min, linearly decreased from 95 %B to 20 %B in 0.2 min, and held at 5 %B for 2.2 min. The flow rate was held at 0.42 mL/min for 8.8 min, linearly increased from 0.42 mL/min to 0.65 mL/min in 0.2 min, and held at 0.65 mL/min for 2.2 min. The total LC run time was 11.2 min. The HPLC system was coupled to an Agilent Technologies 6520 quadrupole time-of-flight mass spectrometer (for LC-QTOF-MS) via a 1:4 post-column split. The QTOF-MS was tuned with the Agilent ESI-L Low concentration tuning mix in the range of 50-1700 m/z. Drying and nebulizing gases were set to 11 L/min and 30 lb/in<sup>2</sup>, respectively, and a drying-gas temperature of 330  $^{\circ}$ C was used throughout. ESI was conducted in the negative ion mode (for [M – H]<sup>–</sup> ions) and a capillary voltage of 3500 V was utilized. The fragmentor, skimmer, and OCT 1 RF Vpp voltages were set to 100, 50, and 170 V, respectively. The data acquisition range was from 50-500 m/z, and the acquisition rate was 0.86 spectra/s. Data acquisition (Workstation B.08.00) and processing (Qualitative Analysis B.06.00 and Profinder B.08.00) were conducted via the Agilent MassHunter software package.

**Proteomics analysis.** Proteins from *S. albus* samples were extracted and tryptic peptides were prepared by following established proteomic sample preparation protocol<sup>10</sup>. Briefly, cell pellets were resuspended in Qiagen P2 Lysis Buffer (Qiagen, Hilden, Germany, Cat.#19052) to promote cell lysis. Proteins were precipitated with addition of 1 mM NaCl and 4 x vol acetone, followed by two additional washes with 80% acetone in water. The recovered protein pellet was homogenized by pipetting mixing with 100 mM Ammonium bicarbonate in 20% Methanol. Protein concentration was determined by the DC protein assay (BioRad, Hercules, CA). Protein reduction was accomplished using 5 mM tris 2-(carboxyethyl)phosphine (TCEP) for 30 min at room temperature, and alkylation was performed with 10 mM iodoacetamide (IAM; final concentration) for 30 min at room temperature in the dark. Overnight digestion with trypsin was accomplished with a 1:50 trypsin:total protein ratio. The resulting peptide samples were analyzed on an Agilent 1290 UHPLC system coupled to a Thermo Scientific Orbitrap Exploris 480 mass spectrometer for discovery proteomics<sup>11</sup>. Briefly, 20 µg of tryptic peptides were loaded onto an Ascentis® (Sigma–Aldrich) ES-C18 column (2.1 mm × 100 mm, 2.7 µm particle size, operated at 60°C) and were eluted from the column by using a 10-minute gradient from 98% solvent A (0.1 % FA in H<sub>2</sub>O) and 2% solvent B (0.1% FA in acetonitrile) to 65% solvent A and 35% solvent B. The eluting peptides were introduced to the mass spectrometer operating in positive-ion mode. Full MS survey scans were acquired in the range of 300-1200 m/z at 60,000 resolution. The automatic gain control (AGC) target was set at  $3 \times 10^6$  and the maximum injection time was set to 60 ms. Top 10 multiply charged precursor ions (2-5) were isolated for higher-energy collisional dissociation (HCD) MS/MS using a 1.6 m/z isolation window and were accumulated until they either reached an AGC target value of  $1e5$  or a maximum injection time of 50 ms. MS/MS data were generated with a normalized collision energy (NCE) of 30, at a resolution of 15,000. Upon fragmentation precursor ions were dynamically excluded for 10 s after the first fragmentation event. The acquired LCMS raw data were converted to mgf files and searched against the latest uniprot *S. albus* protein database plus the protein sequences of the heterologous proteins and common proteomic contaminants using Mascot search engine version 2.3.02 (Matrix Science). The resulting search results were filtered and analyzed by Scaffold v 5.0 (Proteome Software Inc.). The generated mass spectrometry proteomics data have been deposited to the ProteomeXchange Consortium via the PRIDE<sup>12</sup> partner repository with the dataset identifier PXD042863 and 10.6019/PXD04286.

**Extraction of compounds for analysis.** 10 mL cell culture supernatant was obtained by centrifuge 10 mL cell culture in a 15 mL falcon tube at 3,000×g for 10 min. 2 × 10 mL ethyl acetate was mixed with all the HCl-acidified supernatants (pH<2) vigorously for 2 min to extract the BKDL. After spinning down the mixture to get the phase separation at 3,000×g for 10 min, the organic phase was separated from the top layer. The extract was dried by speedvac before analysis by LC-MS.

**Alpha-fold protein structure predictions.** The protein structures were predicted using alpha-fold with corresponding protein sequences<sup>13</sup>.

#### **Techno-Economic Analysis and Life Cycle Assessment of BKDL Production System.**

Bio-production of BKDL process models used in this study was developed in a commercial process modeling software package—SuperPro Designer-V12 (Intelligen: Scotch Plains, NJ.). The process parameters and assumptions for BKDL’s intermediate and optimized scenarios are shown in Supplementary Table 14. Additionally, description and major assumptions for each of the major steps in the production system are presented below. For the bioTAL’s “current technology” scenario, the same assumptions were used as that used for the intermediate scenario, unless otherwise noted in relevant sections below. Similarly, the same assumptions were used for the two “optimized” scenarios in this study, unless otherwise noted in the relevant section.

**Feedstock handling.** Corn stover was assumed as a representative biomass feedstock for the simulated biorefinery. The biorefinery utilizes 2000 bone-dry metric tons of corn stover per day. The modeling parameters were obtained from Xu’s research in 2016<sup>2</sup>. The feedstock handling process includes

transportation from farm to refinery with shipping distance of 31 miles (50 km) and a handling dome. The milled biomass is routed to the biomass deconstruction unit for pretreatment and enzymatic hydrolysis. The greenhouse gas (GHG) emissions for the feedstock handling and supply of corn stover was assumed to be 83.8 kg CO<sub>2</sub>e per metric ton of stover<sup>14</sup>.

#### Corn stover composition

Corn stover composition	wt%
Acetate (bound)	1.81
Ash	4.93
Cellulose	35.05
Hemicellulose	19.53
Lignin	15.76
Other solids	22.93

**Biomass Deconstruction.** The biomass undergoes pre-treatment to break the cell wall made of recalcitrant lignin and that aids in further enzymatic hydrolysis to convert glucose into cellulose. Here, bio-based ionic liquid (IL) cholinium lysinate [Ch][Lys] is chosen as the preferred option for pre-treatment. The biomass deconstruction stage includes pretreatment, enzymatic hydrolysis, solid-liquid separation, and ionic liquid recovery units. The biomass solids loading rate is maintained at 30% by supplying additional water to the biomass and IL mixture. The water is added to ensure better heat and mass transfer when utilizing a high solid loading rate and IL mixture<sup>15</sup>. High IL recovery of 97% for intermediate and “current technology” scenarios (99% for optimistic scenarios) is assumed<sup>2</sup>, where IL is recovered post bioconversion through pervaporation technology. The lignin fraction on cellulose can inhibit enzyme accessible areas and overall sugar yields. Treatment with [Ch][Lys] rectifies this and results in dissolution of 31% (17% for optimistic scenario) of lignin fraction<sup>6</sup>. The pretreated biomass is sent to the enzymatic hydrolysis unit after pH adjustment using sulfuric acid.

**Enzymatic Hydrolysis.** Enzymatic hydrolysis releases fermentable sugars, including glucose from cellulose and xylose from xylan. Cellulose to glucose conversion is modeled at 84% and xylan to xylose conversion is considered to be 80%. The enzyme loading rate is maintained at 20 mg protein g<sup>-1</sup> cellulose. Initial solids loading is at 20 wt%. Enzymatic hydrolysis is operated at a temperature of 48 °C for 72 h. The liquid fraction consisting of glucose and xylose is sent to the bioconversion unit. The solid fraction primarily consisting of lignin is sent to on-site combustor for energy generation. The slurry is cooled to 32 °C for bioconversion with a heat exchanger.



**Bioconversion.** The currently modeled bioconversion process for BKDL uses *Streptomyces*. The bioconversion temperature and time is assumed to be 30°C and 96 h. Xylose to bioTAL conversion is assumed to be 90% of that of glucose to bioTAL conversion. The fermenter requires 10 vol% of inoculum, and the ratio is maintained by sending 10% of the slurry from enzymatic hydrolysis to the seed fermenters, and the rest to the main bioconversion tank. The seed bioconversion consists of five reactors and designed with the modeling assumptions consistent with Humbird's report in 2011<sup>4</sup> and Yang's report in 2020<sup>15</sup>. For both seed bioconversion and main bioconversion unit, the nutrient source is assumed to be corn steep liquor (CSL) and diammonium phosphate (DAP). CSL and DAP are used as a placeholder for a low-cost source of providing nitrogen, phosphorus, and other trace minerals and are not actually used in laboratory experiments. However, for production at scale, an alternate source of nutrients could be explored, which may be separate from both modeled source and media used in experiments. Therefore, in future it is possible to lower the cost of media and obtain consistent yields. Similar assumptions were used for modeling the "optimized" scenario for BKDL, except a residence time of 60 hours was used. For modeling the bioconversion units in the bioTAL scenarios, the bioconversion temperature was assumed to be 22 °C, and a residence time of 74.5 h and 48 h for "current technology" and "optimized" scenarios were used, respectively.

**Product Separation and Recovery.** BKDL production is extracellular, and therefore the first step in product separation and recovery is separation through solids (cell biomass) from liquid (supernatant). Here, separation is modeled through a centrifuge, and the cell biomass solids are sent to the boiler for co-firing for heat and electricity generation. The supernatant stream undergoes solvent extraction using ethyl acetate. The stream is subsequently treated with sulfuric acid to reduce the pH to 2. The acidification is followed by a second round of solvent extraction with ethyl acetate to extract BKDL with limited contaminants. The ethyl acetate is recovered through distillation. The stream with BKDL product undergoes drying using a drum (to simulate vacuum evaporation) and then column chromatography, to obtain a product with purity greater than 95%. Methanol used for column chromatography is also recovered through distillation. For both ethyl acetate and methanol used, a 95% solvent recovery rate is assumed.

**Onsite Energy Generation.** The onsite energy (heat and power) generation relies on a combination of unutilized biomass and supplemental natural gas (when needed). Any excess energy is sold to the grid for a credit based on average U.S. electricity prices. While solvent recovery and recycling increases the facility's on-site energy consumption, the cost associated with hazardous waste management is reduced by maximizing solvent recycling. The process model accounts for waste heat recovery.

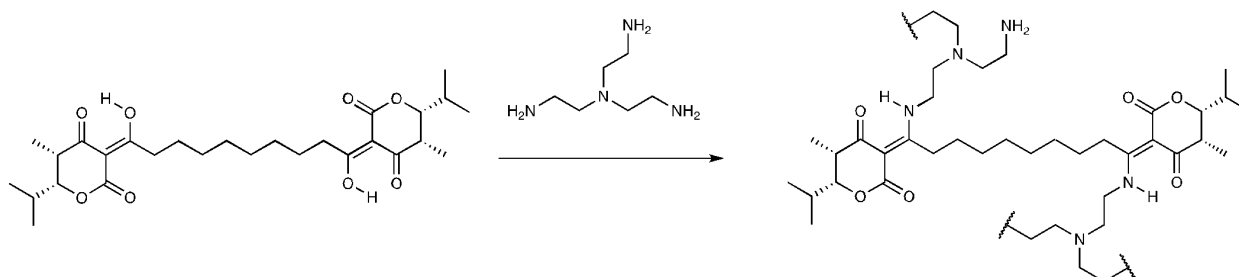
If lignin recovered from biomass is sufficient to meet the facility's heat and electricity demands, no fossil fuels are directly required. Any excess electricity can be sold to the grid; we assume these exports offset the U.S. average grid mix. If lignin is not sufficient, supplemental natural gas is used for on-site combined heat and power generation. The pretreatment process generates the largest contribution to GHG emissions (43% for intermediate scenario) followed by bioconversion process (32% for intermediate scenario).

Implementation of renewable fuels can further reduce the usage of natural gas, leading to a significant reduction in the GHG footprint. Additionally, higher solvent recovery could also lower GHG emissions. In this study, 95% of solvent recovery (ethyl acetate, methanol) is assumed, and the GHG emissions footprint may ultimately be lower than presented here, depending on the mechanism of solvent loss and the fate of unrecovered solvents in the system.

**Comparison of BKDL and bioTAL production.** *Streptomyces* is considered as the host for the state of technology (SOT) scenario, and as such the time of fermentation considered modeling the biorefinery for BKDL bio production is higher than that of bioTAL production (in which *E. coli* is used as the host). Use

of alternate hosts such as industry favored *Corynebacterium* may reduce the time in the bioconversion reactor, which in turn will reduce the MSP. Improving the rate and thus reducing bioconversion time also lowers the amount of energy required on-site, which further reduces the MSP. Production recovery also presents opportunities for improvement, as column chromatography is currently required for recovery of BKDL. Improvements across all aspects of the production system, including improved corn stover production and supply chain, improved sugar yields, higher ionic liquid and product recovery rates, and enhanced titer, rate, and yield are needed to reach these ambitious “optimized” costs. In the near-term, further research can improve BKDL production rates and the BKDL recovery process (e.g, BKDL purification by crystallization, instead of chromatography), which will reduce both the production costs and energy uses. bioTAL is based on similar inputs and assumptions to the BKDL as documented above and in the main text, except in the bioconversion step (a temperature of 22 °C, and time of 74.5 h and 48 h for “current technology” and “optimized” scenarios were used, respectively). More information regarding modeling of BKDL bioproduction can be found in the Supplementary Information, and these assumptions are consistent with previous reports<sup>1</sup>.

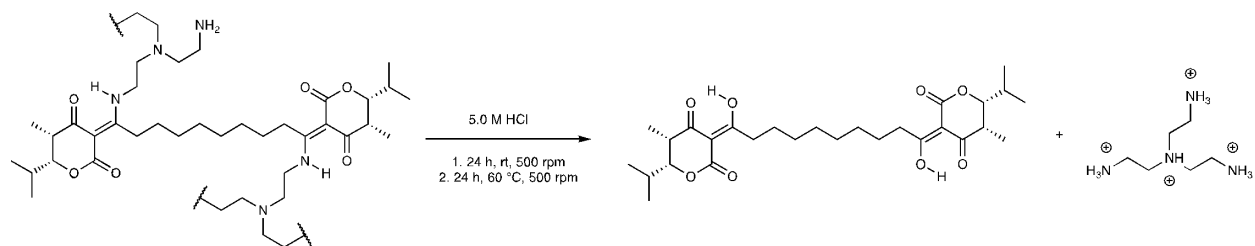
### PDK Polymerization by Ball-Milling



This procedure has been described previously<sup>16</sup>. Ball-milling was performed using a Retsch Planetary Ball-Mill PM100. The container in which the reactions were carried out was a zirconium-coated cylinder either with an inner diameter of 4.5 cm and a height of 3.5 cm (reactor volume ~50 mL) or with an inner diameter of 10 cm and a height of 7 cm (reactor volume ~500 mL). All experiments reported herein used the same weight of zirconium oxide ball bearings (5 mm diameter) and triketone ratio, being 10 times the weight of triketone. The general procedure for all ball-milling reactions involved weighing out the appropriate amount of ditopic triketone monomer (2.0 g) and placing the powder at the bottom of the ball mill, along with the ball bearings (20 g). To the triketone monomer (1 equivalent) was added *tris*(2-aminoethyl)amine (TREN) (1.1 eq. amine) using a pre-calibrated micropipette, which was immediately followed by ball-milling the contents of the closed container for 30 min at a rotation of 500 rpm. The reactor was opened to air and the reactor walls were scraped to bring together the reactants homogeneously. Ball-milling was resumed for an additional 30 min under the same rotation speed. The powder was recovered from the reactor and the residual water removed under vacuum.

**Preparation of solid samples for hydrolysis.** Powdered materials obtained from the ball-mill were pressed into sheets of ~ 1 mm in thickness using a thermal press operating at 100 °C for PDK 1 and PDK 2 and at 100 °C, at 20k psi for 20 min. Small rectangular samples both used for hydrolysis were shaped with dimensions of l = 20 mm, w = 10 mm, t = 1 mm.

### Depolymerization of Chiral PDK Networks



Chiral PDK solid sample (506 mg) was placed in 20-mL glass vials along with 5.0 M HCl (15 mL) and a magnetic stirrer. Depolymerization reaction was conducted over 24 h at room temperature while stirring at 500 rpm, yielding a white PDK solid sample with partially hydrolyzed surface. Depolymerization reaction was pursued over 24 h at 60 °C while stirring at 500 rpm. Chiral Triketone was isolated by extraction with  $\text{CH}_2\text{Cl}_2$  and evaporation of the organic phase. The light brown powder product was dried under vacuum at 80 °C to yield the chiral ditopic triketone monomer (400 mg, yield = 90.1%, purity = 98%). Percent triketone recovery was calculated by the following equation:

$$\text{Percent TK Recovery} = \frac{\text{TK (g)}}{\frac{\text{PDK (g)}}{1 + x - \frac{2(MW_{H_2O})}{MW_{TK}}}} * 100\%$$

Where:

$\text{TK (g)}$  is the mass of recovered ditopic triketone monomer

$\text{PDK (g)}$  is the mass of the PDK to be depolymerized

$x$  is the mass ratio of TREN:Triketone used during PDK polymerization

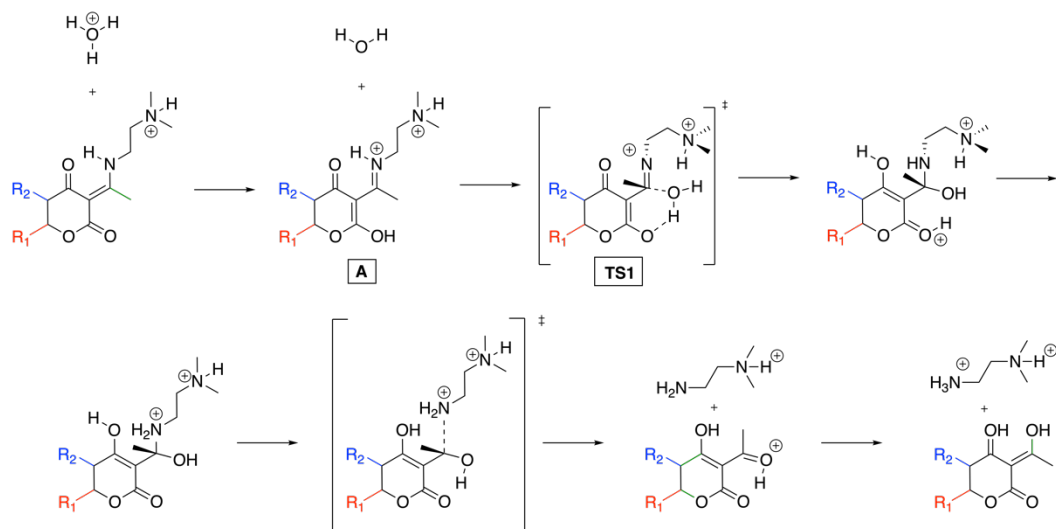
$MW_{H_2O}$  is the molecular weight of  $\text{H}_2\text{O}$

$MW_{TK}$  is the molecular weight of the triketone

**Immersion testing.** Powdered materials obtained from the ball-mill were pressed into sheets of ~ 0.3 mm in thickness using a thermal press operating at 100 °C for b-PDK 1 and b-PDK 2 and at 100 °C at 20k psi for 20 min. The rectangular samples (l = 10 mm, w = 4 mm, t = 0.3 mm) are then immersed in canola oil or vinegar (5% acetic acid) for several hours at room temperature. Visual aspect of these samples is then monitored overtime.

## Computational Methods

To calculate the hydrolysis free energy barrier,  $\Delta G^\ddagger$ , we calculated the difference in free energy for the addition step along the reaction coordinate depicted below,  $G(\text{TS1}) - G(\text{A})$ , according to the mechanism identified in previous work for the hydrolysis of  $\text{R}_1$ -dimethyl substituted BKDL<sup>16</sup>.



To identify the global minimum energy conformers for the addition transition state TS1, we performed a multi-stage conformer search. We reduced the cost of the conformer search by using the lowest-energy conformer found previously for the  $R_1$ -dimethyl substituted BKDL as a template and only performing a conformer search on the substituents at  $R_1$  and  $R_2$ . This assumption allows for high-throughput screening of  $\Delta G^\ddagger$ , and small alkyl substituents far from the reaction center are unlikely to affect the conformation of the  $N,N$ -dimethylethylenediamine moiety or the nucleophile.

For the conformer search, we first used CREST<sup>17</sup> to generate the initial ensemble of conformers, then successively filtered conformers by energy using increasingly accurate DFT levels of theory. All DFT calculations were performed using Gaussian16, calculations were prepared and analyzed using *Pymatgen*<sup>18</sup>, and calculations were automated using *Atomate*<sup>19</sup> and *QUACC* (Rosen, A. QuAcc – The Quantum Accelerator. <https://arosen93.github.io/quacc/>).

We first filtered the initial conformer ensemble by calculating hybrid-DFT electronic energies on the GFN-xTB2 geometries, removing conformers  $> 21 \text{ kJ mol}^{-1}$  higher in energy. We then took the three lowest energy conformers and two randomly selected higher-energy conformers and performed a constrained geometry optimization. We froze the structure of the transition state and optimized it at the B97-D/6-31+G(d,p)/SMD level of theory with density fitting<sup>20,21</sup>. Next, we took the lowest-energy conformer and optimized it to a transition state at the M062-X/6-311+G(d,p)//SMD level of theory<sup>22</sup>. This final conformer was taken to be the lowest-energy conformer of the transition state.

To confirm the transition state geometry and identify the reactant, we perturbed the geometry by the vibrational mode of the single imaginary frequency in the Hessian. We optimized the reactant complex separately, removing the  $\text{H}_2\text{O}$  from the BKDL and performing two independent geometry optimizations at the M062-X/6-311+G(d,p)/SMD level of theory. We separated the reactants both because the energy is extremely sensitive to the precise positioning of the single water molecule and because geometry optimizations are difficult to converge with a single water molecule.

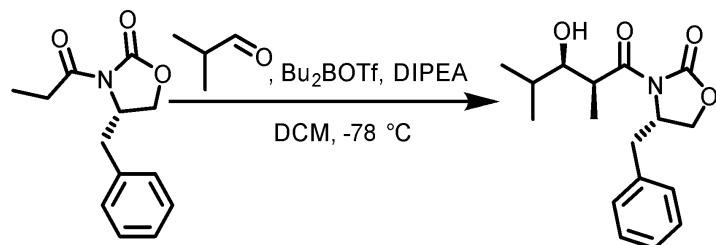
We employed Grimme's Quasi-RRHO free energy model to correct for inaccurate vibrational entropy contributions from low-frequency modes as calculated in Gaussian16 with a pure harmonic oscillator model<sup>23</sup>. Free energies were calculated at 298 K and corrected for the standard state of liquid water,

$$G_{\text{sol}} = G_{\text{Quasi-RRHO}} + RT \ln([H_2O])$$

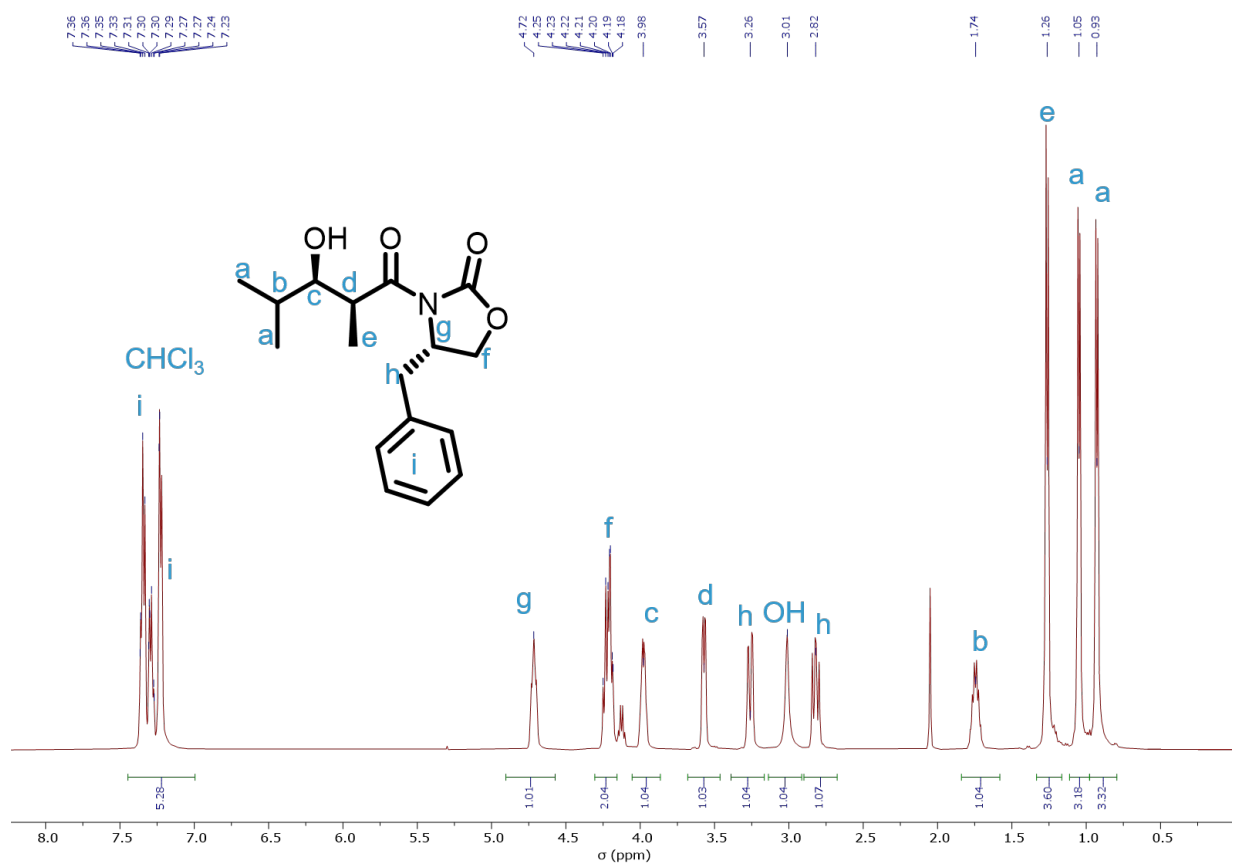
The solvation free energies,  $\Delta G_{solvation}$ , were calculated by taking the difference in free energy between the BKDL reactant structure with and without the SMD implicit solvent model.

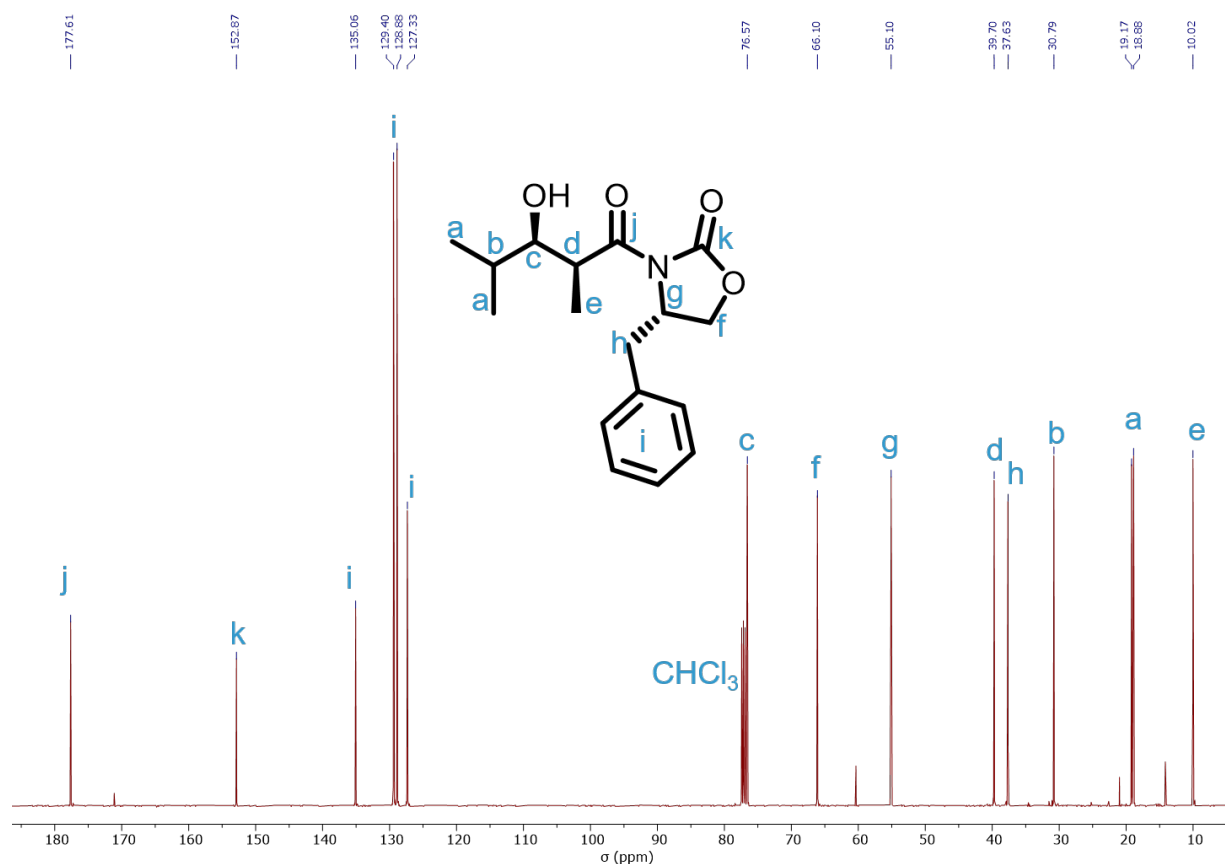
## Synthesis of Aldols

### (*S*)-4-Benzyl-3-((2*S*,3*R*)-3-hydroxy-2,4-dimethylpentanoyl)oxazolidin-2-one

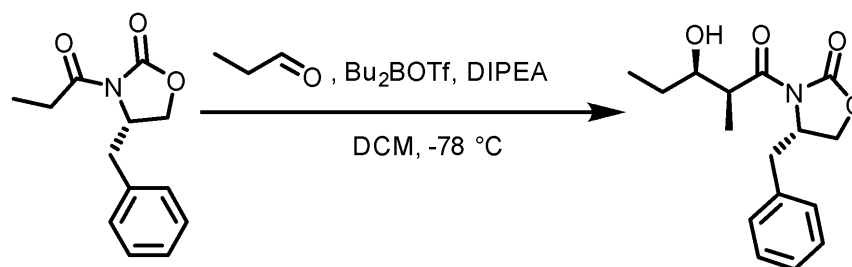


To a stirred solution of (*S*)-4-benzyl-3-propionyloxazolidin-2-one (20.0 g, 86.7 mmol) in DCM (200 mL) under argon atmosphere at  $0^\circ\text{C}$  was dropwisely added  $\text{Bu}_2\text{BOTf}$  (1.0 M in DCM, 100 mL, 100 mmol). Diisopropylethylamine (13.5 g, 104 mmol) was then slowly added to the reaction mixture. The reaction mixture was further stirred at  $0^\circ\text{C}$  for 30 min before cooling to  $-78^\circ\text{C}$ . Redistilled isobutyraldehyde (7.19 g, 99.7 mmol) was slowly added to the reaction mixture under stirring. After stirring the reaction for another 1 h at  $-78^\circ\text{C}$ , the reaction mixture was warmed up to  $0^\circ\text{C}$  and further stirred for 1 h. At  $0^\circ\text{C}$ , the reaction was quenched by slow addition of 350 mL methanol and 100 mL phosphate buffer (1.0 M, pH 7), followed by the slow addition of a solution of 30 wt%  $\text{H}_2\text{O}_2$  (125 mL) in methanol (150 mL). The reaction mixture was stirred for another 1 h before concentration *in vacuo*. The concentrated mixture was extracted by DCM (3 x 100 mL). The organic layers were combined, washed with sat. aq.  $\text{NaHCO}_3$  (100 mL) and brine (100 mL) before being dried over  $\text{MgSO}_4$ . The solvent was removed *in vacuo* to yield the crude product, which was purified by column chromatography (silica gel, 10-50% EtOAc in hexane) to give (*S*)-4-Benzyl-3-((2*S*,3*R*)-3-hydroxy-2,4-dimethylpentanoyl)oxazolidin-2-one as colorless crystalline solids (96% isolated yield,  $R_f = 0.46$ , 1:2 EtOAc/hexane);  $^1\text{H}$  NMR (500 MHz,  $\text{CDCl}_3$ )  $\delta$  ppm, 7.37–7.22 (m, 5H), 4.70 (m, 1H), 4.27–4.16 (m, 2H), 3.98 (dd,  $J = 7.0, 2.8$  Hz, 1H), 3.78 (qd, 7.2, 2.8 Hz, 1H), 3.26 (dd,  $J = 13.5, 3.3$  Hz, 1H), 3.01 (s, 1H), 2.82 (dd,  $J = 13.4, 9.4$  Hz, 1H), 1.74 (m, 1H), 1.26 (d,  $J = 7.2$  Hz, 3H), 1.05 (d,  $J = 6.7$  Hz, 3H), 0.93 (d,  $J = 6.9$  Hz, 3H);  $^{13}\text{C}$  NMR (126 MHz,  $\text{CDCl}_3$ )  $\delta$  ppm, 177.61, 152.87, 135.06, 129.40, 128.88, 127.33, 76.57, 66.10, 55.10, 39.70, 37.63, 30.79, 19.17, 18.88, 10.02.



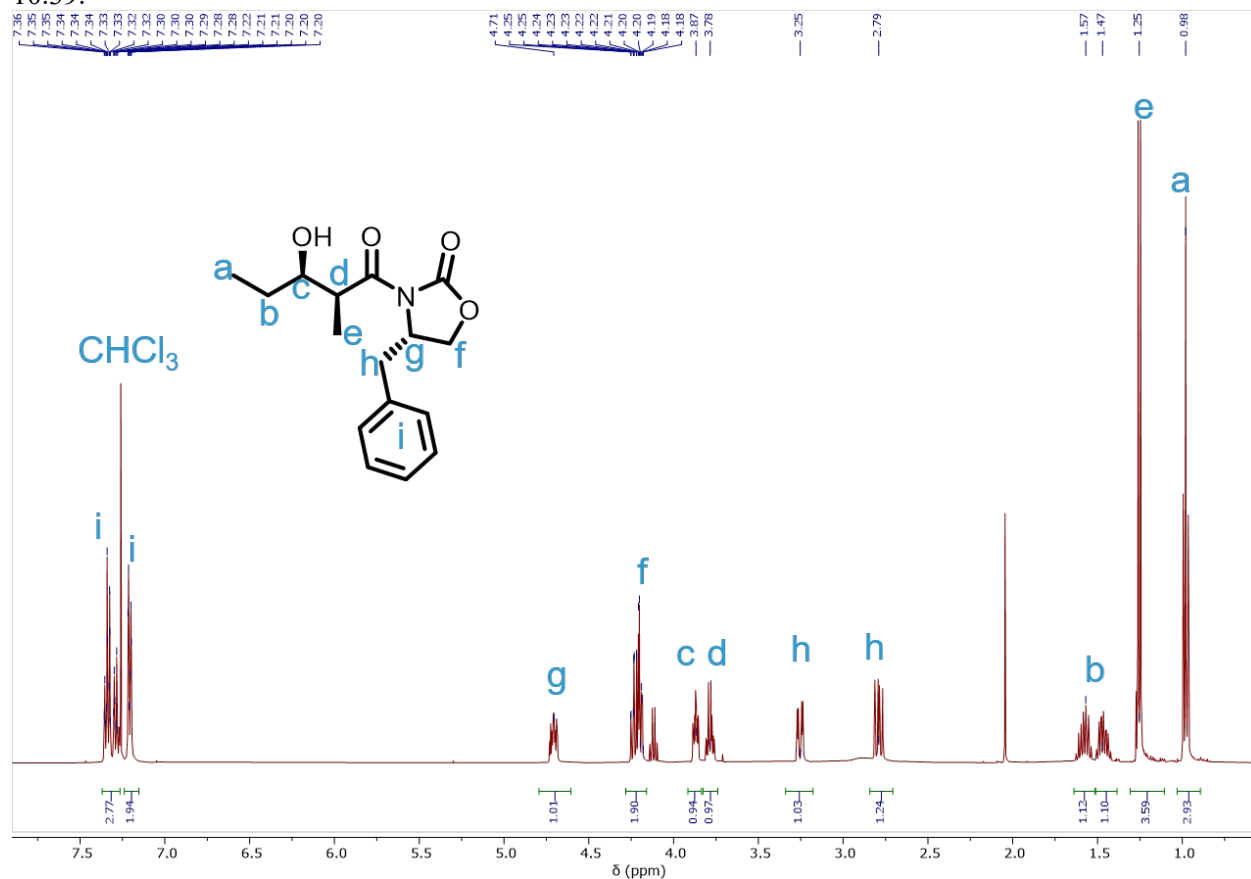


**(S)-4-benzyl-3-((2S,3R)-3-hydroxy-2-methylpentanoyl)oxazolidin-2-one**

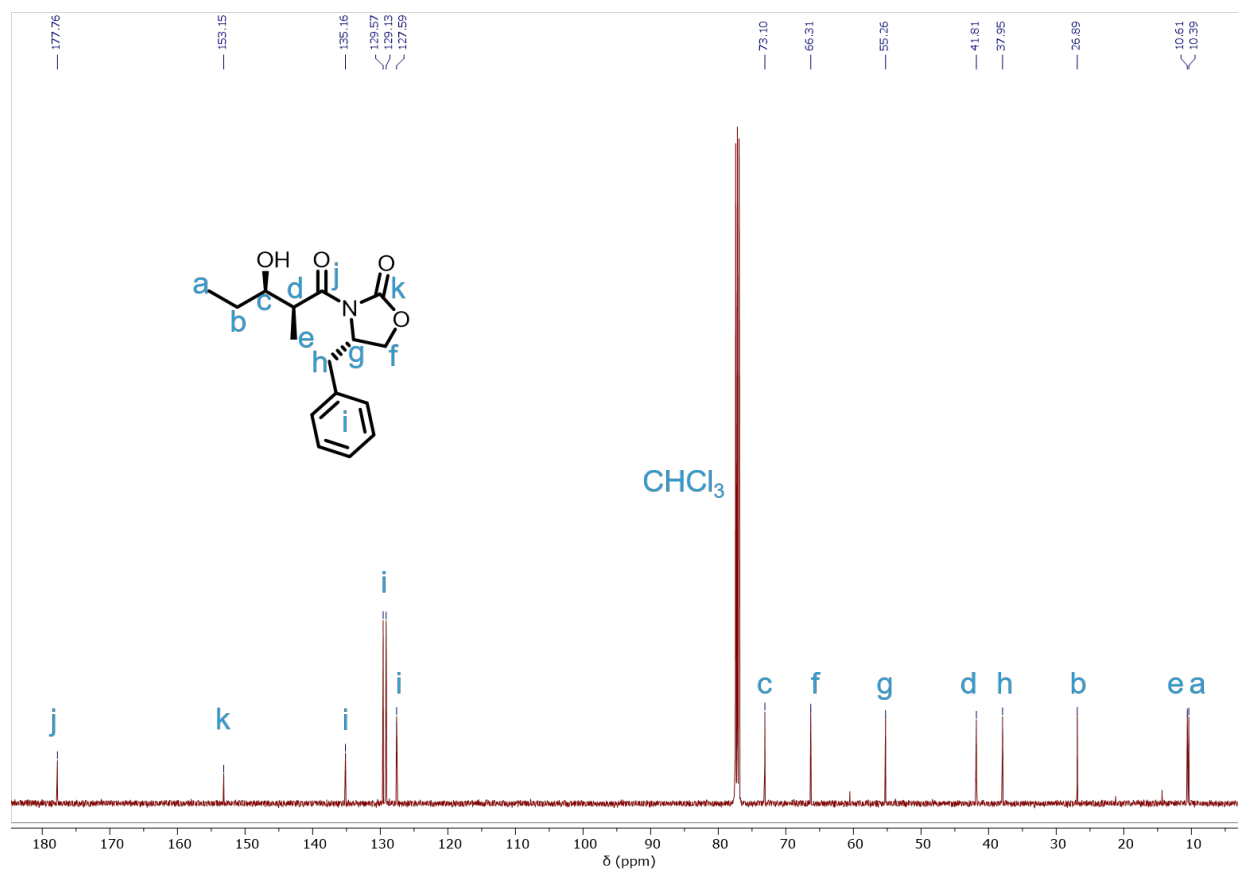


To a stirred solution of (S)-4-benzyl-3-propionyloxazolidin-2-one (4.85 g, 20.8 mmol) in anhydrous DCM (50 mL) under an argon atmosphere at  $0^\circ\text{C}$  was dropwisely added  $\text{Bu}_2\text{BOTf}$  (1.0 M in DCM, 22.9 mL, 22.9 mmol). Diisopropylethylamine (3.50 g, 27.0 mmol) was then slowly added to the reaction mixture. The reaction mixture was further stirred at  $0^\circ\text{C}$  for 30 min before cooling to  $-78^\circ\text{C}$ . Redistilled propionaldehyde (1.81 g, 31.2 mmol) was slowly added to the reaction mixture under stirring. After stirring the reaction for another 1 h at  $-78^\circ\text{C}$ , the reaction mixture was warmed up to  $0^\circ\text{C}$  and further stirred for 1 h. At  $0^\circ\text{C}$ , the reaction was quenched by slow addition of 70 mL methanol and 23 mL phosphate buffer (1.0 M, pH 7), followed by the slow addition of a solution of 30 wt%  $\text{H}_2\text{O}_2$  (25 mL) in methanol (30 mL). The reaction mixture was stirred for another 1 h before concentration *in vacuo*. The concentrated mixture was extracted by DCM (3 x 50 mL). All the organic layers were combined, washed with sat. aq.  $\text{NaHCO}_3$  (50 mL) and brine (50 mL) before being dried over  $\text{MgSO}_4$ . The solvent was removed *in vacuo* to yield the crude product, which was purified by column chromatography (silica gel, 10-50% EtOAc in hexane) to give (S)-4-benzyl-3-((2S,3R)-3-hydroxy-2-methylpentanoyl)oxazolidin-2-one as colorless crystalline solids (60% isolated yield,  $R_f = 0.46$ , 1:2 EtOAc/hexane);  $^1\text{H}$  NMR (500 MHz,  $\text{CDCl}_3$ )  $\delta$  ppm, 7.38–7.25 (m, 3H), 7.23–7.16 (m, 2H), 4.70 (ddt,  $J = 9.5, 7.6, 3.2$  Hz, 1H), 4.27–4.12 (m,

2H), 3.87 (ddd,  $J = 8.1, 5.1, 2.6$  Hz, 1H), 3.78 (qd,  $J = 7.1, 2.6$  Hz, 1H), 3.25 (dd,  $J = 13.4, 3.3$  Hz, 1H), 2.79 (dd,  $J = 13.4, 9.5$  Hz, 1H), 2.98-2.83 (b, 1H), 1.57 (ddq,  $J = 13.6, 8.4, 7.4$  Hz, 1H), 1.47 (ddq,  $J = 13.6, 8.4, 7.4$  Hz, 1H), 1.25 (d,  $J = 7.1$  Hz, 3H), 0.98 (t,  $J = 7.4$  Hz, 3H);  $^{13}\text{C}$  NMR (126 MHz,  $\text{CDCl}_3$ )  $\delta$  ppm, 177.76, 153.15, 135.16, 129.57, 129.13, 127.59, 73.10, 66.31, 55.26, 41.81, 37.95, 26.89, 10.61, 10.39.

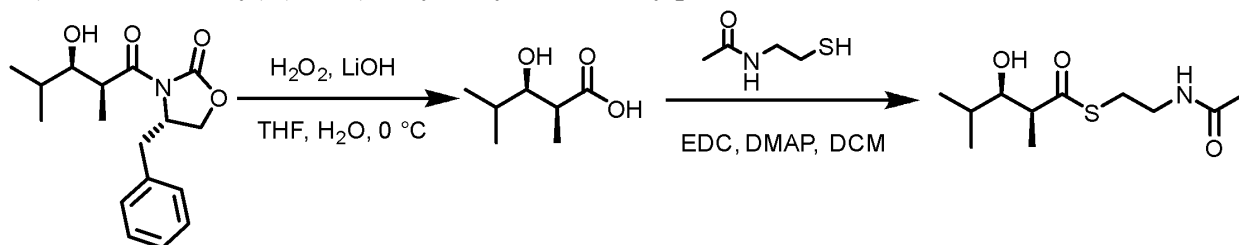






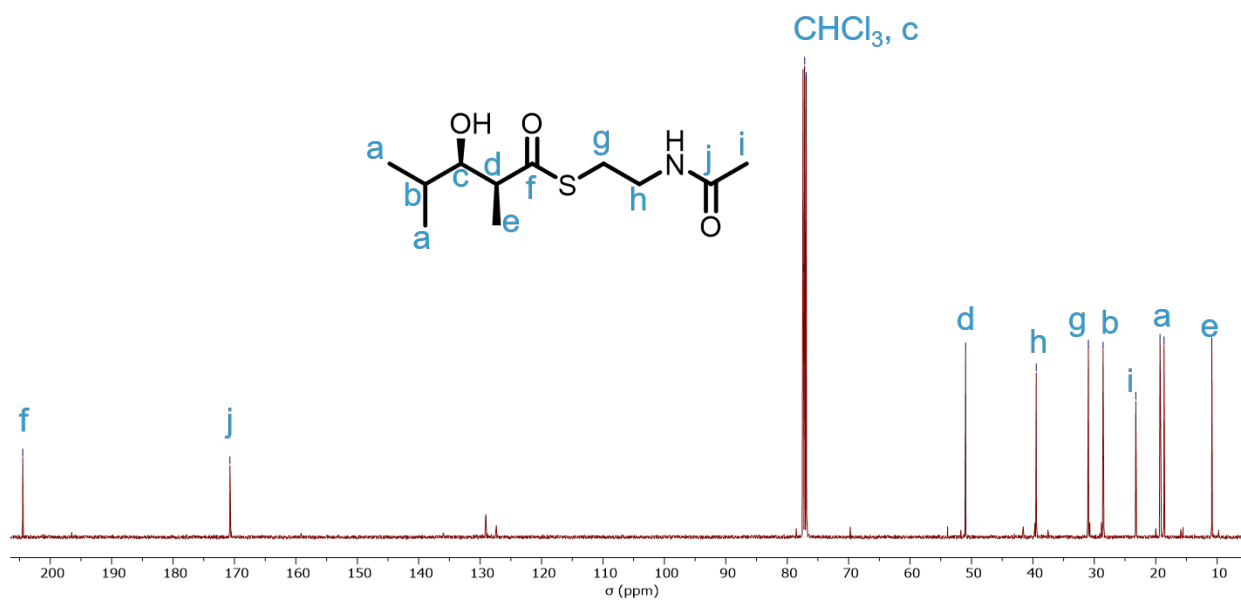
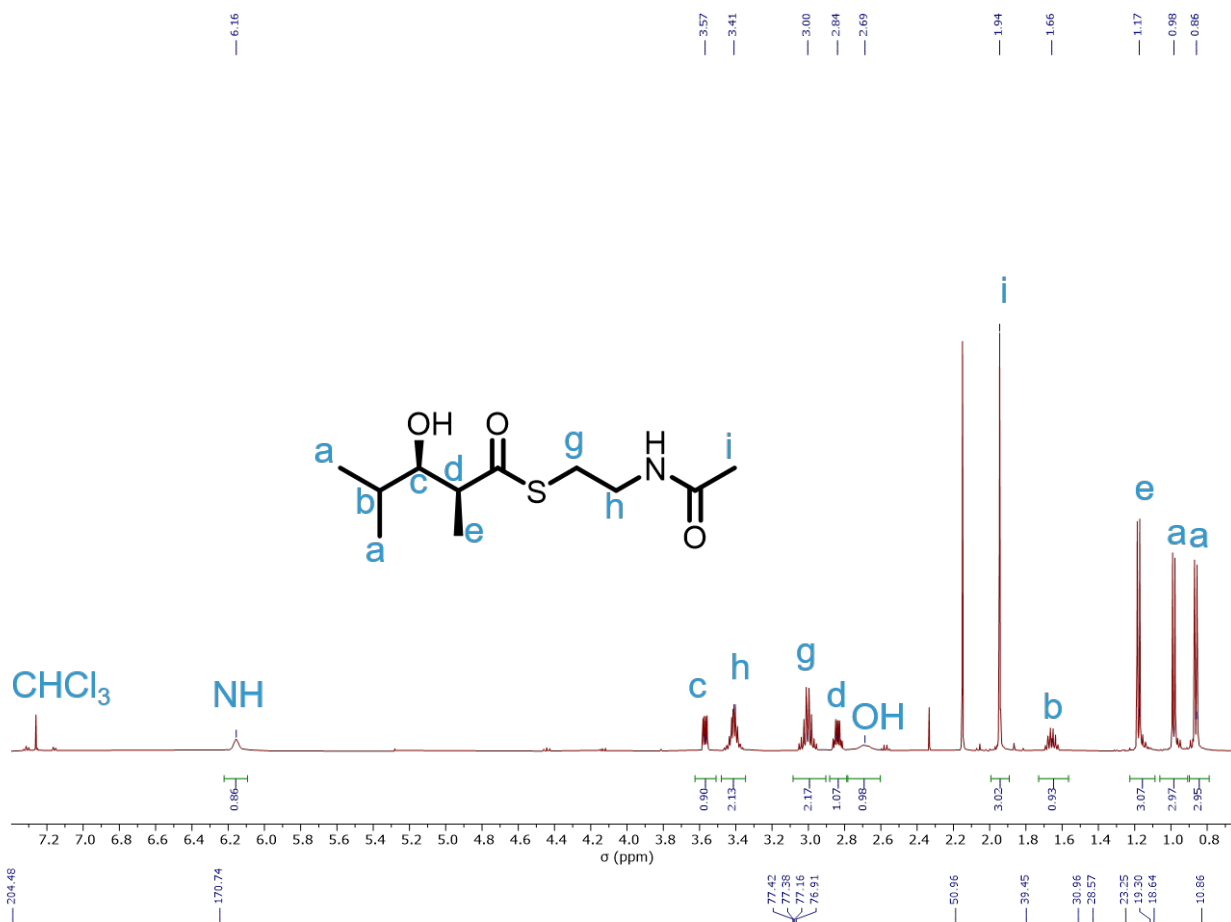
## Synthesis of 3-hydroxy alkyl thiolates (SNAC)

### *S*-(2-Acetamidoethyl) (2*S*,3*R*)-3-hydroxy-2,4-dimethylpentanethioate

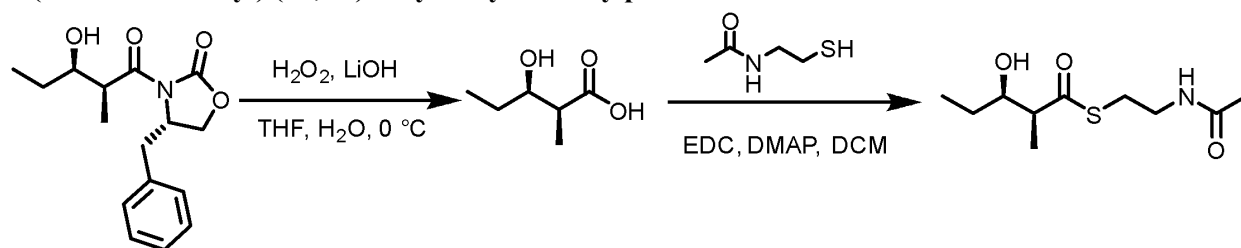


Aldol product ((*S*)-4-Benzyl-3-((2*S*,3*R*)-3-hydroxy-2,4-dimethylpentanoyl)oxazolidin-2-one) (3.20 g, 10.4 mmol) was dissolved in THF/H<sub>2</sub>O (30 mL, v/v = 4:1) to form a clear solution. The mixture was cooled to 0 °C, followed by slow addition of 30 wt% H<sub>2</sub>O<sub>2</sub> (25 mL) under stirring. LiOH (5.32 g, 218 mmol) in H<sub>2</sub>O (15 mL) was slowly added to the reaction, and the reaction mixture was further stirred for another 2 h at 0 °C before thin layer chromatography confirmed full consumption of aldol product. The reaction was quenched by the slow addition of sat. aq. Na<sub>2</sub>SO<sub>3</sub> (30 mL), and extracted by DCM (2 x 50 mL). The organic layers were combined and back-extracted by H<sub>2</sub>O (50 mL). The combined aqueous phase was cooled to 0 °C, and the pH was adjusted to 1 by HCl (2.0 M). The resultant mixture was extracted by EtOAc (3 x 50 mL). The organic layer was combined and washed brine (50 mL) before being dried over Na<sub>2</sub>SO<sub>4</sub>. The solvent was removed *in vacuo* to yield (2*S*,3*R*)-3-hydroxy-2,4-dimethylpentanoic acid (89% isolated yield), used without further purification.

(2*S*,3*R*)-3-hydroxy-2,4-dimethylpentanoic acid (1.36 g, 9.27 mmol) was then dissolved in anhydrous DCM (10 mL) under an argon atmosphere at 0 °C, followed by the addition of EDC (3.56 g, 18.5 mmol) in anhydrous DCM (10 mL) with stirring. The reaction mixture was further stirred for another 20 min before dropwise addition of a solution of *N*-acetylcysteine (1.23 g, 11.1 mmol) and DMAP (56.6 mg, 0.46 mmol) in anhydrous DCM (10 mL). The reaction was allowed to stir for another 4 h at 0 °C and then warmed up to r.t. and further stirred overnight. Brine (40 mL) was added to the mixture to quench the reaction, and the organic layer was separated. The aqueous layer was extracted by EtOAc (3 x 50 mL), and all the organic layers were combined, washed with brine (50 mL) before being dried over Na<sub>2</sub>SO<sub>4</sub>. The solvent was removed *in vacuo* to yield the crude product, which was purified by column chromatography (silica gel, 10-60% acetone in hexane) to give *S*-(2-Acetamidoethyl) (2*S*,3*R*)-3-hydroxy-2,4-dimethylpentanethioate as pale-yellow oil (44% isolated yield, *R*<sub>f</sub> = 0.30, 1:1 acetone/hexane); <sup>1</sup>H NMR (500 MHz, CDCl<sub>3</sub>) δ ppm 6.16 (br, 1H), 3.57 (dd, *J* = 7.7, 3.8 Hz, 1H), 3.45–3.33 (m, 2H), 3.07–2.93 (m, 2H), 2.84 (qd, *J* = 7.1, 3.9 Hz, 1H), 2.69 (br, 1H), 1.94 (s, 3H), 1.73–1.58 (m, 1H), 1.17 (d, *J* = 7.0 Hz, 3H), 0.98 (d, *J* = 6.6 Hz, 3H), 0.86 (d, *J* = 6.8 Hz, 3H); <sup>13</sup>C NMR (126 MHz, CDCl<sub>3</sub>) δ ppm, 204.48, 170.74, 77.38, 50.96, 39.45, 30.96, 28.57, 23.25, 19.30, 18.64, 10.86.

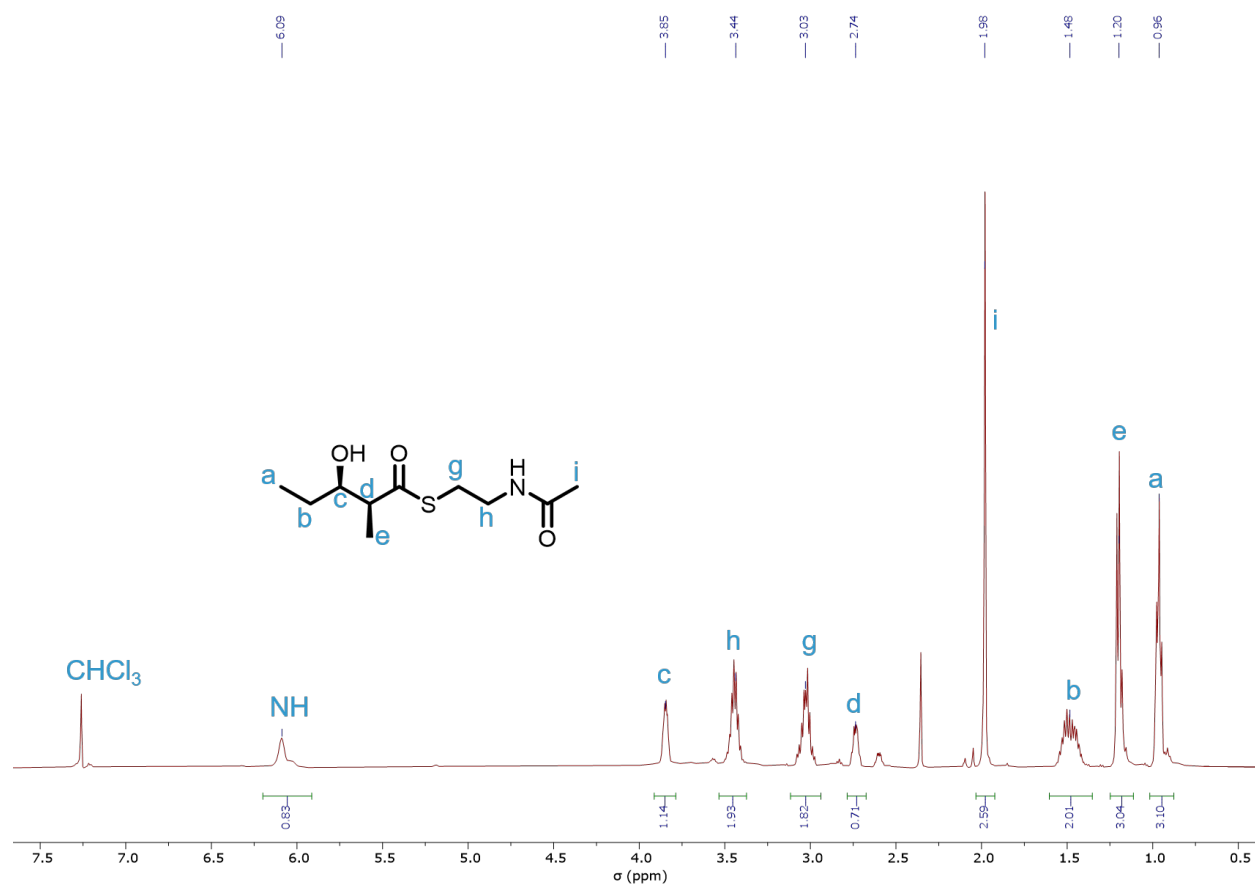


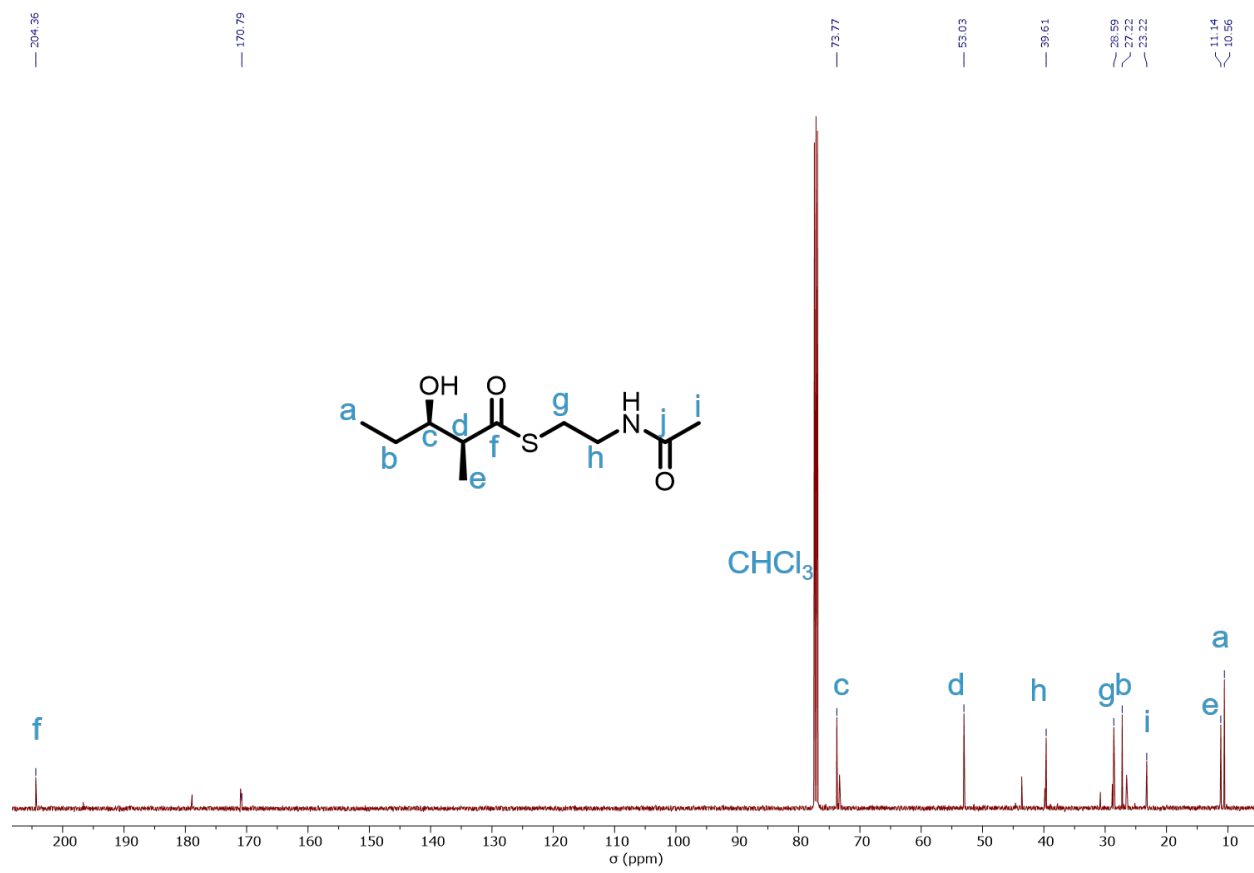
***S*-(2-acetamidoethyl) (2*S*,3*R*)-3-hydroxy-2-methylpentanethioate**



Aldol product ((*S*)-4-benzyl-3-((2*S*,3*R*)-3-hydroxy-2-methylpentanoyl)oxazolidin-2-one) (1.93 g, 6.61 mmol) was dissolved in  $\text{THF}/\text{H}_2\text{O}$  (17 mL, v/v = 4:1) to form a clear solution. The mixture was cooled to  $0\text{ }^\circ\text{C}$ , followed by slow addition of 30 wt%  $\text{H}_2\text{O}_2$  (17 mL) under stirring.  $\text{LiOH}$  (3.31 g, 138 mmol) in  $\text{H}_2\text{O}$  (7 mL) was slowly added to the reaction, and the reaction mixture was further stirred for another 2 h at  $0\text{ }^\circ\text{C}$  before thin layer chromatography confirmed full consumption of aldol product. The reaction was quenched by the slow addition of sat. aq.  $\text{Na}_2\text{SO}_3$  (17 mL), and extracted by  $\text{DCM}$  (2 x 50 mL). All the organic layers were combined and back-extracted by  $\text{H}_2\text{O}$  (50 mL). The combined aqueous phase was cooled to  $0\text{ }^\circ\text{C}$ , and the pH was adjusted to 1 by  $\text{HCl}$  (2.0 M). The resultant mixture was extracted by  $\text{EtOAc}$  (3 x 50 mL). The organic layer was combined and washed brine (50 mL) before being dried over  $\text{Na}_2\text{SO}_4$ . The solvent was removed *in vacuo* to yield (2*S*,3*R*)-3-hydroxy-2-methylpentanoic acid (92% isolated yield), used without further purification.

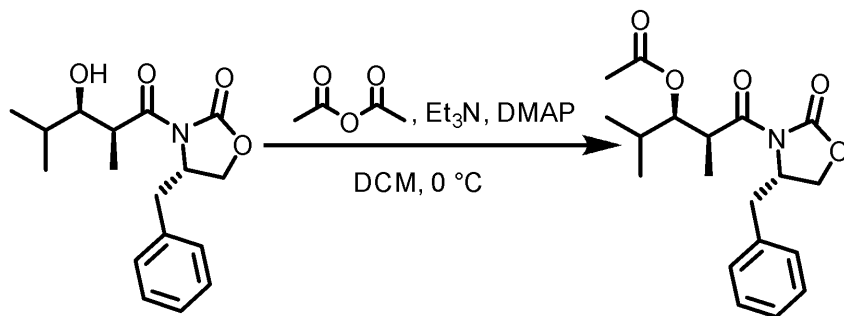
(2*S*,3*R*)-3-hydroxy-2-methylpentanoic acid (802 mg, 6.07 mmol) was then dissolved in anhydrous  $\text{DCM}$  (5 mL) under an argon atmosphere at  $0\text{ }^\circ\text{C}$ , followed by the addition of EDC (2.33 g, 12.1 mmol) in anhydrous  $\text{DCM}$  (5 mL) with stirring. The reaction mixture was further stirred for another 20 min before dropwise addition of a solution of *N*-acetylcysteine (802 mg, 7.28 mmol) and DMAP (37 mg, 0.3 mmol) in anhydrous  $\text{DCM}$  (5 mL). The reaction was allowed to stir for another 4 h at  $0\text{ }^\circ\text{C}$  and then warmed up to r.t. and further stirred overnight. Brine (20 mL) was added to the mixture to quench the reaction, and the organic layer was separated. The aqueous layer was extracted by  $\text{EtOAc}$  (3 x 25 mL), and all the organic layers were combined, washed with brine (50 mL) before being dried over  $\text{Na}_2\text{SO}_4$ . The solvent was removed *in vacuo* to yield the crude product, which was purified by column chromatography (silica gel, 10-60% acetone in hexane) to give *S*-(2-acetamidoethyl) (2*S*,3*R*)-3-hydroxy-2-methylpentanethioate as pale-yellow oil (58% isolated yield,  $R_f$  = 0.3, 1:1 acetone/hexane);  $^1\text{H}$  NMR (500 MHz,  $\text{CDCl}_3$ )  $\delta$  ppm, 6.16–5.97 (br, 1H), 3.93–3.77 (m, 2H), 3.53–3.37 (m, 2H), 3.10–2.96 (m, 2H), 2.80–2.69 (m, 1H), 1.98 (s, 3H), 1.59–1.37 (m, 2H), 1.20 (t,  $J$  = 7.5 Hz, 3H), 0.95 (t,  $J$  = 7.5 Hz, 3H);  $^{13}\text{C}$  NMR (126 MHz,  $\text{CDCl}_3$ )  $\delta$  ppm, 204.36, 170.79, 73.77, 53.03, 39.61, 28.59, 27.22, 23.22, 11.14, 10.56.



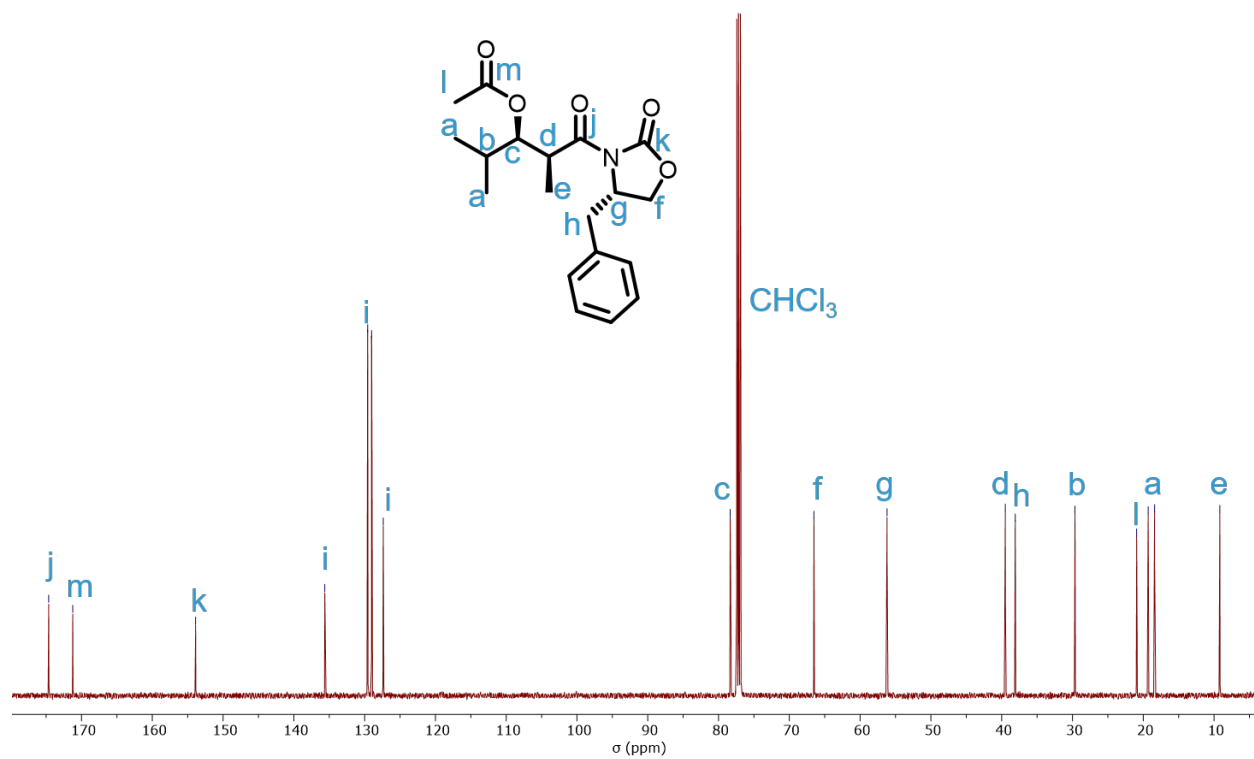
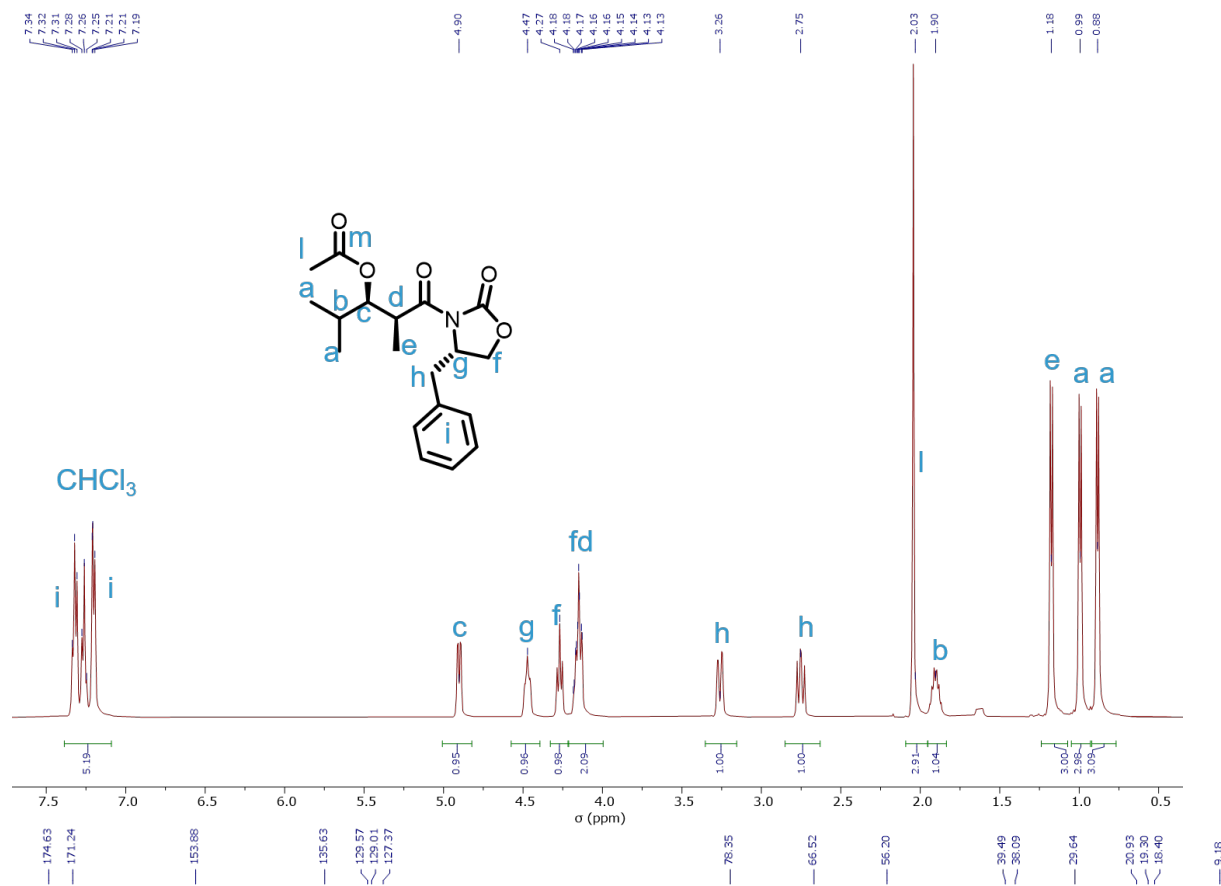


## Synthesis of Beta-keto-lactone (BKDL)

### (2*S*,3*R*)-1-((*S*)-4-benzyl-2-oxooxazolidin-3-yl)-2,4-dimethyl-1-oxopentan-3-yl acetate

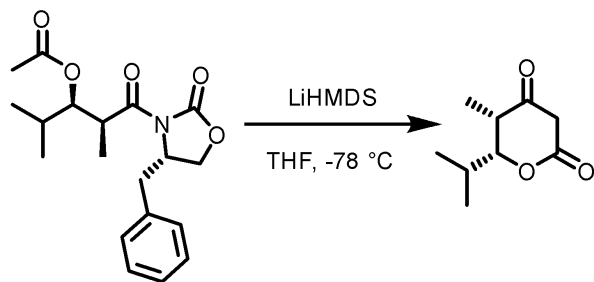


Et<sub>3</sub>N (9.95 g, 98.4 mmol) was added to a stirred solution of (*S*)-4-Benzyl-3-((2*S*,3*R*)-3-hydroxy-2,4-dimethylpentanoyl)oxazolidin-2-one (22.0 g, 75.7 mmol) in anhydrous DCM (200 mL), followed by the addition of freshly distilled acetic anhydride (9.27 g, 90.8 mmol). The solution mixture was cooled to 0 °C, and a solution of DMAP (1.85 g, 15.1 mmol) in DCM (5 mL) was dropwise added. The reaction was allowed to stir at 0 °C for 30 min before warmed up to r.t. and further reacted for another 90 min. The reaction was then quenched by the addition of sat. aq. NH<sub>4</sub>Cl (200 mL) and the aqueous phase was separated and extracted by DCM (2 x 100 mL). All the organic layers were combined, washed with brine (100 mL) before being dried over Na<sub>2</sub>SO<sub>4</sub>. The solvent was removed *in vacuo* to yield the crude product, which was purified by column chromatography (silica gel, 5-30% EtOAc in hexane) to give (2*S*,3*R*)-1-((*S*)-4-benzyl-2-oxooxazolidin-3-yl)-2,4-dimethyl-1-oxopentan-3-yl acetate as colorless crystals (81% isolated yield, R<sub>f</sub> = 0.55, 1:3 EtOAc/hexane); <sup>1</sup>H NMR (500 MHz, CDCl<sub>3</sub>) δ ppm, 7.37–7.08 (m, 5H), 4.90 (dd, *J* = 9.3, 2.9 Hz, 1H), 4.47 (m, 1H), 4.27 (dd, *J* = 8.4, 8.1 Hz, 1H), 4.21–4.03 (m, 2H), 3.26 (dd, *J* = 13.4, 3.4 Hz, 1H), 2.75 (dd, *J* = 13.3, 9.9 Hz, 1H), 2.03 (s, 3H), 1.90 (m, 1H), 1.18 (d, *J* = 6.9 Hz, 3H), 0.99 (d, *J* = 6.8 Hz, 3H), 0.88 (d, *J* = 6.6 Hz, 3H); <sup>13</sup>C NMR (126 MHz, CDCl<sub>3</sub>) δ ppm, 174.63, 171.24, 153.88, 135.63, 129.57, 129.01, 127.37, 78.35, 66.52, 56.20, 39.49, 38.09, 29.64, 20.93, 19.30, 18.40, 9.18.

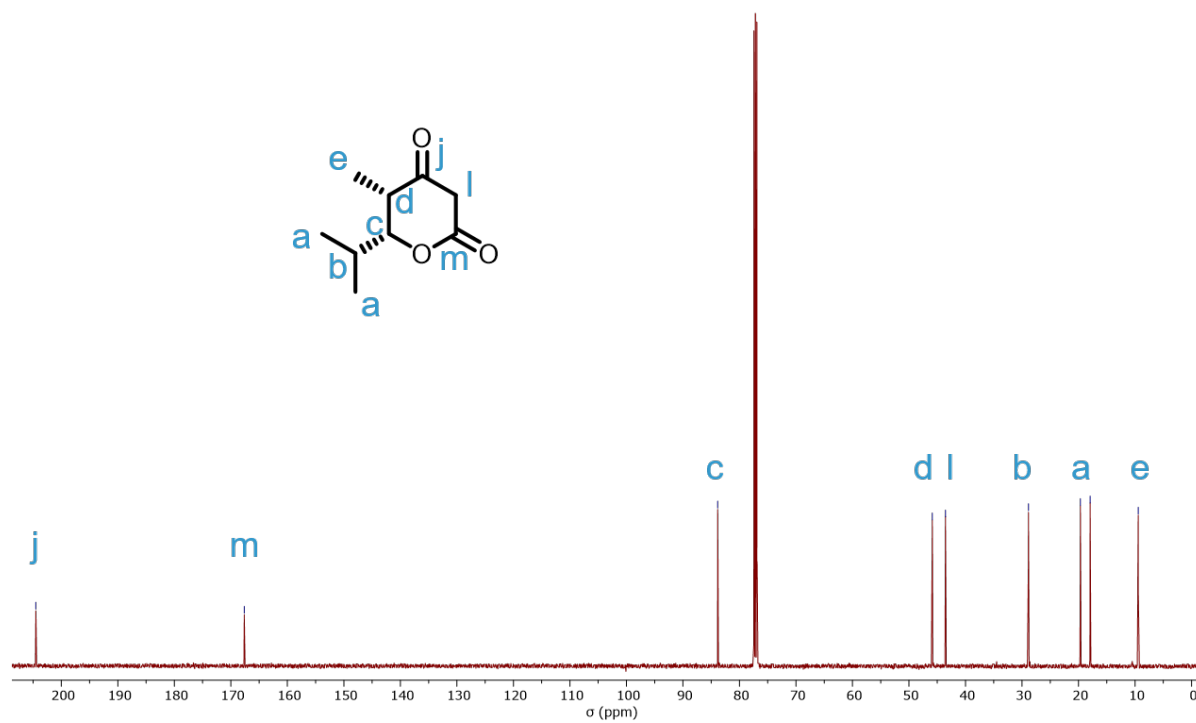
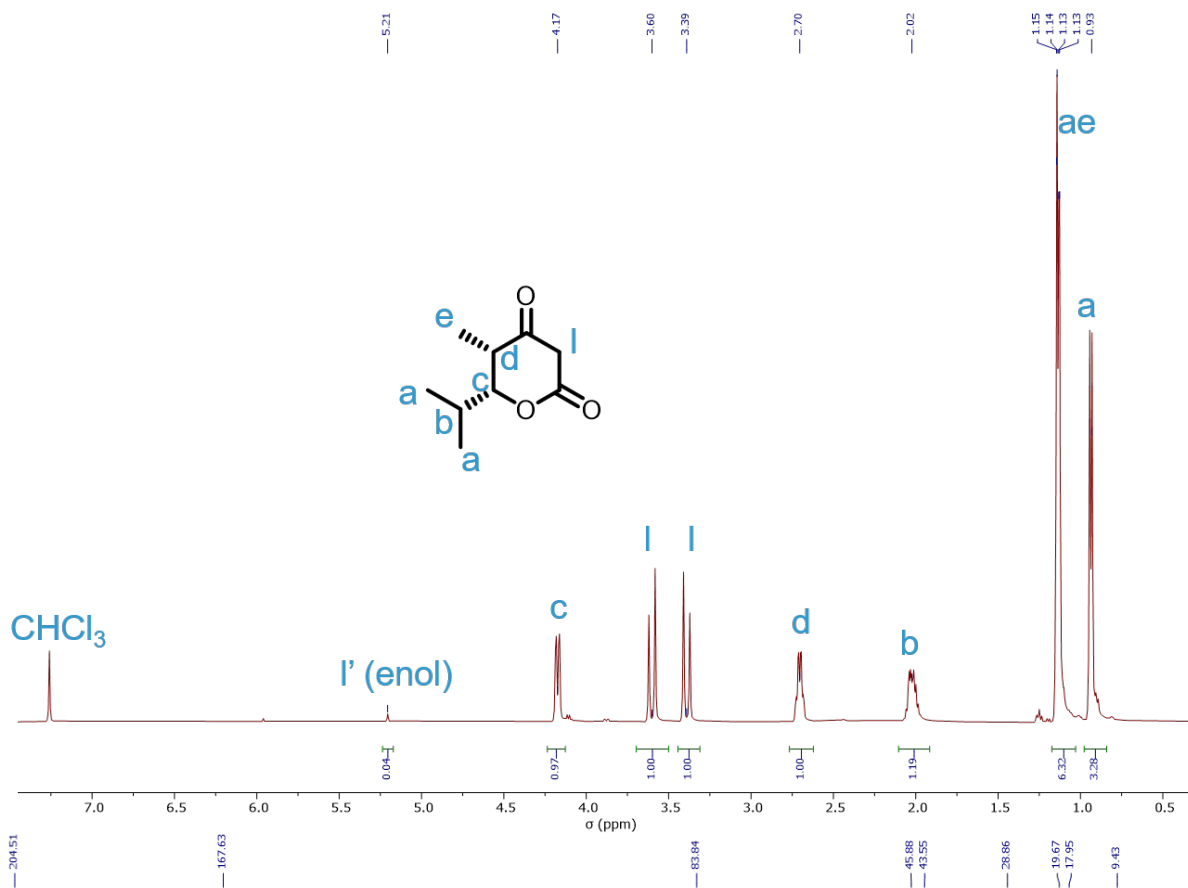


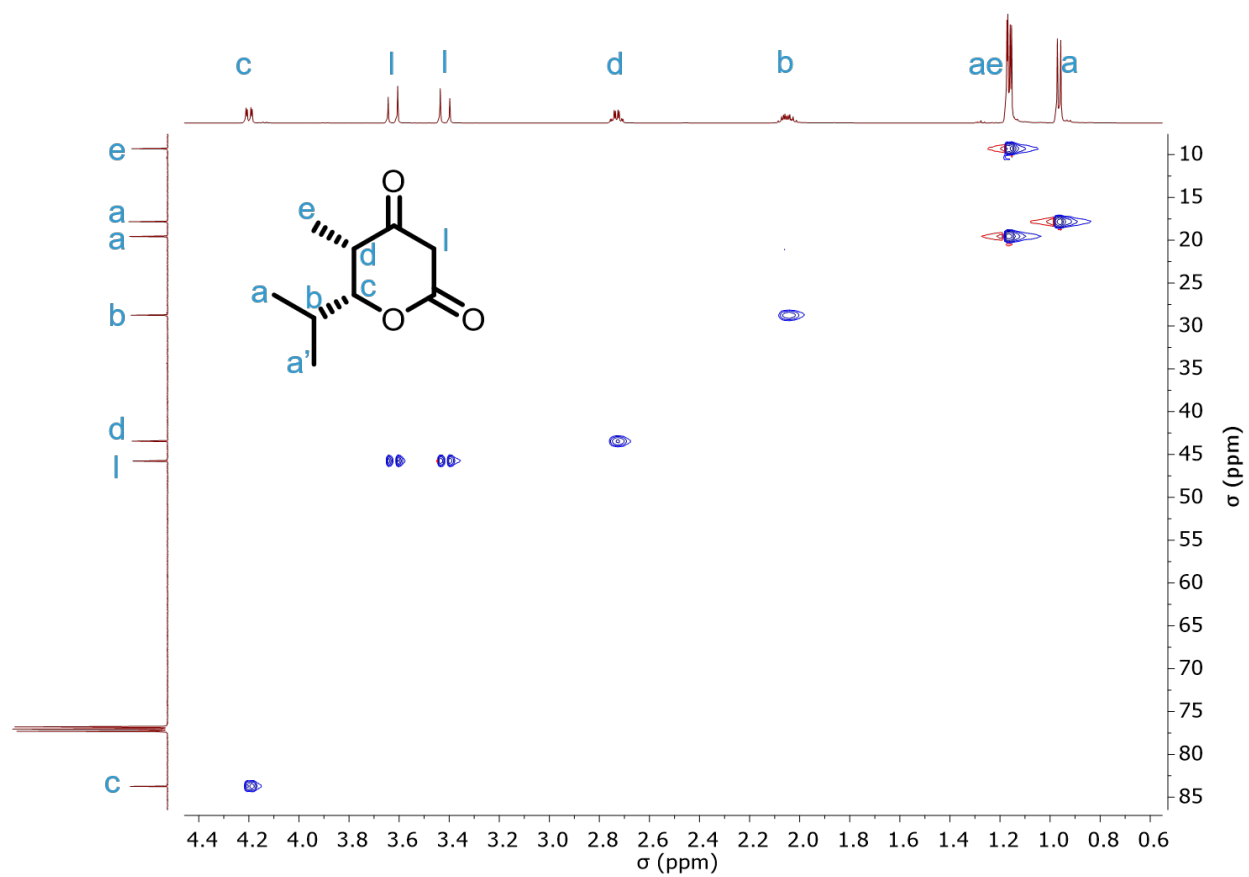


**(5*S*,6*R*)-6-isopropyl-5-methyldihydro-2*H*-pyran-2,4(3*H*)-dione (BKDL 5)**

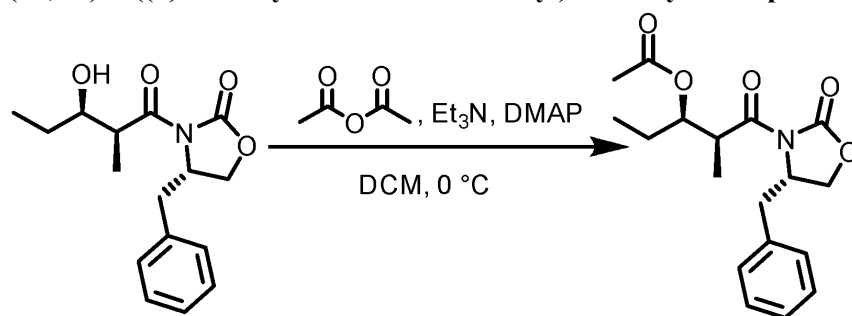


Acetate (2*S*,3*R*)-1-((*S*)-4-benzyl-2-oxooxazolidin-3-yl)-2,4-dimethyl-1-oxopentan-3-yl acetate (3.13 g, 9.01 mmol) was dissolved in anhydrous THF (50 mL), and the solution was cooled to -78 °C, followed by dropwise addition of a pre-cooled (-78 °C) solution of LiHMDS in THF (1.0 M, 50 mL) under vigorous stirring. The reaction was further allowed to stir for 1 h before quenched by a solution mixture of sat. NH<sub>4</sub>Cl/H<sub>2</sub>O/MeOH (v:v:v = 1:1:1, 250 mL). EtOAc (150 mL) was added to the solution, and the aqueous phase was separated and acidified to pH <2 by HCl (2.0 M). The mixture was extracted by DCM (3 x 50 mL), and all the DCM layers were combined before being dried over Na<sub>2</sub>SO<sub>4</sub>. The solvent was removed *in vacuo* to yield the crude product, which was purified by column chromatography (silica gel, 10-60% EtOAc in hexane) to give BKDL **5** as white solids (75% isolated yield, *R*<sub>f</sub> = 0.42, 1:1 EtOAc/hexane); <sup>1</sup>H NMR (500 MHz, CDCl<sub>3</sub>) δ ppm, 5.21 (s, 1H, enol isomer), 4.17 (dd, *J* = 9.8, 2.5 Hz, 1H), 3.60 (d, *J* = 18.9 Hz, 1H), 3.39 (d, *J* = 19.0 Hz, 1H), 2.70 (qd, *J* = 7.5, 2.4 Hz, 1H), 2.02 (dt, *J* = 9.9, 6.6 Hz, 1H), 1.14 (d, *J* = 6.6 Hz, 3H), 1.13 (d, *J* = 7.4 Hz, 3H), 0.93 (d, *J* = 6.8 Hz, 3H); <sup>13</sup>C NMR (126 MHz, CDCl<sub>3</sub>) δ ppm, 204.51, 167.63, 83.84, 45.88, 43.55, 28.86, 19.67, 17.95, 9.43.

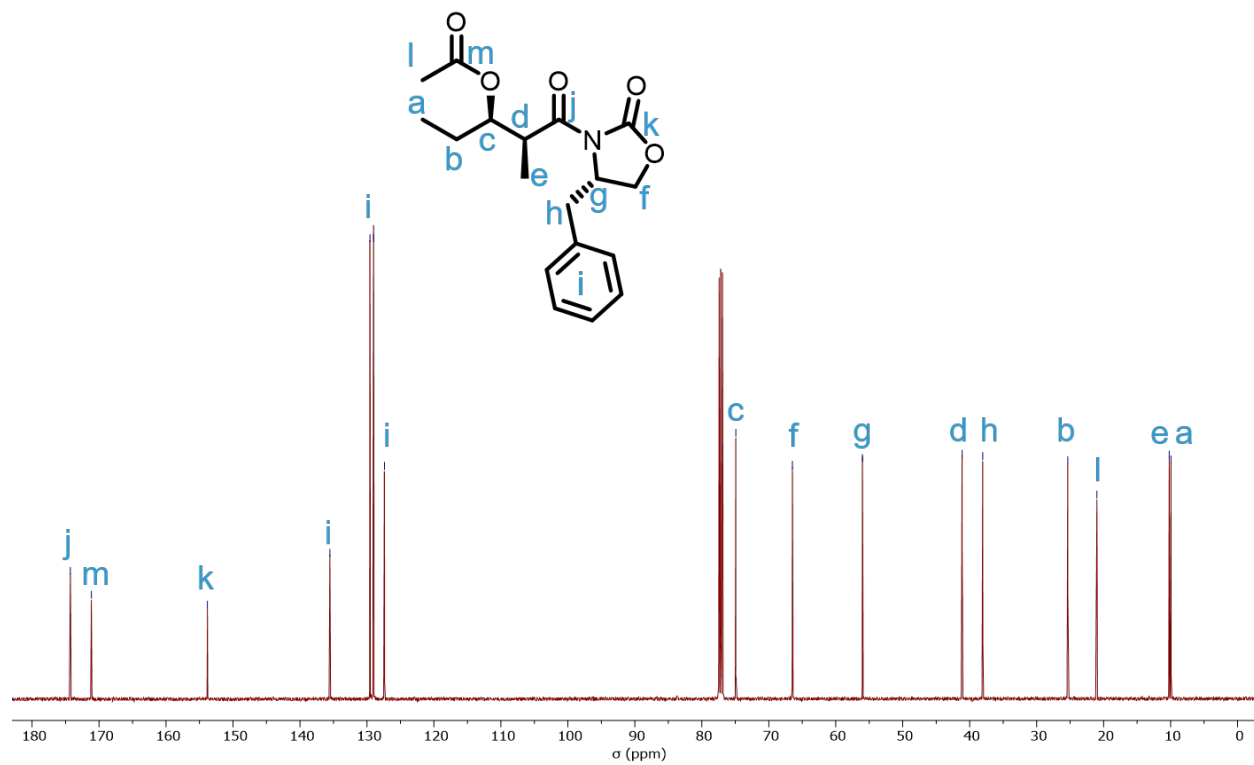
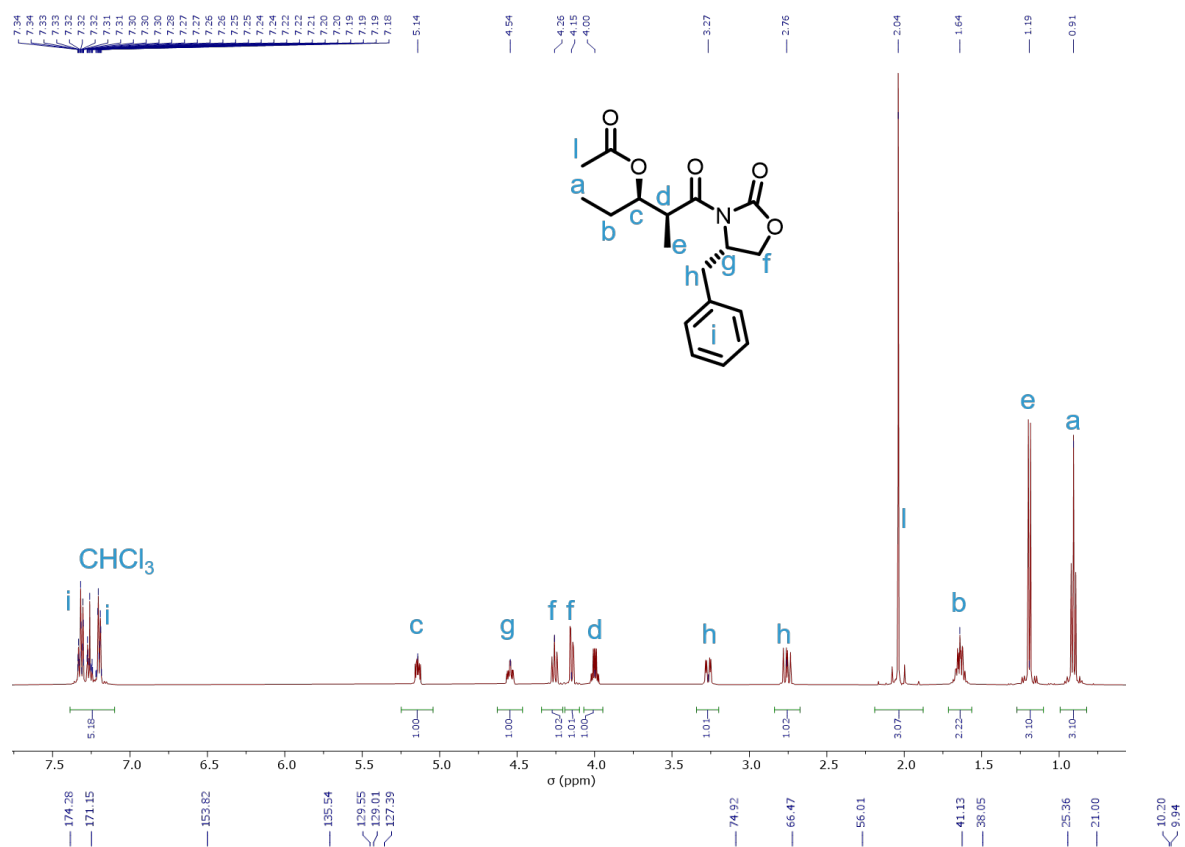




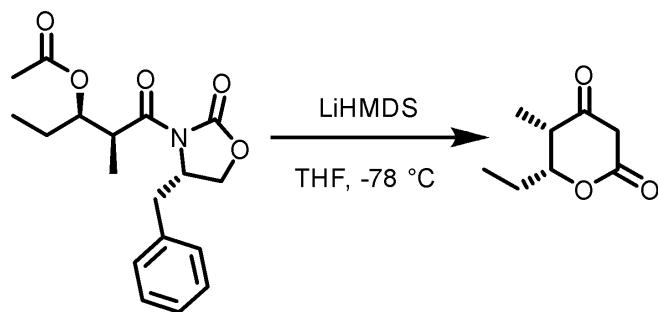
**(2*S*,3*R*)-1-((*S*)-4-benzyl-2-oxooxazolidin-3-yl)-2-methyl-1-oxopentan-3-yl acetate**



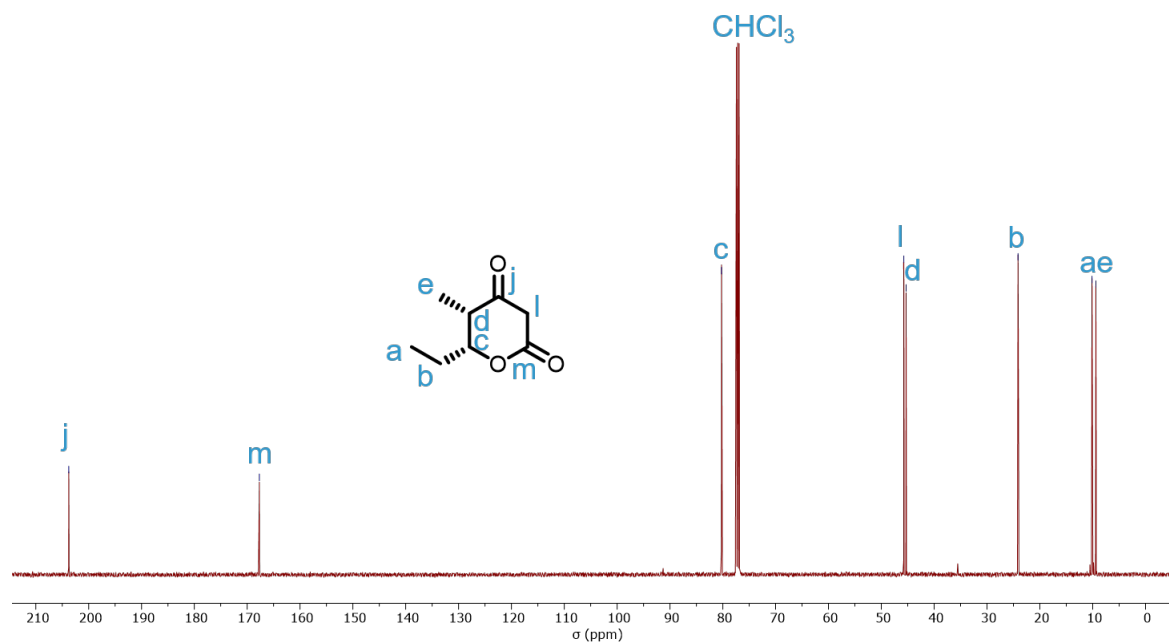
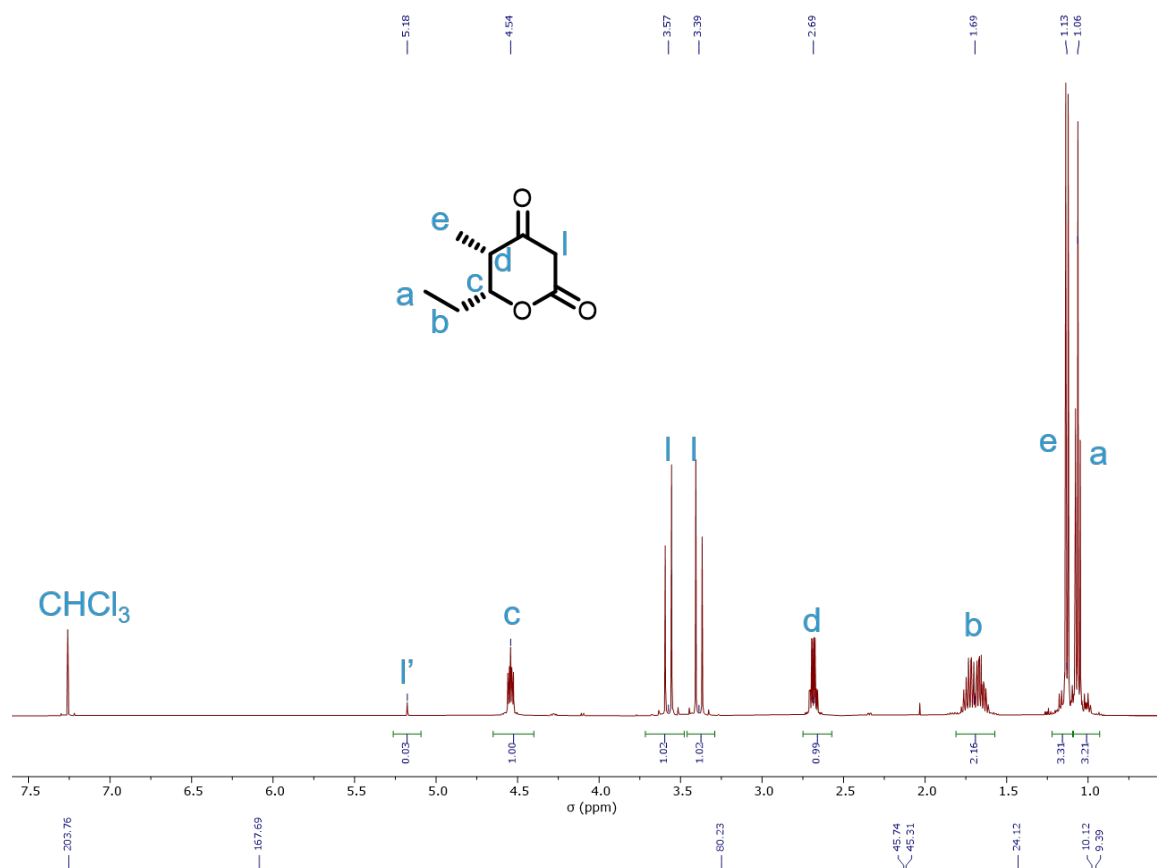
Et<sub>3</sub>N (12.64 g, 125 mmol) was added to a stirred solution of (*S*)-4-benzyl-3-((2*S*,3*R*)-3-hydroxy-2-methylpentanoyl)oxazolidin-2-one (28.0 g, 96.1 mmol) in anhydrous DCM (200 mL), followed by the addition of freshly distilled acetic anhydride (11.8 g, 115 mmol). The solution mixture was cooled to 0 °C, and a solution of DMAP (2.35 g, 19.2 mmol) in DCM (7 mL) was dropwise added. The reaction was allowed to stir at 0 °C for 30 min before warmed up to r.t. and further reacted for another 90 min. The reaction was then quenched by the addition of sat. aq. NH<sub>4</sub>Cl (200 mL) and the aqueous phase was separated and extracted by DCM (2 x 100 mL). All the organic layers were combined, washed with brine (100 mL) before being dried over Na<sub>2</sub>SO<sub>4</sub>. The solvent was removed *in vacuo* to yield the crude product, which was purified by column chromatography (silica gel, 5-30% EtOAc in hexane) to give (2*S*,3*R*)-1-((*S*)-4-benzyl-2-oxooxazolidin-3-yl)-2-methyl-1-oxopentan-3-yl acetate as colorless crystals (57% isolated yield, R<sub>f</sub> = 0.46, 1:3 EtOAc/hexane); <sup>1</sup>H NMR (500 MHz, CDCl<sub>3</sub>) δ ppm, 7.40–7.12 (m, 5H), 5.14 (ddd, *J* = 8.0, 5.7, 3.4 Hz, 1H), 4.54 (dddd, *J* = 9.8, 7.6, 3.4, 2.2 Hz, 1H), 4.26 (dd, *J* = 8.7, 7.7 Hz, 1H), 4.15 (dd, *J* = 8.9, 2.3 Hz, 1H), 4.00 (qd, *J* = 6.9, 3.4 Hz, 1H), 3.27 (dd, *J* = 13.4, 3.5 Hz, 1H), 2.76 (dd, *J* = 13.4, 9.8 Hz, 1H), 2.04 (s, 3H), 1.71 – 1.56 (m, 2H), 1.19 (d, *J* = 6.9 Hz, 3H), 0.91 (t, *J* = 7.4 Hz, 3H); <sup>13</sup>C NMR (126 MHz, CDCl<sub>3</sub>) δ ppm, 174.28, 171.15, 153.82, 135.54, 129.55, 129.01, 127.39, 74.92, 66.47, 56.01, 41.13, 38.05, 25.36, 21.00, 10.20, 9.94.

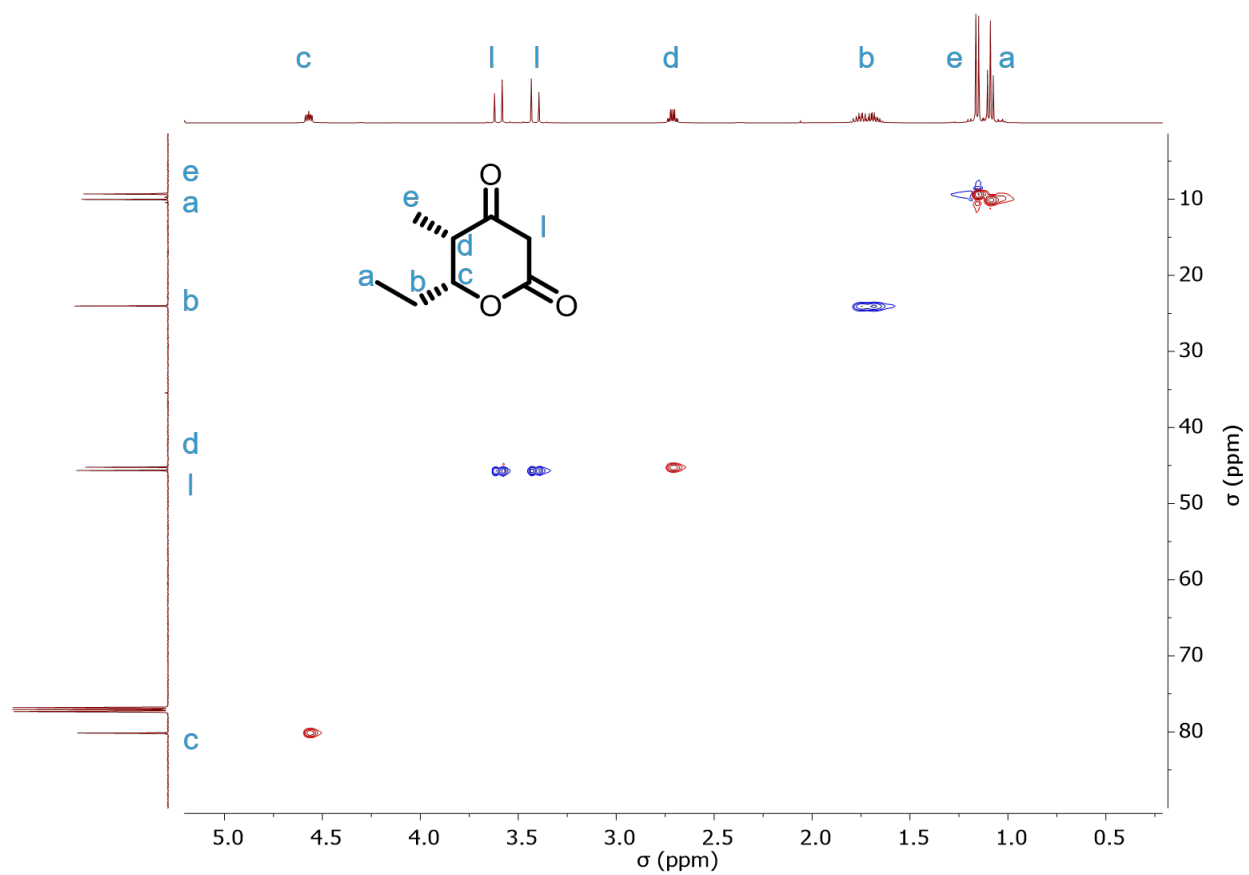


**(5*S*,6*R*)-6-ethyl-5-methyldihydro-2*H*-pyran-2,4(3*H*)-dione (BKDL 2)**



Acetate (2*S*,3*R*)-1-((*S*)-4-benzyl-2-oxooxazolidin-3-yl)-2-methyl-1-oxopentan-3-yl acetate (18.0 g, 54.0 mmol) was dissolved in anhydrous THF (250 mL), and the solution was cooled to -78 °C, followed by dropwise addition of a pre-cooled (-78 °C) solution of LiHMDS in THF (1.0 M, 270 mL) under vigorous stirring. The reaction was further allowed to stir for 1 h before quenched by a solution mixture of sat. NH<sub>4</sub>Cl/H<sub>2</sub>O/MeOH (v:v:v = 1:1:1, 1800 mL). EtOAc (500 mL) was added to the solution, and the aqueous phase was separated and acidified to pH <2 by HCl (2.0 M). The mixture was extracted by DCM (3 x 150 mL), and all the DCM layers were combined before being dried over Na<sub>2</sub>SO<sub>4</sub>. The solvent was removed *in vacuo* to yield the crude product, which was purified by column chromatography (silica gel, 10-60% EtOAc in hexane) to give BKDL 2 as white solids (72% isolated yield, *R*<sub>f</sub> = 0.43, 1:1 EtOAc/hexane); <sup>1</sup>H NMR (500 MHz, CDCl<sub>3</sub>) δ ppm, 5.18 (s, 1H, enol isomer), 4.54 (ddd, *J* = 8.7, 5.1, 3.3 Hz, 2H), 3.57 (d, *J* = 19.6 Hz, 1H), 3.39 (d, *J* = 19.6 Hz, 1H), 2.69 (qd, *J* = 7.4, 3.3 Hz, 1H), 1.93 – 1.42 (m, 2H), 1.13 (d, *J* = 7.4 Hz, 3H), 1.06 (t, *J* = 7.4 Hz, 3H). <sup>13</sup>C NMR (126 MHz, CDCl<sub>3</sub>) δ ppm, 203.76, 167.69, 80.23, 45.74, 45.31, 24.12, 10.12, 9.39.

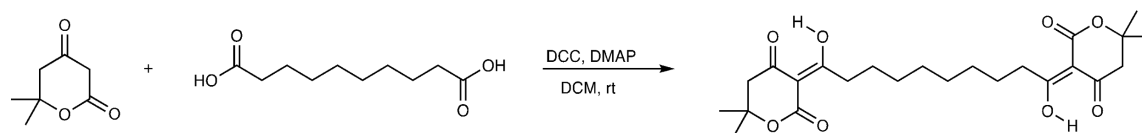




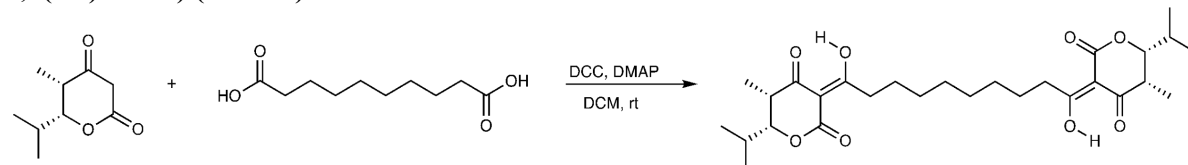


## Synthesis of Triketone Monomers

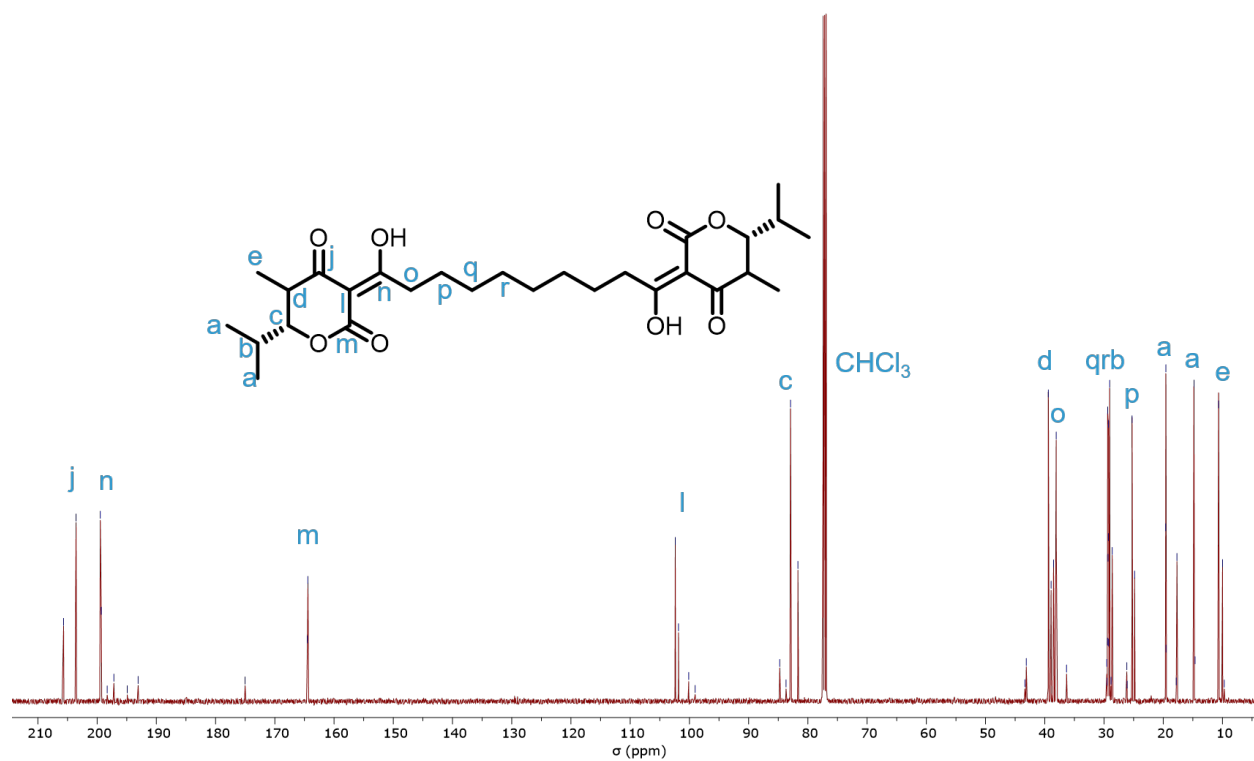
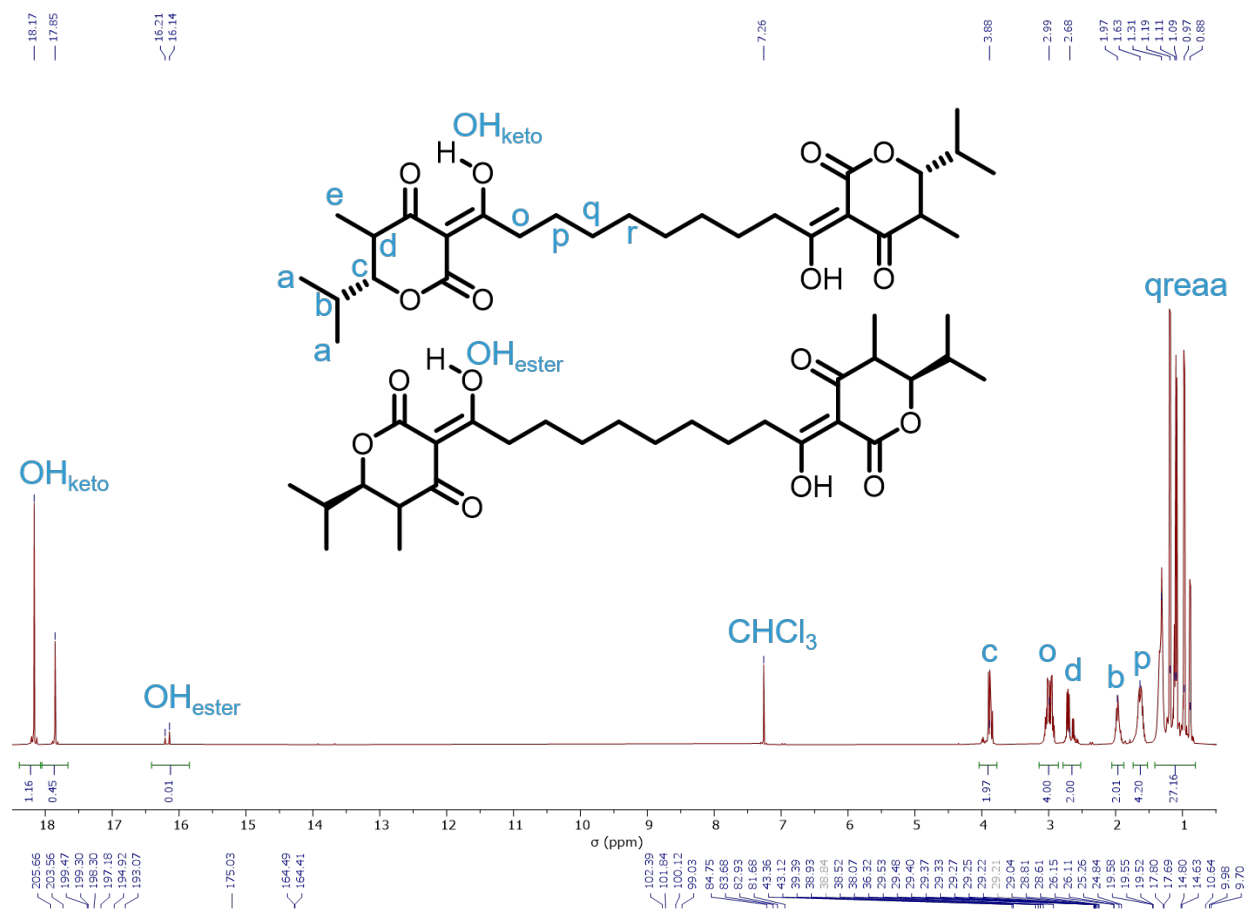
*b*-TK-1 was synthesized according to previously reported procedures<sup>16</sup>.

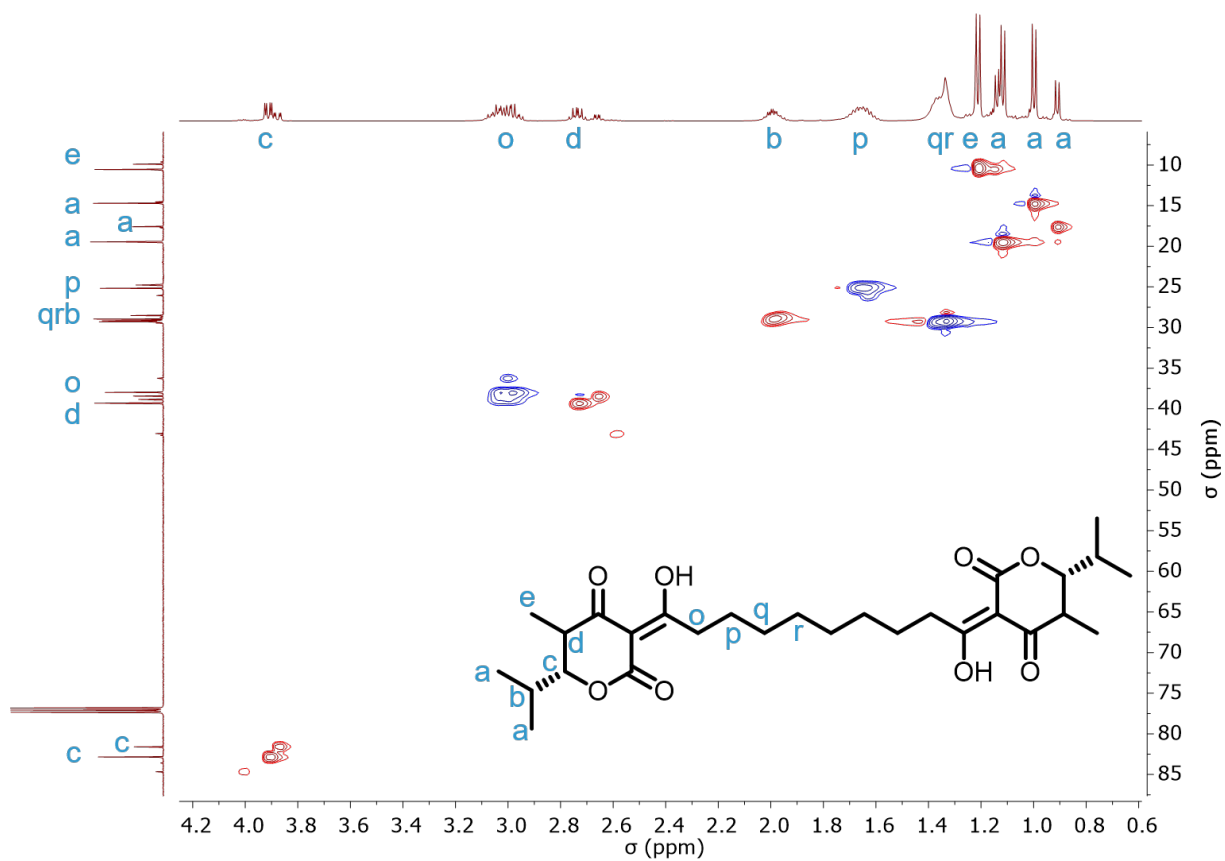


**(6*R*,6'*R*)-3,3'-(1,10-dihydroxydecane-1,10-diylidene)bis(6-isopropyl-5-methyldihydro-2*H*-pyran-2,4(3*H*)-dione) (*b*-TK-2)**



DMAP (5.24 g, 42.9 mmol), sebacic acid (2.90 g, 14.3 mmol), and BKDL **5** (5.00 g, 29.4 mmol) were dissolved in 50 mL DCM under stirring at r.t., followed by slow addition of a solution of DCC (7.08 g, 34.3 mmol) in DCM (40 mL). The reaction was stirred for 24 h before filtered, the residue of which was washed by DCM (10 mL). The residue was washed by HCl (2.0 M) until the aqueous phase's pH is less than 3, before being dried over MgSO<sub>4</sub>. The solvent was removed *in vacuo* to yield the crude product, which was purified by column chromatography (silica gel, 5-40% EtOAc in DCM) to give *b*-TK-2 as a pale-yellow powder (65% isolated yield, *R*<sub>f</sub> = 0.8, 2:8 EtOAc/hexane); <sup>1</sup>H NMR (500 MHz, CDCl<sub>3</sub>) δ ppm, 18.17 (s, 1H), 17.85 (s, 1H), 16.21 (s, 1H), 16.14 (s, 1H), 4.04–3.78 (m, 2H), 3.15–2.88 (m, 4H), 2.78–2.50 (m, 2H), 2.03–1.86 (m, 2H), 1.74–1.52 (m, 4H), 1.42–1.25 (m, 8H), 1.19 (d, *J* = 7.0 Hz, 3H), 1.11 (d, *J* = 6.4 Hz, 3H), 1.09 (d, *J* = 6.9 Hz, 3H), 0.97 (d, *J* = 6.8 Hz, 3H), 0.88 (d, *J* = 6.8 Hz, 3H); <sup>13</sup>C NMR (125 MHz, CDCl<sub>3</sub>): δ ppm, 205.66, 203.56, 199.47, 199.30, 198.30, 197.18, 194.92, 193.07, 175.03, 164.49, 164.41, 102.39, 101.84, 100.12, 99.03, 84.75, 83.68, 82.93, 81.68, 43.36, 43.12, 39.39, 38.93, 38.84, 38.52, 38.07, 36.32, 29.53, 29.48, 29.40, 29.37, 29.33, 29.27, 29.25, 29.22, 29.21, 29.04, 28.81, 28.61, 26.15, 26.11, 25.26, 24.84, 19.58, 19.55, 19.52, 17.80, 17.69, 14.80, 14.63, 10.64, 9.98, 9.70.





## References

1. Demarteau, J. *et al.* Biorenewable circularity in polydiketoenamine plastics. doi:10.26434/chemrxiv-2022-3j68j. (2022)
2. Xu, F. *et al.* Transforming biomass conversion with ionic liquids: process intensification and the development of a high-gravity, one-pot process for the production of cellulosic ethanol. *Energy Environ. Sci.* **9**, 1042–1049 (2016).
3. Davis, R. E. *et al.* *Process design and economics for the conversion of lignocellulosic biomass to hydrocarbon fuels and coproducts: 2018 biochemical design case update; biochemical deconstruction and conversion of biomass to fuels and products via integrated biorefinery pathways.* (2018).
4. Humbird, D. *et al.* *Process Design and Economics for Biochemical Conversion of Lignocellulosic Biomass to Ethanol: Dilute-Acid Pretreatment and Enzymatic Hydrolysis of Corn Stover.* (2011).
5. Baral, N. R. *et al.* Greenhouse gas footprint, water-intensity, and production cost of bio-based isopentenol as a renewable transportation fuel. *ACS Sustain. Chem. Eng.* **7**, 15434–15444 (2019).
6. Magurudeniya, H. D. *et al.* Use of ensiled biomass sorghum increases ionic liquid pretreatment efficiency and reduces biofuel production cost and carbon footprint. *Green Chem.* **23**, 3127–3140 (2021).
7. Vakkilainen, E. K. Boiler Processes. in *Steam Generation from Biomass* 57–86 (2017).
8. Xu, X., Xu, X., Zavalij, P. Y. & Doyle, M. P. Dirhodium(II)-catalyzed formal [3+2+1]-annulation of azomethine imines with two molecules of a diazo ketone. *Chem. Commun.* **49**, 2762–2764 (2013).
9. Blin, K. *et al.* antiSMASH 6.0: improving cluster detection and comparison capabilities. *Nucleic Acids Res.* **49**, W29–W35 (2021).
10. Chen, Y., Gin, J. & Petzold, C. J. Alkaline-SDS cell lysis of microbes with acetone protein precipitation for proteomic sample preparation in 96-well plate format V.1. *protocols.io* (2023).
11. Chen, Y., Gin, J. & Petzold, C. J. Discovery proteomic (DIA) LC-MS/MS data acquisition and analysis v1. *protocols.io* (2022).
12. Perez-Riverol, Y. *et al.* The PRIDE database and related tools and resources in 2019: improving support for quantification data. *Nucleic Acids Res.* **47**, D442–D450 (2019).
13. Baek, M. *et al.* Accurate prediction of protein structures and interactions using a three-track neural network. *Science* **373**, 871–876 (2021).
14. Baral, N. R., Quiroz-Arita, C. & Bradley, T. H. Uncertainties in corn stover feedstock supply logistics cost and life-cycle greenhouse gas emissions for butanol production. *Appl. Energy* **208**, 1343–1356 (2017).
15. Yang, M., Baral, N. R., Anastasopoulou, A., Breunig, H. M. & Scown, C. D. Cost and life-cycle greenhouse gas implications of integrating biogas upgrading and carbon capture technologies in cellulosic biorefineries. *Environ. Sci. Technol.* **54**, 12810–12819 (2020).
16. Demarteau, J. *et al.* Circularity in mixed-plastic chemical recycling enabled by variable rates of polydiketoenamine hydrolysis. *Sci. Adv.* **8**, eabp8823 (2022).
17. Pracht, P., Bohle, F. & Grimme, S. Automated exploration of the low-energy chemical space with fast quantum chemical methods. *Phys. Chem. Chem. Phys.* **22**, 7169–7192 (2020).
18. Ong, S. P. *et al.* Python Materials Genomics (pymatgen): A robust, open-source python library for materials analysis. *Comp. Mater. Sci.* **68**, 314–319 (2013).
19. Mathew, K. *et al.* Atomate: A high-level interface to generate, execute, and analyze computational materials science workflows. *Comp. Mater. Sci.* **139**, 140–152 (2017).
20. Grimme, S. Semiempirical GGA-type density functional constructed with a long-range dispersion correction. *J. Comput. Chem.* **27**, 1787–1799 (2006).
21. Marenich, A. V., Cramer, C. J. & Truhlar, D. G. Universal solvation model based on solute electron density and on a continuum model of the solvent defined by the bulk dielectric constant and atomic surface tensions. *J. Phys. Chem. B* **113**, 6378–6396 (2009).

22. Zhao, Y. & Truhlar, D. G. Density functionals with broad applicability in chemistry. *Acc. Chem. Res.* **41**, 157–167 (2008).
23. Grimme, S. Supramolecular binding thermodynamics by dispersion-corrected density functional theory. *Chem. Eur. J* **18**, 9955–9964 (2012).